Characterisation and Crystallisation of a Bacterial Light-Harvesting Complex

by

Neil Guthrie

A thesis submitted for the degree of Doctor of Philosophy

University of Glasgow
Department of Chemistry
October 1992

ProQuest LLC.
789 East Eisenhower Parkway
P.O. Box 1346
Ann Arbor, MI 48106 – 1346

Summary

The B800–820 light harvesting antenna complex, an integral membrane protein, from *Rhodopseudomonas acidophila* strain 7750 has been characterised. The antenna complex is comprised of four low molecular weight pigment binding apoproteins, namely the B800–820α_1, B800–820α_2, B800–820β_1 and B800–820β_2. The apparent molecular weights of bands corresponding to these apoproteins have been determined using tricine SDS polyacrylamide gel electrophoresis as 2550 daltons, 3350 daltons, 6300 daltons and 6600 daltons. Differences in the true molecular weight (M_r) deduced from the amino acid sequence and these apparent molecular weights, make it impossible to determine which is the α_1, β_1 or β_2 aprotein. Electrospray mass spectrometry indicates that the unsequenced α_2 may be the heaviest of these four apoproteins. The stoichiometric ratio of bacteriochlorophyll *a*: carotenoid has been determined as 2:1, which confirms work by Evans in 1989. Polyacrylamide gel electrophoresis shows that the complex exists as an oligomeric assembly with an apparent molecular weight of 92,000 daltons.

The integrity of the antenna complex has been maintained after exchange of lauryl dimethyl *N*-amine oxide for any of the following detergents: heptyl glucoside, β octyl-glucoside, nonyl glucoside, lauryl maltoside, heptyl thioglucoside, *N*-dodecyl-*N*, *N*-dimethyl-3-ammonio-1-propane sulfonate, CHAPS, CHAPSO and MEGA8. This integrity was demonstrated by examination of the near infrared spectra and circular dichroism studies. Ultraviolet circular dichroism demonstrated the presence of α-helix which is thought to span the lipid bilayer. Infrared circular dichroism showed that the absorption of both carotenoid and bacteriochlorophyll pigments in

the antenna complex are influenced by their surrounding environment, with possible excitonic coupling between bacteriochlorophyll molecules.

Microcrystals of the antenna complex could be grown in a variety of different detergents in the presence of a small amphiphilic molecule. Crystals of the antenna complex could be grown using β-octyl glucoside and *N*-dodecyl-*N*, *N*-dimethyl-3-ammonio-1-propane sulfonate, in the presence of the small amphiphile benzamidine hydrochloride. These diffracted X-rays to a resolution of 10Å and 15Å respectively.

Crystallisation using β octyl glucoside was then optimised with respect to different physical parameters. This led to an increase in the crystal size, with a decrease in crystallisation time, and also an improvement in the resolution of X-ray diffraction (by approximately 5Å). X-ray diffraction data were collected on two forms(#1 and #2) of tabular plate crystal, which both indexed as hexagonal cells with space group *R32*. The cell dimensions of crystal form #1 were a=b=120.01Å, c=293.91Å and those of crystal form #2 were a=b=121.81Å, c=283.11Å.

The crystal density in both forms was determined to be 1.17g/cm^3. Assuming a molecular weight of 83.5 kDa in the asymmetric unit, this indicates a V_m of 2.47Å^3/dalton for crystal form #1 and 2.42Å^3/dalton for crystal form #2. This gives a solvent composition of 49.2% and 50.8% for crystal form #1 and #2. Using the percentage solvent, the density was back calculated as 1.17g/cm^3. This indicates that the B800–820 antenna complex has an asymmetric unit consisting of a trimer of tetramers. This is consistent with the experimentally derived stoichiometric ratio of bacteriochlorophyll *a*: carotenoid (2:1).

Analysis of the Rotation function indicates the presence of a local two fold symmetry axis parallel to the z axis. It is possible there is also a local

three fold axis parallel, or at a few degrees to the z axis. The z=0 section of the Patterson map shows regular ordering of distinct sets of peaks, with interatomic vector lengths consistent with the distances between α helices arranged as a trimer of tetramers. On the basis of the biochemical and X-ray data, a model of the asymmetric unit was proposed which consisted of a trimer of molecular assemblies, with each assembly consisting of $\alpha_1\alpha_2\beta_1\beta_2$ proteins, six bacteriochlorophyll and three carotenoid molecules.

The close similarity in the unit cell and space group of these protein crystals and crystals of the B800–850 antenna complex suggests a similar asymmetric unit in both cases.

ACKNOWLEDGEMENTS

I would like to thank both my supervisors, Prof. Richard Cogdell and Prof. Neil Isaacs for all their help and guidance during the past three years. I would also like to thank everyone in Protein Crystallography including Gerry MacDermott, Dr Andy Freer, Allison Littlejohn, Fran Young, Debbie Harris, Jacqui Coll, Sean Tierney and Keith McKellar. I would like to thank everbody in Botany especially Jehan Bahkt (the "expert") for all his assistance with the gels and Evelyn Halloren for general advice and the odd bottle of purple bacteria.

I would like to acknowledge Sharon Kelly and Dr Nick Price for helping with the circular dichroism measurements at the SERC CD facility at Stirling University. I would also like to acknowledge Andrea Schneier, of the University of Cambridge, for performing the Electrospray Mass Spectrometry.

I would like to acknowledge the SERC for funding my PhD and my attendance at different scientific meetings.

Finally I would like to thank Kate for all her patience, help and support.

DECLARATION

This thesis is less than 100,000 words in length, exclusive of tables, maps, bibliographies and appendices. The work reported in this thesis was performed entirely by myself unless otherwise cited or acknowledged. Its contents have not previously been submitted for any other degree. The research for this thesis was performed between October 1989 and October 1992.

signed

Neil Guthrie

21st October 1992

TABLE OF CONTENTS

Appendices

LIST OF FIGURES

LIST OF TABLES

PAGE

SYMBOLS AND ABBREVIATIONS USED IN THE TEXT

SDS	sodium dodecyl sulphate
CHAPS	3-[(3-cholamidopropyl)dimethylammonio]-1-propane sulphonate
CHAPSO	3-[(3-cholamidopropyl)dimethylammonio]-2-hydroxy-1-propane sulphonate
MEGA8	octanoyl - *N* - methyl glucamide
NDA	*N*-dodecyl- *N*,*N*-dimethyl-3-ammonio-1-propane sulphonate
LDAO	lauryl dimethyl- *N*-amine oxide
9-OG	nonyl glucoside
ATP	adenosine triphosphate
NADP	nicotinamide adenine dinucleotide phosphate
LH1	core light-harvesting antenna complex
LH2	peripheral light-harvesting antenna complex
B	bulk (pigment)
CD	circular dichroism
DEAE	diethylethyl-amino ethyl cellulose
FRAMBO	frame buffer operation program
SANTA	SAXII area detector network transfer agent

To my Mum and Dad

CHAPTER 1. Introduction

1.1. Classification of the Purple Non-Sulphur Photosynthetic Bacteria *Rhodopseudomonas acidophila*

The order Rhodospirillales comprise those bacteria which carry out anoxygenic photosynthesis and contain bacteriochlorophyll (Pfennig and Trüper, 1971, 1974) (**Figure 1.1.**). Rhodospirillales has two sub-orders (Trüper and Pfennig, 1978):

(1). Chlorobiineae – green photosynthetic bacteria

(2). Rhodospirillineae – purple photosynthetic bacteria

The sub-order Rhodospirillineae can be classified into three families of purple phototrophic bacteria (Imhoff *et al.*, 1984):

(1). Ectothiorhodospiraceae – sulphur

(2). Chromatiaceae – sulphur

(3). Rhodospillaceae – non-sulphur

So far twenty five species of Rhodospirillales have been divided into six genera. Most species of purple bacteria contain bacteriochlorophyll *a* (*Rhodopseudomonas viridis*, *Ectothiorhodospira halochloris, Ectothiorhodospira abdelmalekii* and *Thiocapsa pfenningii*, are exceptions which contain bacteriochlorophyll *b*, (Imhoff, 1988)). Carotenoid pigments are also associated with the intracytoplasmic membrane which is continous with the cytoplasmic membrane. Most of these purple bacterial photosynthetic membranes appear to arise by invagination (Clayton 1978). The types of intracytoplasmic membrane systems range from vesicular (*Rhodobacter sphaeroides, Rhodobacter capsulatus* and *Chromatium vinosum*), to tubular (*Thiocapsa pfennigii*) and lamellar (*Rhodopseudomonas viridis, Rhodopseudomonas palustris* and *Rhodopseudomonas acidophila*) (**Figure 1.2.**)

The genus *Rhodopseudomonas*, with spherical, ovoid or rod shaped cells, was first isolated by Pfennig in 1969 and named due to its preference

for an acidic medium of pH 5.2.

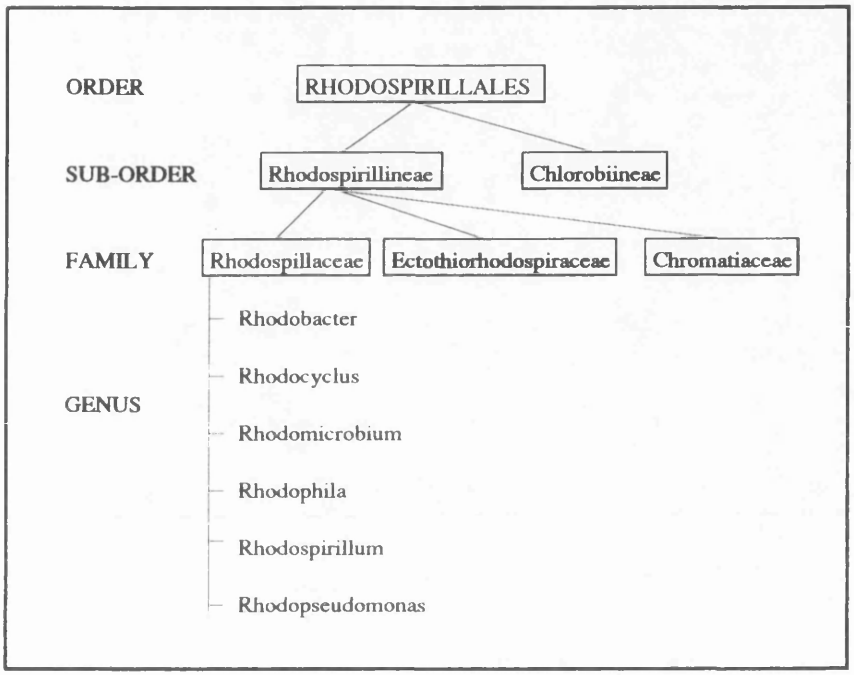

Figure 1.1. Classification of Phototrophic Bacteria (only genera of the family Rhodospillaceae are shown).

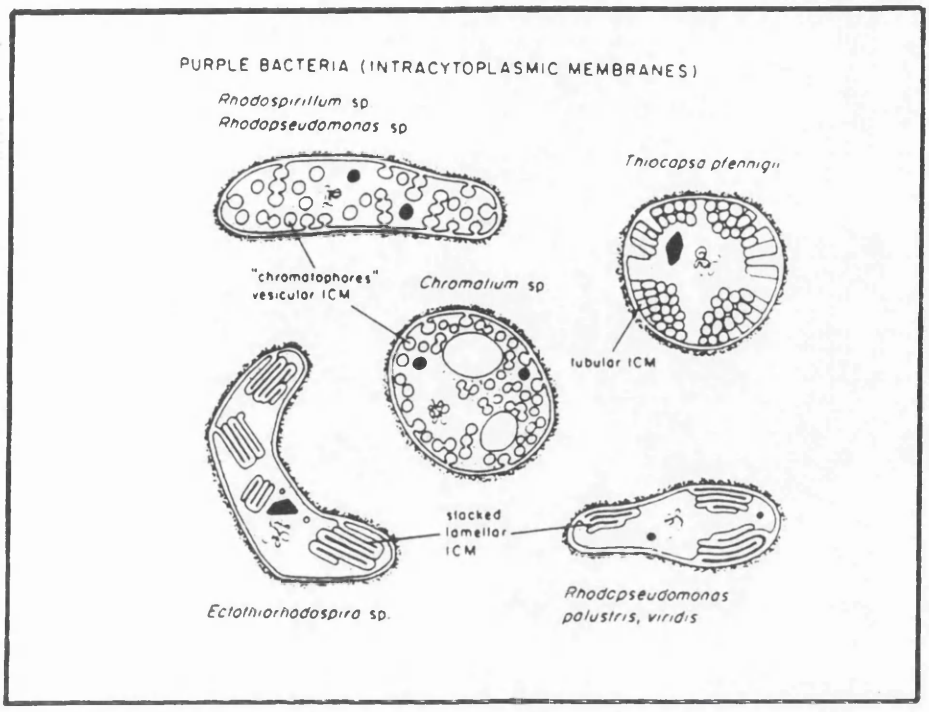

Figure 1.2. Cell Shapes and Different Forms of the Intracytoplasmic Membranes of Purple Bacteria (Sprague and Varta, 1986).

1.2. Environmental Adaptation of Purple Photosynthetic Bacteria

In the anaerobic depths of ponds and lakes, organic material is fermented by microbes which release carbon dioxide and fermentative end products e.g. hydrogen, propionate, lactate and butyrate. Purple non-sulphur bacteria, such as *Rhodopseudomonas acidophila*, are facultative anaerobes which can switch from deriving energy via aerobic respiration to utilising carbon dioxide and these fermentative end products to perform anaerobic photosynthesis. This situation arises in a typical aquatic environment shown in **Figure 1.3.** The upper strata of a such an environment are occupied by

cyanobacteria, algae and higher plants which absorb in the visible region of light. In response to the remaining near infrared wavelengths of light, which filter to levels with reduced oxygen tension, purple non-sulphur bacteria have evolved light-harvesting pigment protein complexes to perform anaerobic photosynthesis.

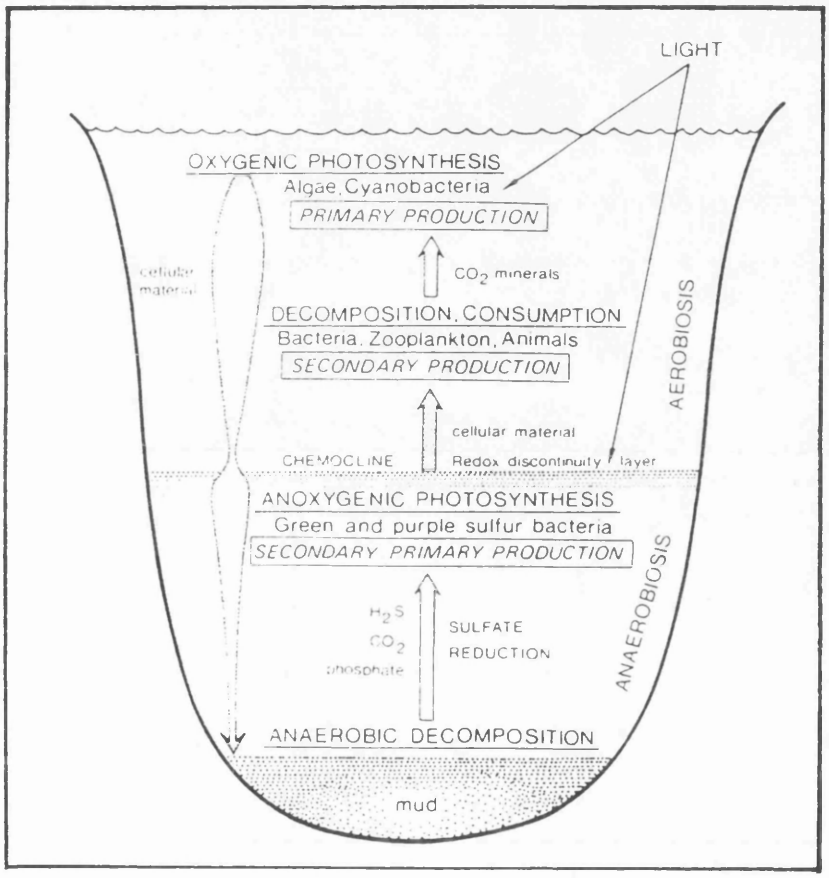

Figure 1.3. A Schematic Diagram of a Typical Aquatic Environment Containing Purple Photosynthetic Bacteria (Clayton 1978).

1.3. Bacterial Photosynthesis–An Overview

1.3. (i) Introduction

Photosynthesis is a complex series of biochemical reactions in which incident solar radiation is captured and converted into chemical energy, which is used to maintain essential cellular processes. These reactions were described by van Niel using the general equation:

$$2H_2A + CO_2 \longrightarrow 2A + H_2O + (CH_2O) \qquad \text{(van Niel, 1941)}$$

The processes represented by this equation can be divided into those reactions which require light to generate "high energy" compounds, and other reactions which subsequently use these compounds to drive light-independent reactions. The light-dependent reactions take place in and on the highly pigmented intracytoplasmic membranes of purple bacteria (**Figure 1.4.**). The light reactions of photosynthetic bacteria comprise several steps:

(1). Light harvesting

(2). Energy trapping

(3). Electron transfer and the generation of a membrane potential

(4). The formation of chemical bond energy (ATP) and reducing power (NADP)

The structure and function of antenna complexes will be described in detail after a brief discussion of other processes important in bacterial photosynthesis.

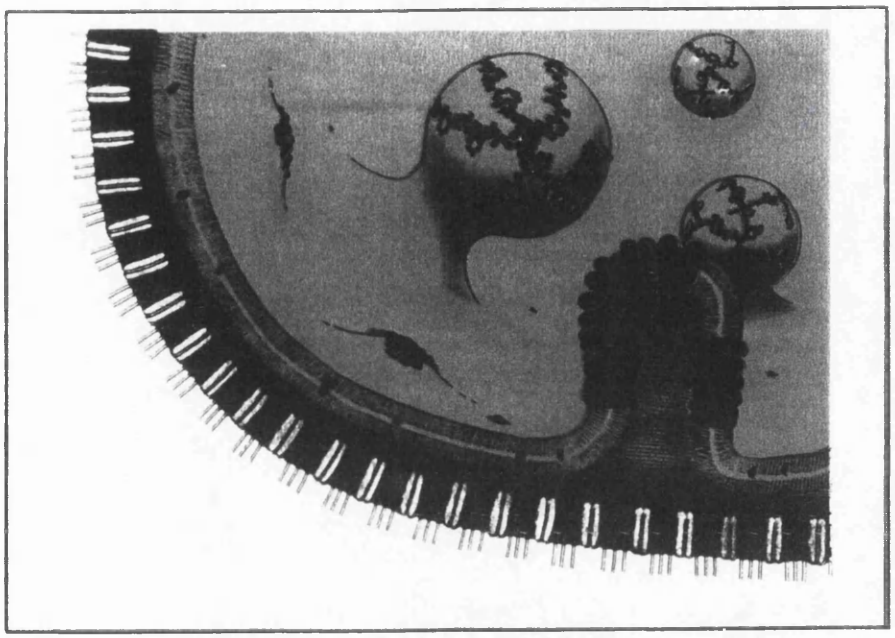

Figure 1.4. Cartoon of the Intracytoplasmic Membrane. Reaction centres (blue) form core complexes with LH1 antenna proteins (red). These in turn are surrounded and interconnected by LH2 complexes (green) (Jones and Hunter, 1992).

1.3. (ii) The First Molecular Steps of Photosynthesis

The existence of the photosynthetic reaction centre was first postulated by Emerson and Arnold (1932), with isolation from photosynthetic membranes reported by Reed and Clayton in 1968. Reaction centres contain three transmembrane proteins labelled heavy (H), medium (M) and light (L), (these labels were chosen according to the apparent molecular weights of the subunits determined by gel electrophoresis) (Clayton & Haselkorn, 1972). In *Rhodopseudomonas viridis* these contain 258, 323 and 273 amino

acid residues respectively, compared with 260, 307 and 281 residues in *Rhodobacter sphaeroides* (Williams *et al.*, 1983, Michel and Deisenhofer, 1986). In addition to transmembrane proteins, *Rhodopseudomonas viridis* also contains a tightly bound molecule of cytochrome *c* (336 amino acid residues) (Weyer *et al.*, 1987). Reaction centres of purple bacteria contain one carotenoid molecule, four bacteriochlorophylls, two bacteriopheophytins, one non-heme iron and two quinone molecules. Excitation energy from light-harvesting antenna complexes is funnelled to two exciton-coupled bacteriochlorophyll molecules known as the "special-pair" (McElroy *et al.*, 1969, Norris *et al.*, 1971, Norris *et al.*, 1973 and Netzel *et al.*, 1973). This excitation energy induces a transition of the "special-pair" to its lowest excited singlet state, followed by donation of an electron to bacteriopheophytin, the primary acceptor (Fleming *et al.*, 1988).

The bacteriochlorophyll molecule, which lies between the dimer and the bacteriopheophytin, facilitates electron transfer and acts as an electron acceptor (Shreve *et al.*, 1992). A transient charge separation occurs between the bacteriochlorophyll dimer and the bacteriopheophytin (Parson and Holten, 1986). Within 200 picoseconds the electron is transferred further across the membrane to a quinone molecule ($\mathbf{Q}_A$). A cytochrome *c* molecule then donates an electron to the electron depleted dimer which stabilises the charge separation, and the electron on $\mathbf{Q}_A$ is transferred to the membrane quinone pool via a second reaction centre quinone $\mathbf{Q}_B$. Light therefore initiates a redox reaction which results in a charge separation and the formation of a reduced quinone.

The first three-dimensional structure of a photyosynthetic reaction centre, (from *Rhodopseudomonas viridis*), was determined at atomic resolution, using the technique of X-ray crystallography (Deisenhofer *et al.*, 1984,

Deisenhofer *et al.*, 1989). This was subsequently followed by the three dimensional structures of reaction centres from *Rhodobacter sphaeroides* Strain R-26 (Chang *et al.*, 1986, Allen *et al.*, 1987a, Allen *et al.*, 1987b, Yeates *et al.*, 1987, and Chang *et al.*, 1991) and *Rhodobacter sphaeroides* 2.4.1. (Allen *et al.*, 1988 and Yeates *et al.*, 1988). Crystals from wild type *Rhodobacter sphaeroides* Y have recently diffracted X- rays to atomic resolution (Reiss–Husson *et al.*, 1992).

The orientation of the reaction centre cofactors and proteins of *Rhodopseudomonas viridis* are illustrated in **Figure 1.5** and **Figure 1.6.** Each of the L and M subunits contain five membrane spanning polypeptide segments, folded into long helices. The L and M subunits can be superimposed by carrying out a rotation of ~180° around an axis running perpendicular to the membrane surface. These transmembrane helices are labelled A–E with the central D and E helices from each protein crossing each other to form a core complex encasing the pigments. The H subunit contributes another membrane-spanning helix with its N-terminus near the periplasmic membrane. The C-terminal half of the H-subunit forms a globular domain that is bound to the L–M complex near the cytoplasmic membrane surface. This protein is not required for primary photochemistry and does not bind any of the cofactors, but it may be involved in electron transfer from the primary to the secondary quinone. It may also help to stabilise the reaction centre, bind antenna complexes or act as a target site in the cytoplasmic membrane for the synthesis of new photosynthetic units (Michel and Deisenhofer, 1986).

The pigments are arranged within the core in two branches labelled A and B, co-ordinated to the L and M polypeptide subunits respectively (Deisenhofer *et al.*, 1989). The cytochrome on the periplasmic side of the mem-

brane feeds electrons to the "special-pair" bacteriochlorophyll dimer. Electrons travel across the membrane via the A branch pigments to the primary quinone Q_A and pass around the non-heme iron as they are transferred to the B branch quinone (Q_B) (**Figure 1.7**). When Q_B has accepted two electrons it dissociates from the reaction centre and reduces a ubiquinone in the large, membrane quinone pool. The role of the non-heme iron is still uncertain. Its removal does not affect the rate of electron transfer from Q_A to Q_B. But it does form six co-ordinate bonds with surrounding amino acids which may help to stablise the reaction centre.

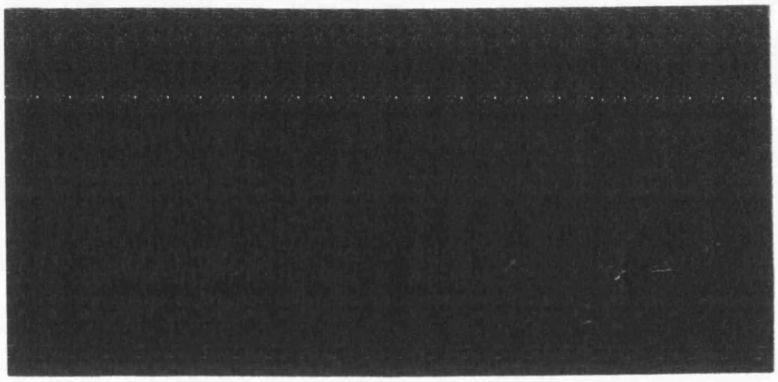

Figure 1.5. Stereoview Showing the Arrangement of the Co-factors in the Reaction Centre of *Rhodopseudomonas viridis* (Deisenhofer *et al.*, 1989). The co-factors of the M branch are shown in purple and those of the L branch are shown in green. The co-factors of the M branch can be transformed onto the co-factors of the L branch (transformed co-ordinates shown in red). This transformation superimposes only the bacteriochlorophyll special pair of each branch.

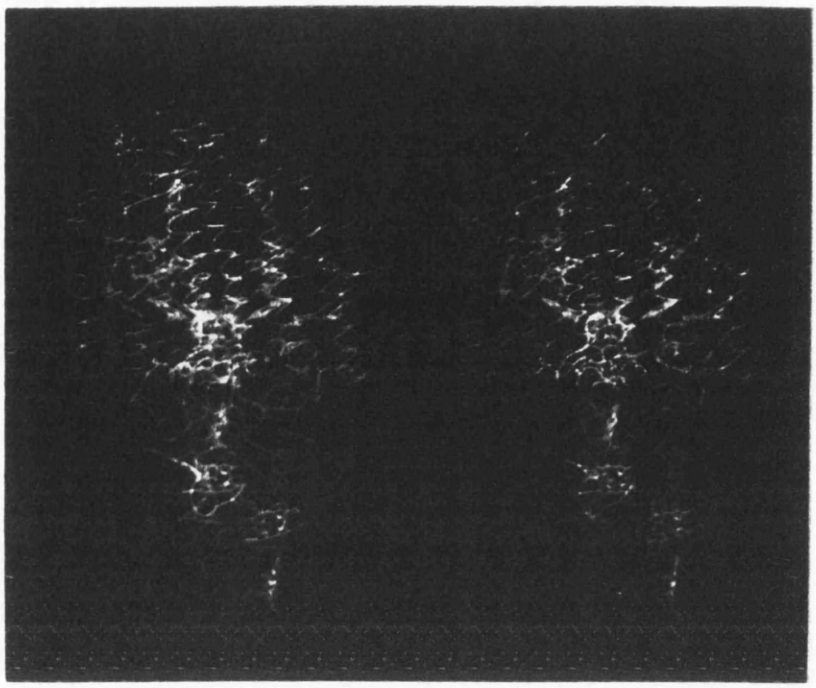

Figure 1.6. Stereoview showing an overall view of the reaction centre from *Rhodopseudomonas viridis*. Protein chains are represented as smoothed backbone drawings (Deisenhofer *et al.*, 1989). **Proteins**: Green – cytochrome, Purple – H subunit, Blue – M subunit, Brown – L subunit. **Cofactors**: Yellow – carbons, Blue – nitrogens, Red – oxygens, Green – magnesium. The reaction centre is situated in the membrane with the periplasm at the top of the diagram and the cytoplasm at the bottom.

1.3. (iii) Energy Flow and the Synthesis of ATP and NADH

The membrane quinol pool supplies electrons to the transmembrane cytochrome bc_1 complex (Gabellini *et al*, 1982) which is used in both photosynthesis and photorespiration. In photosynthesis electrons are transferred from the membrane quinone pool through the cytochrome bc_1 complex to

the reaction centre donor cytochrome c_2 (Robertson and Dutton, 1988). The electrons from the quinone pool are transferred to protein-associated quinone sites in the complex. Electrons from the Q_c site and some from Q_z site reduce the cytochrome b_h which is then thought to reduce the membrane quinone pool (**Figure 1.7**). The remaining electrons from the Q_z site reduce soluble cytochrome c_2 in the periplasmic space, which then diffuses across and donates electrons to the reaction centre. Overall there is a net oxidation of one quinol and a net reduction of two cytochromes c_2.

As electron flow proceeds the combined Δ pH and $\Delta\psi$ ($\Delta\mu_{H+}$) increases and can be used to drive three processes (**Figure 1.8**):

(1). Reduction of nicotinamide adenine dinucleotide (NAD) to (NADH) in an energy linked reversed transfer process, by membrane bound NADH-quinone oxidoreductase enzymes.

(2). Synthesis of adenosine triphosphate (ATP) by proton flow across the membrane through the ATP synthase complex (chemiosmotic hypothesis) (Mitchell, 1961, Nicolls, 1982, and Jackson and Crofts, 1969).

(3). Active transport of metabolites across the cytoplasmic membrane.

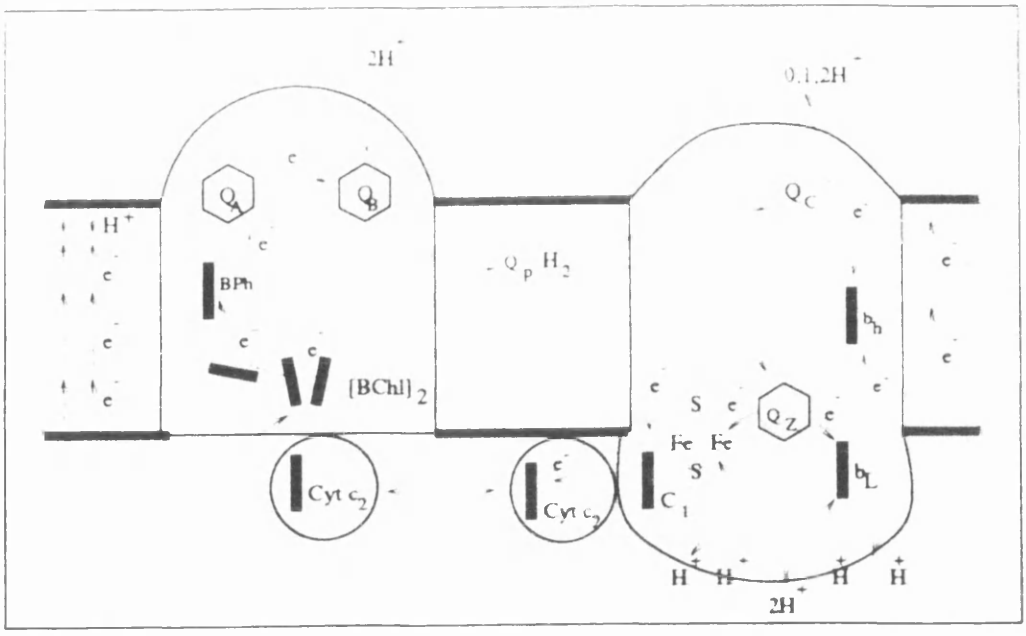

Figure 1.7. Cyclic Electron Flow Between the Reaction Centre and the Cytochrome bc_1 complex. Membrane pool quinones reduce two quinones in the cytochrome bc_1 complex (Q_C and Q_Z). Electrons then flow to cytochrome b_H and back to the membrane quinone pool, or to cytochrome c_2 in the periplasmic or lumenal space. Cytochrome c_2 then donates electrons to the reaction centre "special-pair" to complete the cycle. The cyclic electron flow results in a net transport of protons across the membrane (Robertson and Dutton, 1988).

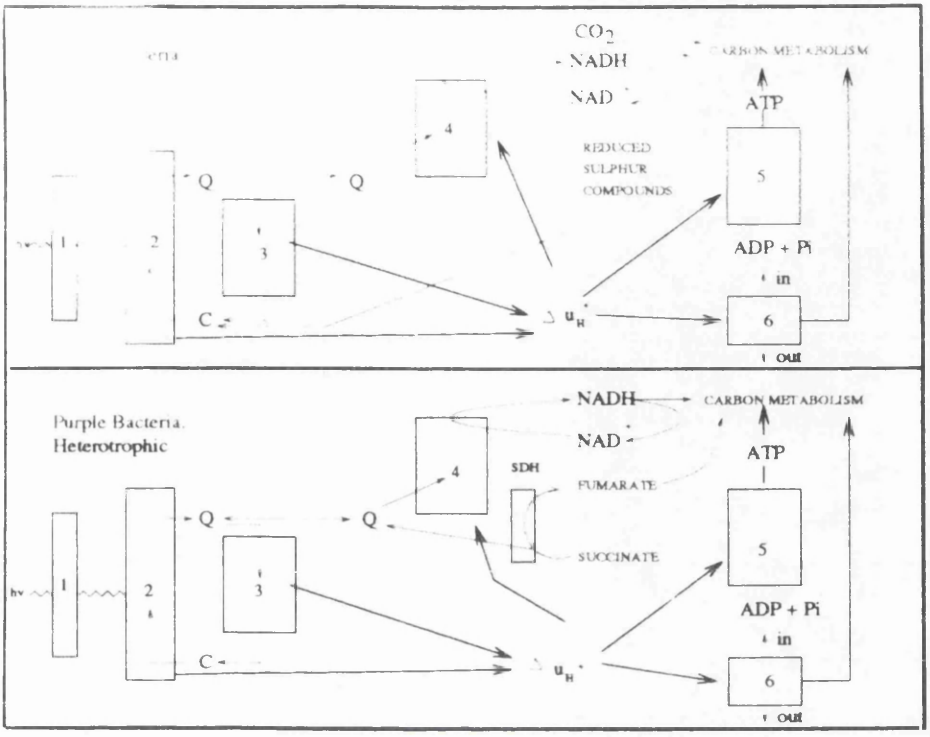

Figure 1.8. Electron Flow and Electron Transfer in Autotrophic and Heterotrophic Nutritional Modes in Purple Bacteria. (**1**) Light- harvesting antenna complexes, (**2**) Reaction centre, (**3**) Cytochrome bc_1 complex, (**4**) NADH-quinone oxidoreductase, (**5**) ATP synthase complex, (**6**) Transmembrane metabolite transporters (**Q**) Membrane pool quinone, (**C**) Cytochrome c_2., (**SDH**) Succinate dehydrogenase (Dutton, 1986).

1.4. The Light-Harvesting Antenna Complexes of Purple Photosynthetic Bacteria

1.4. (i) Introduction

The absorption spectrum of bacteriochlorophyll shows three main absorption bands (**Figure 1.9 (i)**). The Soret, UV (380nm) band results from an electronic transition to the second excited singlet state. The Q_x absorption band at 590nm and the Q_y absorption band at 772nm result from excitations into the first excited singlet state. After excitation into the Soret band, rapid internal conversion to the first excited singlet state occurs. The Q_x and Q_y bands arise from two different, perpendicular transition dipoles across the porphyrin ring (**Figure 1.9 (ii)**). Light absorption into the Q_x band at $\simeq$590nm induces a different molecular orbital electron distribution, and hence a different orientation compared to the Q_y dipole.

Nomenclature for light harvesting antenna complexes is assigned with reference to their intense near infrared Q_y absorption bands (Vredenberg and Amesz, 1967). This is shifted from the absorption of unbound bacteriochlorophyll at 772nm. The carotenoid band is also positioned further to the red in the native complex which suggests that the chromophores are involved in specific interactions with other molecules.

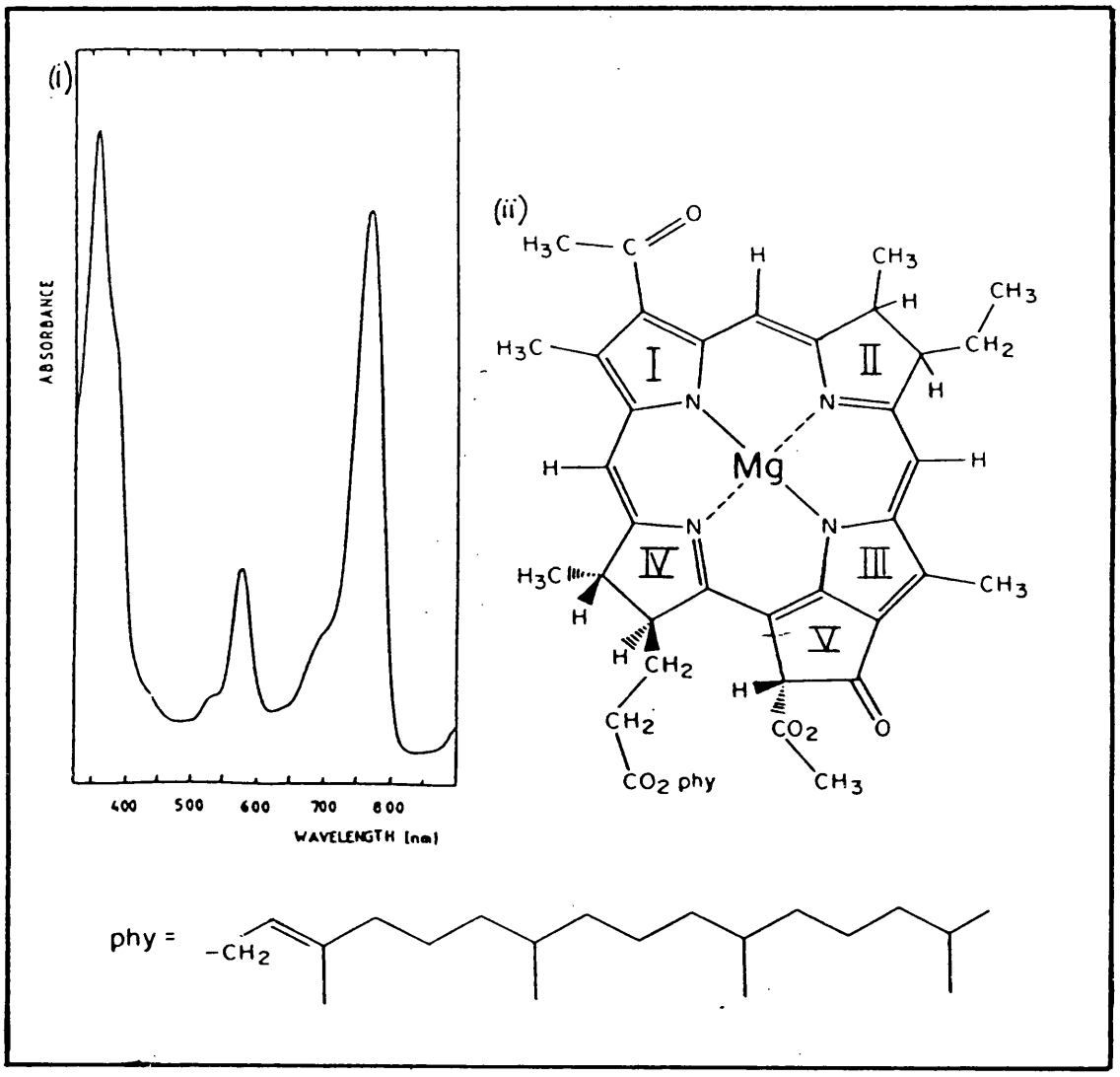

Figure 1.9. **(i)** Electronic Absorption Spectrum of Unbound Bacteriochlorophyll in Acetone. **(ii)** Molecular structure of bacteriochlorophyll *a*. The isoprenoid phtyl side-chain (phy) is replaced in *Rhodospirillum rubrum* by a geranylgeranyl side-chain.

Bril (1958) and Clayton (1962) obtained a partial separation of the antenna bacteriochlorophyll forms, by treatment of chromatophores (photosynthetic membranes) with Triton X-100 and DOC (deoxycholate) respectively. Since then a great deal of progress has been made in both the isolation and purification of antenna complexes from the chromatophores of different species (Cogdell, 1986). There are two main classes of antenna

complex which differ in spectral properties (Thornber *et al.*, 1983).

The "core" antenna complex is characterised by a single strong bacteriochlorophyll *a* Q_y absorption band in the wavelength ranges 870–890nm. The exact wavelengths of their Q_y maxima vary slightly, but these are grouped as B880 complexes for convenience (where "B" stands for bulk pigment followed by the wavelength of absorption). This class of antenna complexes is also termed LH1 (light harvesting). The B880 "core" antenna complex is present in all species of purple photosynthetic bacteria situated adjacent to the reaction centre and delivers excitation energy directly to it. The "core" complex has a fixed stoichiometry with respect to the reaction centre (Aagard & Sistrom, 1972). Examination of the structure of the photosynthetic membranes from species containing bacteriochlorophyll *b*, using high–resolution electron microscopy and image reconstruction techniques, have suggested that the B880 "core" antenna complexes (B1012 in *Rhodopseudomonas viridis*) form a well defined core complex of twelve heterodimers surrounding the reaction centre (Miller *et al.*, 1982, Stark *et al.*, 1984, & Engelhardt *et al.*, 1985). Recent studies of "core" complexes from the 7750 and 10050 strains of *Rhodopseudomonas acidophila*, show a hexagonal lattice of heterodimers surrounding the reaction centre (Gall A., personal communication, 1992).

A second type of antenna complex can be isolated from the chromatophores of most species of purple bacteria (*Rhodospirillum rubrum* and *Rhodopseudomonas viridis* are some exceptions). These complexes differ from the "core" complex in the first instance by having two distinct Q_y bacteriochlorophyll bands in the near infrared (**Figure 1.10.**). The amount and type of peripheral antenna complex expressed in most strains is also dependent on environmental factors such as light intensity and/or temper-

ature to which the bacterium is exposed. In the two most widely studied species, *Rhodobacter sphaeroides* and *Rhodobacter capsulatus*, the effect of growing cells at different light intensities has been well documented (Agaard & Sistrom, 1972, Oelze *et al.*, 1981 and Drews *et al.*, 1985). In these species the major response to lowering the light intensity is increased synthesis of the variable B800–850 complex. There are however a number of less well studied species which not only regulate the size of their photosynthetic unit in response to changes in the ambient environment, but also have the capacity to alter the type of peripheral antenna complex synthesised (Hayashi *et al.*, 1981, Hayashi *et al.*, 1982b and Cogdell *et al.*, 1983). *Chromatium vinosum*, *Rhodopseudomonas palustris* and *Rhodopseudomonas acidophila* are examples of species which show this type of response (**Figure 1.11**). Both the 7750 and the 7050 strains of *Rhodopseudomonas acidophila* can synthesise a B800–820 peripheral antenna complex in response to low temperature and/or low light. However only the 7750 strain can synthesise the B800–820 complex free of associated B800–850 complex.

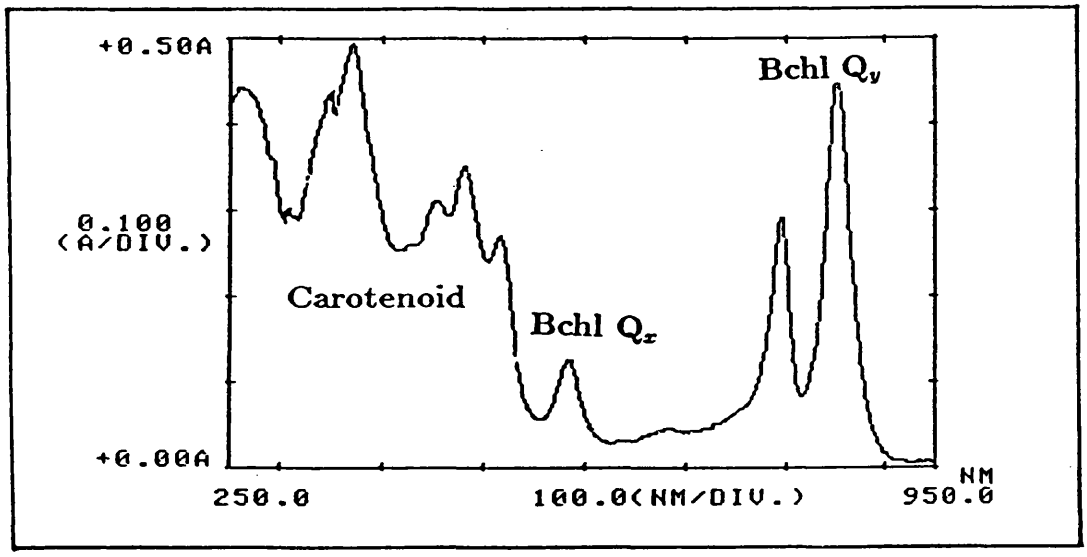

Figure 1.10. Absorption Spectrum of the B800–850 Antenna Complex from *Rhodopseudomonas acidophila* strain 10050.

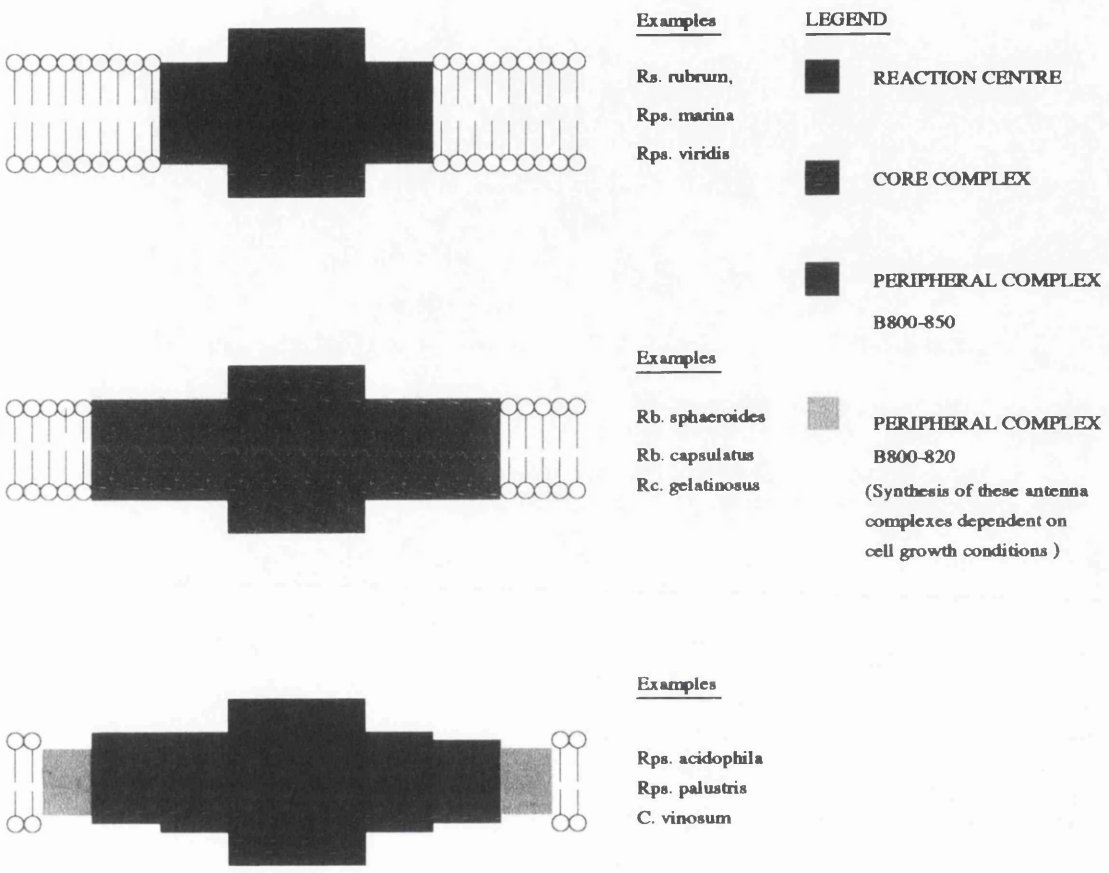

Figure 1.11. Relationships Between Different Species of Photosynthetic Purple Bacteria and Different Types of Light-Harvesting Complexes (Zuber, 1991).

1.4 (ii) The Molecular Structure of Light-Harvesting Antenna Complexes

Since the first light-harvesting antenna polypeptide, from the B890 complex from *Rhodospirillum rubrum*, was sequenced in 1981 (Brunisholz *et al.*), a large variety of both core and peripheral antenna complexes from many different species of purple bacteria have been sequenced (**Figure 1.12 (a), (b)**) (Zuber, 1990).

Hydropathy plots have indicated a hydrophobic stretch of 20-23 amino acids flanked by polar N- and C-termini. The N-terminal region is exposed to the cytoplasmic side of the photosynthetic membrane, with the C terminal portion located on or near the periplasm (Brunisholz *et al.*, 1986). The location of these regions was determined via protease experiments (Brunisholz *et al.*, 1986). On the basis of labelling experiments (Jay *et al.*, 1983), ultra violet circular dichroism and infrared spectroscopy (Breton and Nabedryk, 1984, Cogdell and Scheer, 1985), it has been demonstrated that the central hydrophobic domain consists of an α helical segment. Using infrared dichroism Breton and Nabedryk (1984) have suggested that the α-helices lie at 30 to 35° to the membrane normal. In 1986 Brunisholz *et al.* proposed a model for the membrane location of the B890 "core" complex from *Rhodospirillum rubrum* (**Figure 1.14.**).

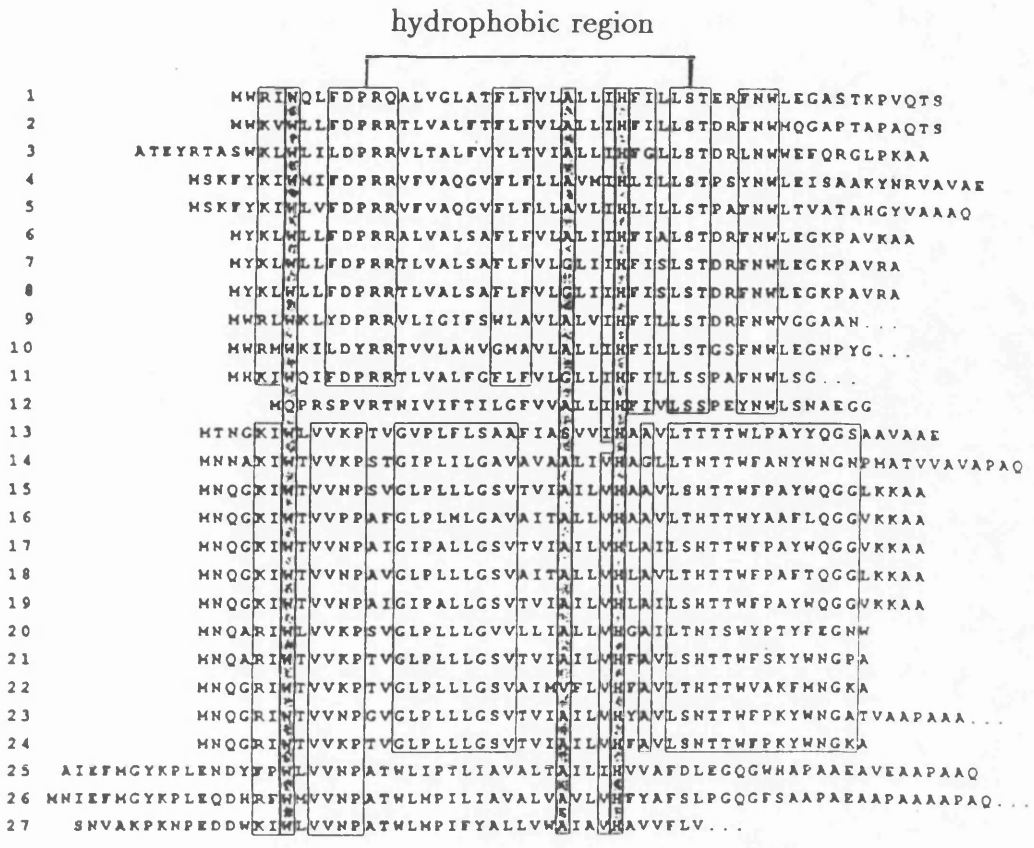

Figure 1.12. (a). Primary Structures of α Polypeptides of the Core and Peripheral Antenna Complexes of Purple Bacteria (Zuber 1990). The conserved histidine residue (H), which is the proposed bacteriochlorophyll binding site is shaded. Boxes: conserved clusters of amino acid residues. The function of these clusters is unknown. Dots represent C–Terminal sequences which are still unknown. For a key to the one letter amino acid codes see **Figure 1.13.**

1 Rhodospirillum rubrum B890-β
2 Rhodopseudomonas marina B880-β
3 Rhodopseudomonas viridis B1015-β
4 Rhodobacter sphaeroides B870-β
5 Rhodobacter capsulatus B870-β
6 Rp. acidophila Ac7050 B890-β
7 Rp. acidophila Ac7750 B890-β
8 Rp. acidophila Ac10050 B890-β
9 Ectothiorhodospira halochloris β-Polypeptid
10 Ectothiorhodospira halophila $B890_1$-β
11 Ectothiorhodospira halophila $B890_2$-β
12 Chromatium vinosum $B890_1$-β
13 Chromatium vinosum $B890_2$-β
14 Chloroflexus aurantiacus J-10-fl B806-866-β
15 Rhodobacter sphaeroides B800-850-β
16 Rhodobacter capsulata B800-850-β
17 Rp. acidophila Ac7050 B800-850-β
18 Rp. acidophila Ac7050 B800-820-β
19 Rp. acidophila Ac7750 B800-850-β
20 Rp. acidophila Ac7750 B800-820-β_2
21 Rp. acidophila Ac7750 B800-820-β_1
22 Rp. acidophila Ac10050 B800-850-β
23 Rp. palustris 2.6.1 B800-850-β_1
24 Rp. palustris 2.6.1 B800-850-β_2
25 Rp. palustris 2.6.1 B80Q-850-β_3
26 Chromatium vinosum B800-850-β
27 Chromatium vinosum B800-820-β_1
28 Chromatium vinosum B800-820-β_2
29 Chromatium vinosum B800-820-β_3

Figure 1.12. (b). Primary Structures of β Polypeptides of the Core and Peripheral Antenna Complexes of Purple Bacteria. Boxes: conserved complex specific structural elements (cluster of amino acid residues). Again the function of these clusters is also unknown. (Zuber, 1990).

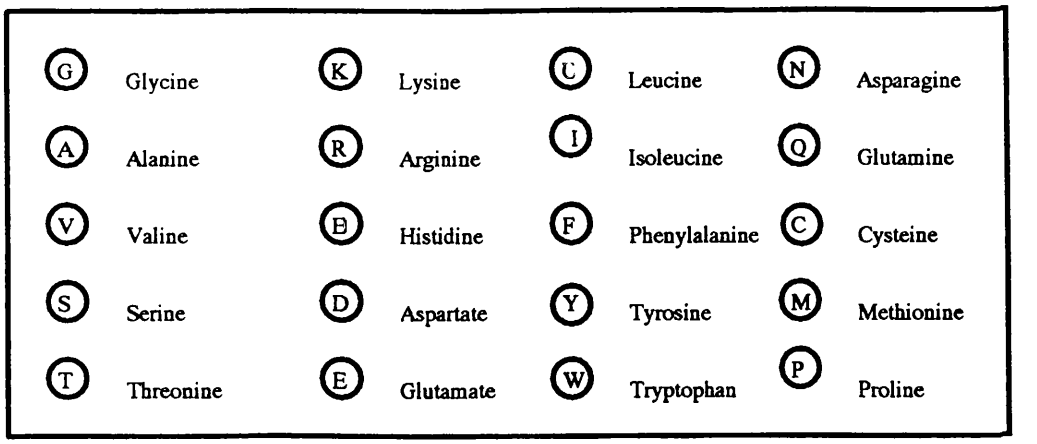

Figure 1.13. Key to the One-Letter Amino Acid Codes [IUPAC-IUB Joint Commission on Biochemical Nomenclature (1984)]

The presence of conserved histidine residues (**Figure 1.12. (a), (b)**) has led to the suggestion that a bacteriochlorophyll dimer is non-covalently liganded between the two adjacent histidines. A high resolution X-ray analysis of crystals of a water-soluble bacteriochlorophyll *a* protein complex from the green bacteria *Prosthecochloris aestuarii* has demonstrated the presence of co-ordinate bonds between the central magnesium atom of bacteriochlorophyll and a nitrogen atom orbital of the amino acid histidine (Fenna and Matthews, 1975, Fenna *et al.*, 1977 and Pearlstein, 1987).

Resonance Raman spectroscopy was used to probe the vibrational interactions of the bacteriochlorophyll chromophores in isolated antenna complexes (Robert and Lutz, 1985). This data confirmed that the magnesium atom of the bacteriochlorophyll has five ligands, four of which are presumably co-ordinated to the dihydrophorbin ring. The fifth ligand is therefore co-ordinated to an external structure. By comparing the Raman spectra of bacteriochlorophyll-imidazole models with those of the antenna complexes, Robert and Lutz concluded that the B890/B850 chromophores are liganded

to histidine residues. However a different Raman spectrum was found for the B800 chromophores which has been interpreted as meaning that the B800 bacteriochlorophylls are not co-ordinated to histidine residues as has been suggested.

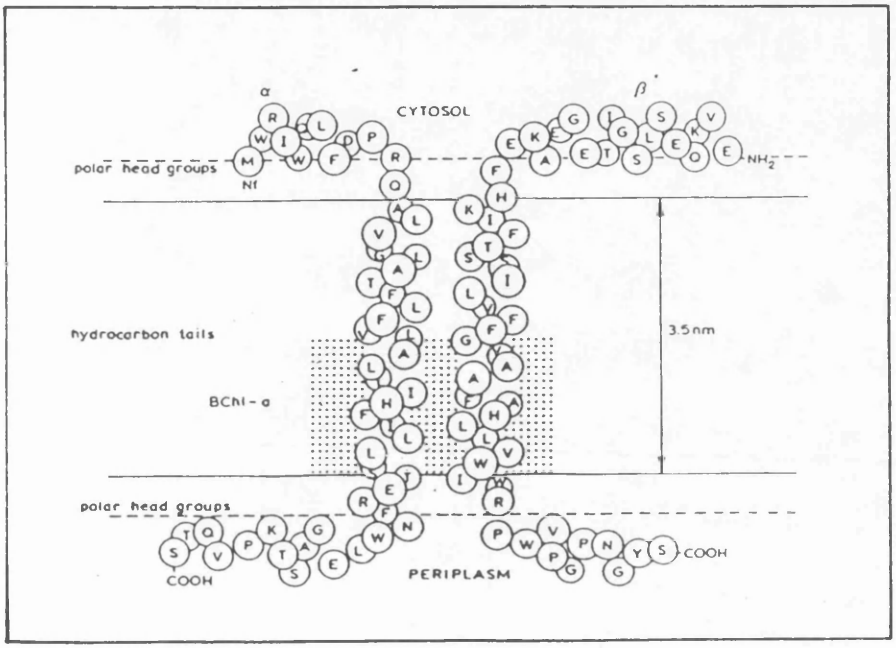

Figure 1.14. Structural Model of the Light-Harvesting "Core" Antenna Apoproteins from Purple Photosynthetic Bacteria (Brunisholz *et al.*, 1986). α– and β– subunits traverse the membrane as an α–helix, and the polar domains protrude on either side.

1.4. (iii) *In Vivo* Bacteriochlorophyll Q_y Absorption

The same bacteriochlorophyll *a* molecule can either multiply or singularly absorb at numerous wavelengths (800-890nm) in different antenna complexes. These *in vivo* near infrared maxima, observed in detergent solubilised antenna complexes are a property of the specific interactions of

bacteriochlorophyll with its immediate environment. Pigment-protein complexes which absorb at different wavelengths are of fundamental importance in the processes of light capture and directed heterogenous energy transfer to the reaction centre. The route of bacteriochlorophyll energy transfer within a photosynthetic unit of *Rhodopseudomonas acidophila* strain 7750 grown at 27°C, is shown in **Figure 1.15**. The transfer of energy from the outermost B800–820 antenna complex to the reaction centre is an energetically favourable process (the energy of an electronic transition is inversely proportional to the absorption wavelength).

Many factors can alter the wavelength at which the Q_y bands absorb e.g. the strain of bacterium, the oxygen tension, growth conditions and age (Thornber *et al.*, 1978). Wavelength shifts have also been noted during detergent solubilisation of antenna complexes e.g. 5nm and 12nm blue shifts in LDAO (lauryl dimethyl N-amine oxide) extracts from *Rhodobacter sphaeroides*, wild type, and R-26 carotenoidless mutant respectively (Reed, 1970, Clayton and Clayton, 1972). *In vitro*, bacteriochlorophyll and bacteriopheophytin oligomers have been found in small Triton X-100 and LDAO detergent micelles (Cotton *et al.*, 1978, Gottstein and Scheer, 1983, Scherz and Parson, 1984 and Scherz *et al.*, 1986). These oligomers have Q_y bands which can absorb at wavelengths as high as 880nm. It is thought that their pyrrole rings III overlap, giving rise to exciton coupling and inducing the red shift (**Figure 1.9**). However in very dry non-nucleophilic solvents aggregation does not occur (Katz *et al.*, 1977, Cotton *et al.*, 1978). It has been proposed that during aggregation nucleophiles, solvent hydroxyl groups, form lone-pair coordinate bonds with the central magnesium atom of one of the chlorophylls. The solvent can then hydrogen-bond the keto group on ring V of the second chlorophyll to form the aggregate. Hanson

and Hofrichter (1985) formed water-free phaeophorbide *a* crystals which had red shifts high enough to account for the *in vivo* Q_y bacteriochlorophyll forms, by just π–π orbital interactions.

Although this evidence demonstrates that *in vitro* bacteriochlorophyll molecules can form oligomers resulting in a red shift, resonance Raman spectroscopy has indicated that such oligomerisation does not occur *in vivo.* This does not however dismiss the overlap of excited state wavefunctions of closely positioned molecules.

There is some evidence to suggest interactions with carotenoids can effect a bathochromic shift in the Q_y maximum (Griffiths *et al.*, 1955). The α– and β– apoproteins of antenna complexes from wild type *Rhodospirillum rubrum* and the $G9^+$ carotenoidless mutant strain have identical amino acid sequences (Brunisholz *et al.*, 1984), however the Q_y maxima of these two strains differs by 8nm (Wild type 881nm, mutant strain 873nm (Parkes-Loach *et al.*, 1988)). Thus the difference in wavelength seems to be associated with the carotenoid.

It is also possible that bathochromicity is partly due to bacteriochlorophyll–protein interactions, especially with charged or aromatic amino acids. The evidence for bacteriochlorophyll–histidine ligation has already been discussed. With rare exceptions both the N-terminal and C-terminal polar domains of antenna polypeptides contain clusters of two–four conserved aromatic amino acid residues (see **Figure 1.12.**) The B800–850 antenna complexes from the 7050 and 7750 strains of *Rhodopseudomonas acidophila* have identical absorption spectra. Although there are some differences in primary structure, there is a conserved cluster of aromatic amino acids in the C-terminals of the α–apoproteins, i.e. Y_{44}-W_{45} (Brunisholz & Zuber, 1987). When strain 7050 is grown under low light

intensity it synthesises a B800–820 complex, which has a different aromatic cluster (F_{44}-L_{45}). In the B800–820 complex of cells of the 7750 strain grown at low temperature, the cluster is replaced by F_{44}-T_{45}. As these are the only major differences in the C–terminal regions of the polypeptides it was suggested that these aromatic amino acids are specifically responsible for the variation in the Q_y band absorption maxima of these complexes (Zuber & Brunisholz , 1991). This has recently been confirmed by site-directed mutagenesis experiments producing genetically modified antenna complexes with these blue–shifted absorbance bands (Fowler *et al.*, 1992).

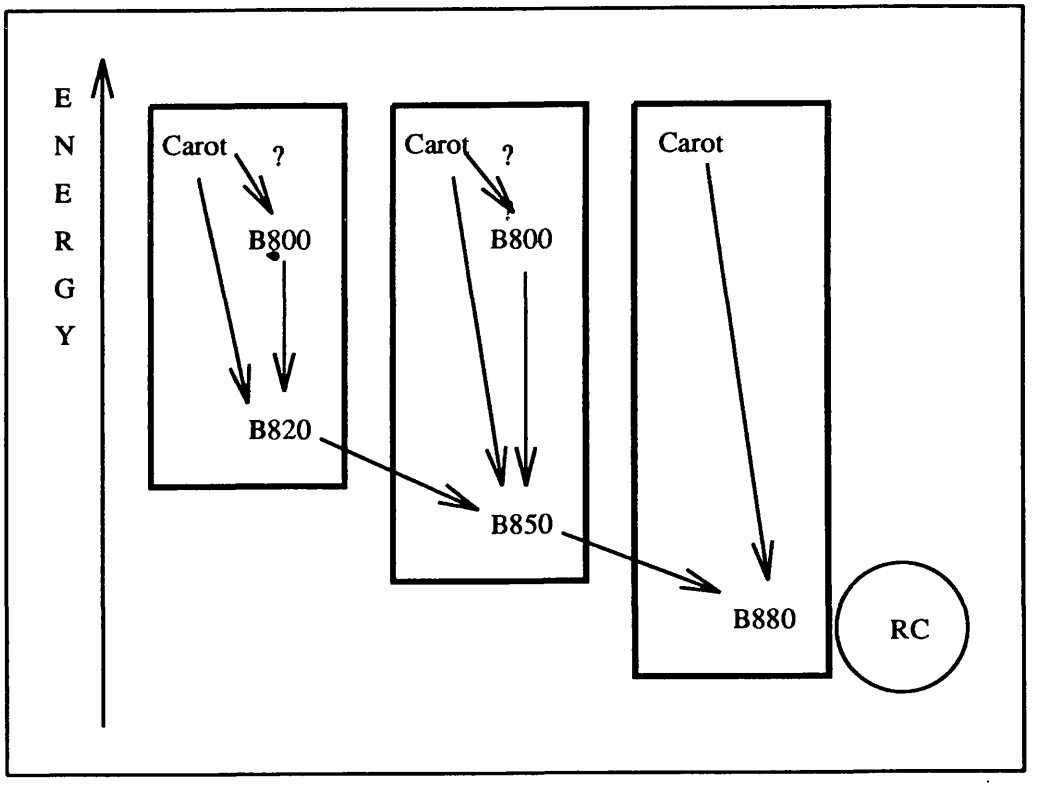

Figure 1.15. Photosynthetic Unit from *Rhodopseudomonas acidophila* strain 7750 grown at 27°C. An efficient directional flow of excitation energy from the antenna complexes to the reaction centre is possible by a combination of chemically identical bacteriochlorophyll pigments absorbing at different wavelengths.

The differences in near infrared circular dichroism intensities and variation in the wavelength at which the core antenna complexes absorb (880–890nm) can be correlated from a comparison of the primary sequences of the polypeptides (Brunisholz and Zuber, 1987). The B880/B890 core antenna complexes have an intense biphasic near infrared CD signal (Cogdell and Scheer, 1985, Thornber, 1986), whilst the CD signals of the slightly blue shifted B875 core antenna complexes have a much weaker CD signal. The structural features of the polypeptides of core antenna complexes with intense CD signals are:

i. in the α–polypeptides: the adjacent amino acid of the conserved histidine is a phenylalanine.

ii. in the C-terminal domain of the β–polypeptides a tyrosine/tryptophan residue is present adjacent to an extreme turn constellation (**Figure 1.16.**). These specific structural elements are not present in the polypeptides of the core antenna complexes with weak CD intensities indicative of a possible structural and functional role for the strongly interacting core antenna pigments.

Both bacteriochlorophyll–bacteriochlorophyll and bacteriochlorophyll–amino acid interactions were found to be present in the light–harvesting antenna complex from *Prosthecochloris aestuarii*, when the structure was determined to atomic resolution by Fenna and Matthews in 1975. Although this antenna complex binds bacteriochlorophyll *a*, it is water–soluble and thus different to the hydrophobic antenna complexes of purple bacteria.

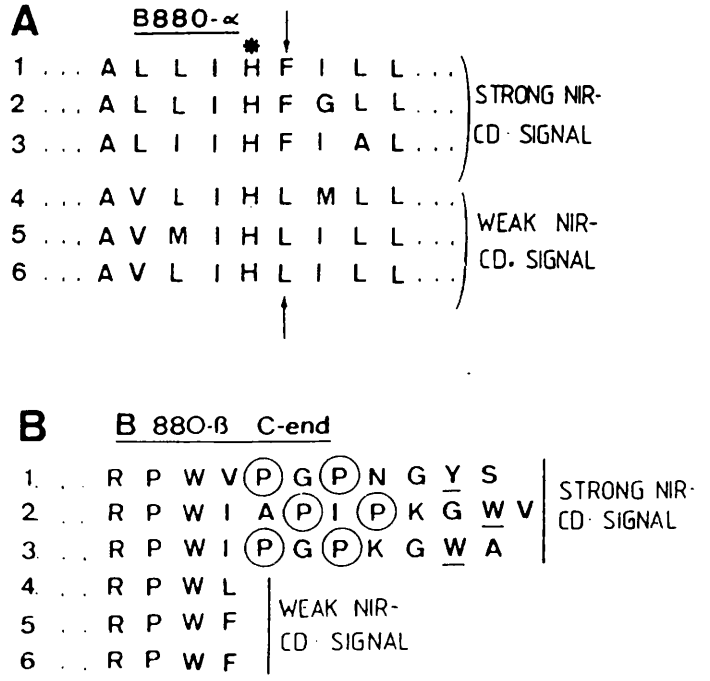

Figure 1.16. Correlation of the Near Infrared CD Intensities of the Core Antenna with Specific Structural Features of the α– and β–polypeptides. **A**: Amino acid sequence constellation in the vicinity of the conserved histidine ($*$) of the core α-polypeptides. **B**: A comparison of the C-terminal domains of the β–polypeptides of the core antenna complexes. 1. *Rs. rubrum*, 2. *Rps. viridis*, 3. *Rps. acidophila*, 4. *Rc. gelatinosus*, 5. *Rb. sphaeroides*, 6. *Rb. capsulatus* (Brunisholz and Zuber, 1987).

In summary the observed bathochromicity of the bacteriochlorophyll Q_y bands is probably due to a combination of different bacteriochlorophyll interactions. The bacteriochlorophyll-bacteriochlorophyll interaction in the B800–850 dimer will induce a red shift of unknown magnitude. The coordinate ligation of both the dimer and monomer to histidine residues will alter

the first excited state wavefunctions of the bacteriochlorophyll and induce a red shift. And finally, the presence of aromatic amino acids in the environment of the antenna bacteriochlorophylls may play a role in "fine-tuning" the near infrared absorption maxima.

1.4. (iv) Pigment Stoichiometry

B875/B890 complexes contain one bacteriochlorophyll dimer per α/β–polypeptide pair whereas peripheral antenna complexes contain a dimer and a monomer giving a stoichiometry of three bacteriochlorophylls per polypeptide pair (Sauer and Austin, 1978, Broglie *et al.*, 1980, Picorel and Gingras, 1988). The ratio of bacteriochlorophyll to carotenoid appears to be antenna complex specific. B875 complexes are believed to have ratios of 1:1 (Broglie *et al.*, 1980, Evans, 1989), but B890 complexes are believed to have ratios of 2 bacteriochlorophyll *a* to 1 carotenoid (Cogdell *et al.*, 1982, Picorel *et al.*, 1983, Ueda *et al.*, 1985). The ratio for all B800–820 complexes was initially reported to be 3:1 (Thornber *et al.*, 1970, Cogdell *et al.*, 1983a), but the ratio for the B800–820 complex from *Rhodopseudomonas acidophila* strain 7750 has recently been redetermined as 2:1 (Evans, 1989). The ratio of pigments in this complex is the subject of investigation in **Chapter 3.**

1.4. (v) Orientation of Pigments

The position of non-covalently bound carotenoid molecules in antenna complexes is unknown. Carotenoids perform energy transfer and provide photoprotective functions, which are restored after these pigments are reconstituted into complexes isolated from carotenoidless mutants (Davidson and Cogdell, 1981). To act as photoprotectors the carotenoids must be positioned $\leq$ 0.5nm from bacteriochlorophyll molecules. Zuber (1985) suggests that the carotenoid may be located within the short α–helical regions of the α– and β–polypeptides at the N–terminal side of the membrane. Brun-

isholz *et al.*, (1986) described differences in the action of proteases on the N–terminal domains of the apoproteins of *Rhodospirillum rubrum* wild-type and the carotenoidless mutant strain $G9^+$, which they suggest indicates that the carotenoid may lie in this region.

From fluorescence polarisation and linear dichroism studies, Breton *et al.* (1984) have proposed a model in which the porphyrin ring of the bacteriochlorophyll 800nm absorbing monomer lies almost parallel with respect to the plane of the membrane, and perpendicular to the carotenoid. The porphyrin rings of bacteriochlorophylls absorbing between 820–850nm lie perpendicular with respect to the plane of the membrane and are apparently located in the same bilayer half as the "special pair" of the reaction centre (Brunisholz *et al.*, 1984, Brunisholz *et al.*, 1986). It is proposed that they are orientated so that their Q_y transition moments are mutually perpendicular.

1.4. (vi) The Arrangement of Antenna Polypeptide Aggregates

The structural basis for the strict organisation of pigment molecules is the hierarchical organisation of the α– and β– antenna polypeptides within and between the antenna complexes.The results of recent excitation migration studies of different cultures of *Rhodopseudomonas acidophila* have shown that differences exist in the transfer of energy (Deinum *et al.*, 1991). On the basis of these results Deinum *et al.* proposed a general model for the structural arrangement of antenna complexes in the photosynthetic membrane (**Figure 1.17.**). This model depicts small clusters of B880 core complexes separated from each other by a more or less continous array of B800–820 or B800–850 antenna complexes.

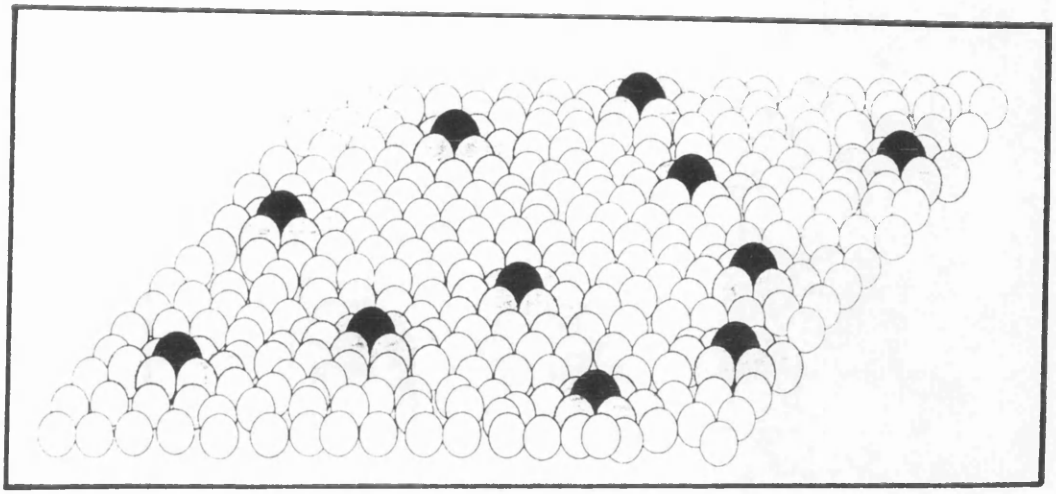

Figure 1.17. Model for the Photosynthetic Antenna Complexes of *Rhodopseudomonas acidophila.* The peripheral antennae (B800–820 and/or B800–850, depending on the culture) are indicated by white circles, the reaction centre plus core antennae (B880) by black and grey circles, (Deinum *et al.*, 1991).

Electron microscopy and image processing, of photosynthetic membranes from *Rhodopseudomonas viridis* suggest that the B1015 complex has a hexagonal arrangement around the reaction centre (Englehardt *et al.*, 1985, Stark *et al.*, 1984). Assuming a tilt of 30° of the α–helices (Breton and Nabedryk, 1984) a speculative model for the circular arrangement of α/β–apoprotein pairs has been proposed (Zuber *et al.*, 1985, Zuber, 1986). The model envisages an aggregate which forms a left–handed superhelix; the individual apoproteins interacting at the centre (**Figure 1.18.**). X-ray diffraction data indicates that the observed three–fold axis of symmetry of the polypeptide arrangement corresponds with the three-fold functional symmetry of the $3\alpha_2\beta_2$ subunits (Papiz *et al.*, 1989).

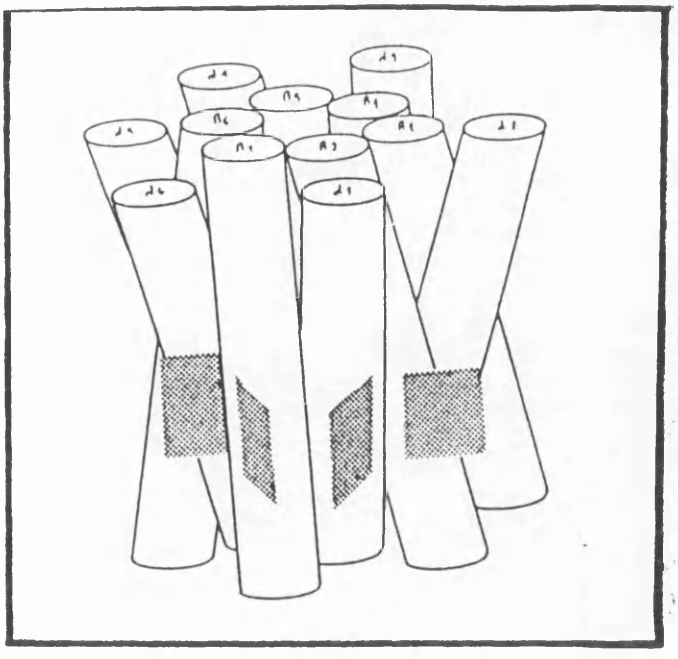

Figure 1.18. Model of the Arrangement of α/β– Polypeptide Aggregates (Zuber, 1986). The α–helices of the polypeptides are tilted about 30° with respect to the membrane normal and arranged in a hexameric aggregate.

CHAPTER 2. Experimental Methods

2.1. Culture Storage

Cell cultures were maintained in agar at a temperature of 20°C or in glycerol at approximately -70°C.

2.2. Cell Culture

Rhodopseudomonas acidophila, strain 7750 was grown photoheterotrophically at pH 5.2 (**Appendix A**), in Pfennigs medium (Pfennig, 1969). Liquid starter cultures were prepared from stored cultures and grown in 25ml bottles positioned between arrays of 100 and 150 Watt electric light bulbs at a temperature of 30°C. After 2 days the cultures were transferred to 500ml flat-sided screw capped bottles. Cells were grown at 23°C in a thermostatically controlled waterbath. The light intensity was 50μmoles/sec/m^2 (six 60 Watt electric light bulbs). Since large quantities of the cells were required, the contents of the culture bottles were transferred after 3 days during the late log phase, into a 10 litre stoppered flask.

2.3. Isolation of the Photosynthetic Membranes

Cells were harvested from the liquid culture, during the late log phase by centrifugation at 2800rpm, for 100min at 4°C (Fisons MSE COOLSPIN centrifuge). After re-suspending in MES-KCl buffer, pH 6.8, the cells were further centrifuged at 12000rpm for 20min at 4°C (Fisons MSE18 centrifuge). The pelleted cells were re-suspended in 20mM Tris-HCl pH 8.0, and then used immediately or stored at -20°C until required The cell suspension was stirred together with a few grains of bovine pancreatic DNAaseI (Sigma) and magnesium chloride for 10min. A French press (Frenkel and Nelson, 1971), chilled prior to use, was used to rupture the cells under a pressure of 7–10 tonnes/in^2.

tonnes/in^2. The broken cells were centrifuged at 12000rpm for 20min at 4°C, and the supernatant further centrifuged at 45000rpm in a fixed angle rotor (Dupont, Sorvall T865), for 1hr at 4°C (Cogdell *et al.*, 1983b). The pellets from the low and high speed spins were combined and re-suspended in 20mM Tris-HCl, pH 8.0.

2.4. Solubilisation of the Photosynthetic Membranes and Isolation of the Crude Preparations of Antenna Complexes

The photosynthetic membrane suspension was adjusted by dilution with 20mM Tris-HCl at pH 8.0, to give an absorbance at a wavelength of 800nm of 50cm^{-1}. The diluted membrane solution was then incubated for 20mins, at room temperature with 1%(v/v) LDAO(lauryl dimethyl *N*-amine oxide) (Oxyl). Centrifugation at 12000rpm for 10min was used to pellet the unsolubilised material. The supernatant containing the crude preparations of antenna complex was retained and used immediately or stored at -20°C.

2.5. Separation of the B880 Core and the B800–820 Peripheral Antenna Complexes

Two methods were used for the separation of the B880 core complex from the B800–820 peripheral antenna complex.

2.5(i) DEAE Anion-Exchange Chromatography

Whatman DE52 diethylethyl-aminoethylcellulose (DEAE) anion exchanger was pre-equilibrated with 20mM Tris-HCl, pH 8.0 and poured into a sintered glass column to a height of 5–10cm. Five column volumes of buffer were used to equilibrate the pH of the anion exchanger, and also to level the anion exchanger – buffer interface. The crude preparation of antenna com-

plex was diluted twofold using buffer and loaded onto the column, making sure that the interface surface remained intact. After loading was complete, a gradient of sodium chloride solutions (30mls each of 50mM, 60mM, 70mM, 100mM and 150mM) in 0.1% LDAO was used to elute first the B880 core complex and then the B800–820 peripheral antenna complex (**Figure 2.1.**). The eluted complexes were collected automatically in 1ml fractions (Biorad-econofraction collector). The electronic absorption spectra of each fraction was monitored in the wavelength ranges 750–900nm (Shimadzu UV-160A spectrophotometer). Fractions containing only the B800–820 peripheral antenna complex free of B880 core complex were pooled. Samples of B800–820 peripheral antenna complex still containing B880 core complex were retained for complete purification using sucrose-density centrifugation.

To concentrate the complex, an identical second anion exchange column was poured using Whatman DE52 anion exchanger, pre-equilibrated with 20mM Tris-HCl, pH 8.0. The pooled fractions were reloaded and again eluted using the same gradient of sodium chloride solutions in 0.1% LDAO. 1ml fractions were collected and their electronic absorption spectra monitored (wavelength range 250–900nm). The pigment/protein ratio of :

$$\frac{bacteriochlorophyll\ a\ Abs(800nm)}{aromatic\ amino\ acid\ Abs(280nm)}$$

was taken as a purity index. Only fractions which had a purity index of 2 or greater were retained. Damaged antenna preparations contain more free pigment and hence less 800nm-absorbing bacteriochlorophyll. This gives a low pigment/protein ratio.

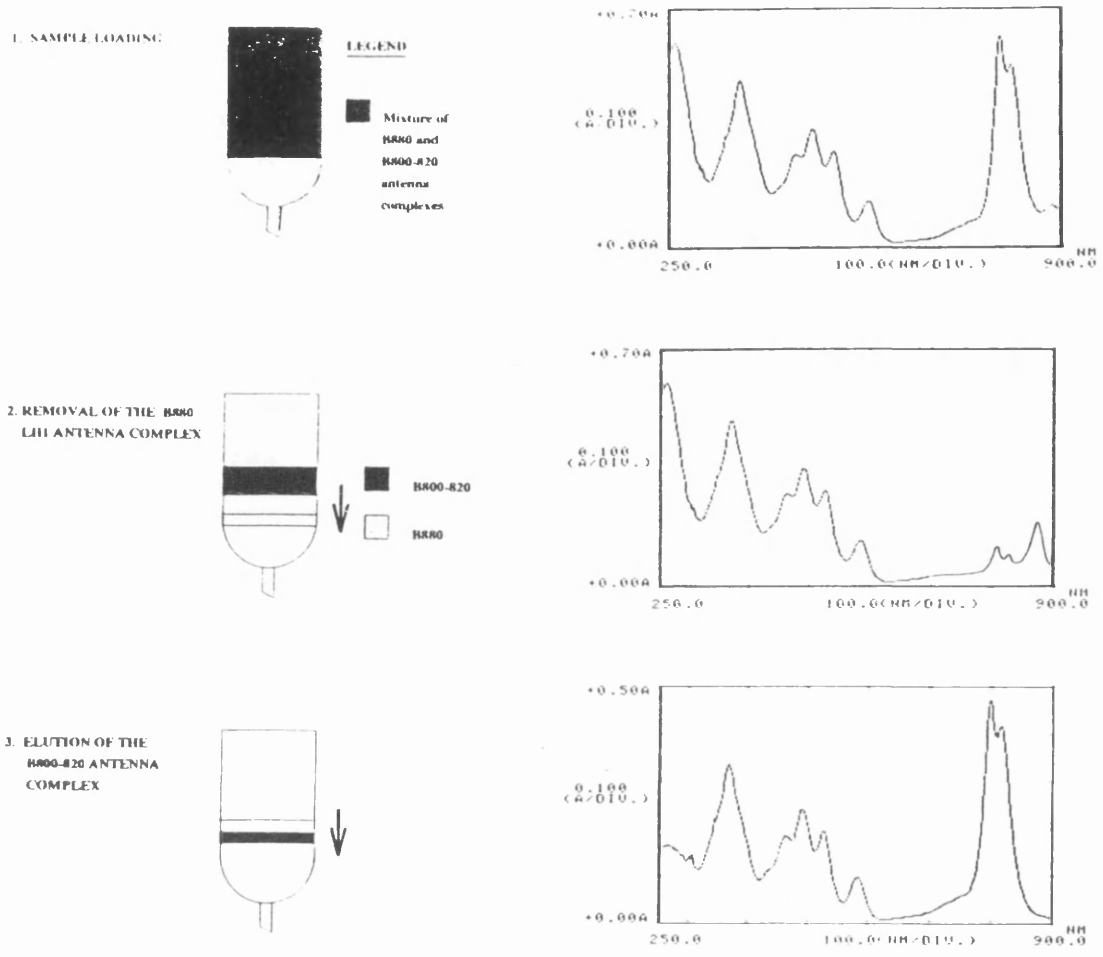

Figure 2.1. Removal of the B880–LH1 Complex using Anion Exchange Chromatography.

2.5 (ii) Sucrose Density-Gradient Centrifugation

Sucrose gradients were carefully prepared in 27ml polycarbonate centrifuge tubes (Dupont) (Garcia *et al.*, 1966). The gradients were layered using 6ml steps of 0.6M, 0.4M, 0.3M and 0.2M sucrose, all in 20mM Tris-HCl, pH 8.0, 0.2% LDAO. A 3ml sample of mixed complexes was layered on top of the gradient. The samples were then centrifuged at 45000rpm for 16hrs at 4°C. The mixed complexes separate into two distinct bands, the upper and lower bands containing the B800-820 peripheral antenna complex and the B880 LH1 core complex respectively. The B800–820 complex was transferred using a pasteur pipette to a membrane (BDH, visking size 2-18/32") and dialysed overnight against 2litres of 20mM Tris-HCl, pH 8.0, 0.1% LDAO at 4°C.

2.6. Gel Filtration Chromatography

Gel filtration chromatography was used to further purify the B800–820 peripheral antenna complex. 3ml preparations from anion exchange chromatography or sucrose -gradient centrifugation were passed down a 1 metre long column of Sephacryl S200 high resolution gel (Pharmacia), pre-equilibrated with approximately 500mls of 20mM Tris-HCl, pH8.0, 0.1% LDAO, at 4°C. 1ml fractions were collected and monitored spectrophotomerically as detailed previously. Fractions with a purity index of 3 or greater were pooled.

2.7. Concentration of the B800–820 Peripheral Antenna Complex and Detergent Exchange

A mini-column poured in a pasteur pipette, containing Whatman DE52

anion exchanger, was equilibrated with approximately 10mls of 20mM Tris-HCl, pH 8.0. The B800–820 peripheral antenna complex was diluted four-fold in the same buffer and loaded onto the column. The complex was then washed with 4 column volumes (6ml) of detergent-free buffer and the detergent exchanged by loading 1 column volume of new detergent (**Appendix B**) (1% concentration in 20mM Tris-HCl, pH 8.0). The complex was eluted using 350mM sodium chloride in 20mM Tris-HCl, pH 8.0, 1% new detergent.

Samples of protein in each of these detergents were assessed for stability by initially observing the electronic absorption spectra. The samples were then stored at -20°C and checked weekly over a period of 4 months, by observation of the electronic absorption spectra.

2.8. Isolation of α– and β–Apoproteins for Electrospray Mass Spectrometry Studies

A 3ml sample of concentrated and detergent-exchanged B800–820 antenna complex was freeze dried for 4 days. The lyophilised complex was added to 20ml of 1:1 (v/v) dichloromethane/methanol in the presence of 100mM ammonium acetate and 1mM dithiothreitol. The sample was then left in the dark for 30 min and extracted via centrifugation at 6000rpm. The green supernatant was removed and extraction of the pellet repeated until the supernatant was colourless. All supernatant fractions were pooled.

A Sephadex LH60 gel filtration column (150x2.5cm) was prepared in 1:1 (v/v) dichloromethane/methanol and 100mM ammonium acetate. A 10ml volume of extracted supernatant was loaded evenly across the gel surface. The eluate was monitored by absorption at 280nm using an LKB Uvicord ultraviolet monitor and collected in 1ml fractions. These fractions were

dried using a rotary evaporator and the white precipitate resuspended in the minimum volume (2ml) of 1:1 (v/v) formic acid:methanol and 50mM ammonium acetate.

2.9. Circular Dichroism

Samples of 20-40μl of final concentrated and detergent exchanged protein were diluted in 3mls of glass-distilled water. All samples were scanned at 4 °C. The absorption spectra of each sample were recorded before and after accumulation of the CD spectra to ensure that no denaturation had occurred during the measurements. A JASCO J/600 Spectropolarimeter was used to measure the absorbance of circularly polarised light in the ultra violet (190–260nm) and infrared (400–950nm) regions (SERC facility, University of Stirling). For measurements in the ultra violet region, a scan speed of 10nm/min was used, with pathlengths of 0.02 and 0.05cm (pathlength determined by the concentration of protein). The infrared measurements were made using a pathlength of 1cm and a scan speed of 20nm/min. Molar ellipticities (deg.cm^2.dmol^{-1}) were calculated using the relationship;

$$ellipticity(molar) = \frac{Mw.\Theta}{100.L}$$

Mw–average molecular weight of 110, L–pathlength,

Θ–observed ellipticity.

Secondary structure estimations were carried out via the absorbance in the ultra violet region using the fitting procedure of Provencher and Glöckner (1981), based on 11 polypeptides of known secondary structures.

2.10. Extraction of the Photosynthetic Pigments

A 7:2 (v/v) acetone:methanol solution was used to extract both the bacteriochlorophyll and carotenoid pigments from the B800–820 peripheral antenna complex. The pigments were extracted in 5mls of solvent in the dark, and centrifuged at 3000rpm in a bench centrifuge for 5 min. This pelleted the protein leaving the free pigments in the solvent. The absorption coefficient for bacteriochlorophyll *a* in an acetone/methanol pigment extract is $76mM^{-1}cm^{-1}$ at 772nm (Clayton, 1966). An average absorption coefficient for the total carotenoid of $134mM^{-1}cm^{-1}$ was used in the determination of pigment ratios (Evans, 1989). The electronic absorption spectra were recorded in the wavelength range 400-900nm (Shimadzu UVPC2101).

2.11. Tricine-Sodium Dodecyl Sulfate-Polyacrylamide Gel Electrophoresis

2.11.(i). Gel Preparation

A discontinous sodium dodecyl sulfate-polyacrylamide gel electrophoresis (SDS-PAGE) system was used to resolve low molecular weight proteins between 5 and 20kDa (Schägger and Von Jagow, 1987). This was performed using a notched plate 'Studier'-type apparatus (Studier, 1973).

Chemicals. SDS and Tricine(Sigma), acrylamide and bisacrylamide (specially purified for gel electrophoresis), glycerol AR and ammonium persulphate GPR (BDH). TEMED (N, N, N', N'- tetramethylethylenediamine) was purchased from Aldrich and Tris-HCl from Boehringer-Mannheim.
The compositions of stock solutions and electrolyte prepared for tricine- gel electrophoresis are given in **Appendix C**. The compositions of the acrylamide mixtures and of all gels are defined by the letters T and C (Hjerten, 1962). T denotes the total percentage concentration of both monomers

(acrylamide and bisacrylamide). C denotes the percentage of crosslinker relative to the total concentation T. All solutions were kept at room temperature with the exception of the acrylamide:bisacrylamide mixtures which were stored at 4°C.

A gel-former kit consisting of two thick glass plates (one notched), two nylon 'spacers', two plastic screw-clamps and a plastic sealing stand(Biorad), was used.

A nylon 'spacer' was placed along either side of the un-notched plate. The notched plate was positioned on top and the two plates fixed together using the two screw-clamps. This assembly was clamped into the sealing stand. Ammonium persulphate was added to the separating gel(16.5%T, 6%C), which was then degassed under vaccuum. TEMED, the second polymerisation catalyst was added and the separating gel was poured continously to a height of 10cm.

The separating gel was overlayed with 50% H_2O:50% Methanol solution and left to polymerise for 30min. The 50% H_2O:50% Methanol solution was removed and the degassed spacer gel(10%T, 3%C) containing the polymerisation catalysts was poured to a height of 4cm. This was again left to polymerise for 30min before the stacking gel(4%T, 3%C) was added. The well-forming comb was inserted between the gel plates and the stacking gel allowed to polymerise.

2.11. (ii) Sample Preparation and Application

The gel and screw-clamps were then attached into the 'Studier' apparatus (Biorad, Protean II). The upper and lower reservoirs were then filled with electrolyte (**Appendix C**). A kit of low molecular weight markers with molecular weights in the range 2.5-17kDa (**Appendix D**) were used

as standard proteins (Sigma). Protein concentrations of antenna complexes were previously determined using tannin and modified Lowry protein assays (see (**2.13** & **2.14.**) An equal volume of boiling solution (**Appendix C**) was added to the sample in an Eppendorf vial and heated for 5min in a boiling waterbath. The correct volume of the solubilised protein solution was added to each well with a Hamilton microliter syringe, giving protein loadings of 10-15μg.

2.11. (iii) Electrophoresis

The electrophoresis was performed at room temperature, with a tank enabling the passage of cold water placed behind the gel. This prevented any local heating effects in the gel. A constant current of 20mA was applied until the the marker dye was within 1cm of the aniodic end of the gel (18hrs).

2.11. (iv) Staining/Destaining

The apparatus was disassembled and the gel was stained for 3hrs with Brilliant Blue R stain (Aldrich). The gel was then transferred to destaining solution for 1-2 days (**Appendix C**).

2.12. SDS Polyacrylamide Gel Electrophoresis

2.12. (i) Gel Preparation

Polyacrylamide gel electrophoresis was performed using a notched plate 'Studier'-type apparatus (Studier, 1973) and a discontinous buffer system (Laemmli, 1970). Different concentrations of polyacrylamide were used to determine the intact molecular weight of the B800–820 peripheral antenna complex(13.5-18.0% T, 2.5%C).

Chemicals. SDS (Sigma), acrylamide and bisacrylamide (specially purified for gel electrophoresis), glycine, glycerol AR and ammonium persulphate GPR (BDH). TEMED (N, N, N', N'- tetramethylethylenediamine) was purchased from Aldrich and Tris-HCl from Boehringer-Mannheim.

The compositions of stock solutions and electrolyte buffer prepared for SDS polyacrylamide gel electrophoresis are given in **Appendix E.** All solutions were kept at room temperature with the exception of the acrylamide:bisacrylamide mixtures which were stored at 4°C.

Gel plates were cleaned and assembled as described in **2.11 (i)**. Ammonium persulphate was added to the acrylamide(13.5-18.0%T, 2.5%C), which was then degassed. TEMED, the second polymerisation catalyst was added and the gel was poured between the plates to a height of 13cm. This was covered with a layer of 50% H_2O:50% Methanol solution and left to polymerise. After polymerisation, the 50% H_2O:50% Methanol solution was removed and the stacking gel (4.5%T, 3.0%C) layered on top to a height of 3cm. The well-forming comb was inserted between the gel plates and the stacking gel allowed to polymerise.

2.12. (ii) Sample Preparation

A standard protein solution containing 5mg/ml horse heart cytochrome c (11.7 kDa), horse heart myoglobin (16.95kDa), horse liver alcohol dehyrogenase (41kDa), and bovine serum albumin (68kDa) were prepared to run as molecular weight markers alongside the sample proteins. An equal volume of boiling solution was mixed with the sample in an eppendorf vial.

Sample application, Gel electrophoresis and gel staining/destaining were performed as described in **2.11 (ii), (iii), (iv).**

2.13. Tannin Protein Assay

Following the addition of tannin reagent (**Appendix F**) to a protein solution, turbidity appears as a result of formation of tannic acid-protein complexes (Mejbaum-Katzenellenbogen and Drobryszycka, 1959). With 10-100μg protein in solution, the relationship between absorbance at 500nm and the amount of protein is linear.

A series of dilutions of standard protein (bovine serum albumin, Sigma) of known concentration was prepared in 20mM Tris-HCl buffer, pH8.0. 1ml volumes were equilibrated at 30°C using a thermostatically controlled waterbath, for 30min. 1ml volumes of tannin reagent were added and incubated for 10min. Stabilisation of the reaction was achieved using gum acacia (0.2% w/v) and a calibration curve of absorbance at 500nm versus μg protein constructed. The assay was repeated using the protein samples of unknown concentration. The concentration of the protein stock solution was estimated from absorbance measurements at 500nm and interpolation of the calibration curve.

2.14. Modified Lowry Protein Assay

The Lowry assay is a measure of the colour change of an alkaline copper reagent following the addition of a protein sample solution. The application of the Lowry procedure (Lowry *et al.*, 1951) to samples containing membranes can require extensive pretreatment of the sample for solubilisation before analysis. A modified procedure containing sodium dodecyl sulphate in the alkali reagent and an increase in the amount of copper tartrate reagent was used (Markwell *et al.*, 1987).

1ml of solution B was added to 100ml of solution A, to give the alkaline copper sulphate solution C (see **Appendix F** for an explanation of solutions A, B & C). A volume of 3ml of solution C was added to 1ml volumes of standard protein. After 15min at room temperature, 0.3ml of solution was added and left for 30min. A calibration curve was constructed of absorbance at 660nm versus μg of protein. The assay was repeated for samples of unknown concentration and the concentration of the protein stock solution was estimated from the absorbance at 660nm and interpolation of the calibration curve.

2.15. Electrospray Mass Spectrometry

Samples of 20μl of both final concentrated, detergent-exchanged protein and isolated α/β apoproteins were added to 20μl volumes of the carrier solvent (50:50:1 (v/v) solution of methanol/water/acetic acid). A VG BioQ mass spectrometer with a quadrupole mass detector was used to identify the molecular weights of protein species which were present (SERC facility, University of Cambridge). The mass spectrometer was calibrated using myoglobin (Sigma) and the protein sample in the carrier solvent infused into the hollow electrospray needle (**Figure 2.2**) at a flow rate of 4μl/min.

The mass spectrometer was repetitively scanned at a rate of 3sec/scan and profile data accumulated over 10 scans. The resulting m/z versus % relative abundance profile data was directly converted into mass versus % relative abundance profile using a deconvolution procedure which followed the algorithmns of Mann *et al.* (1989).

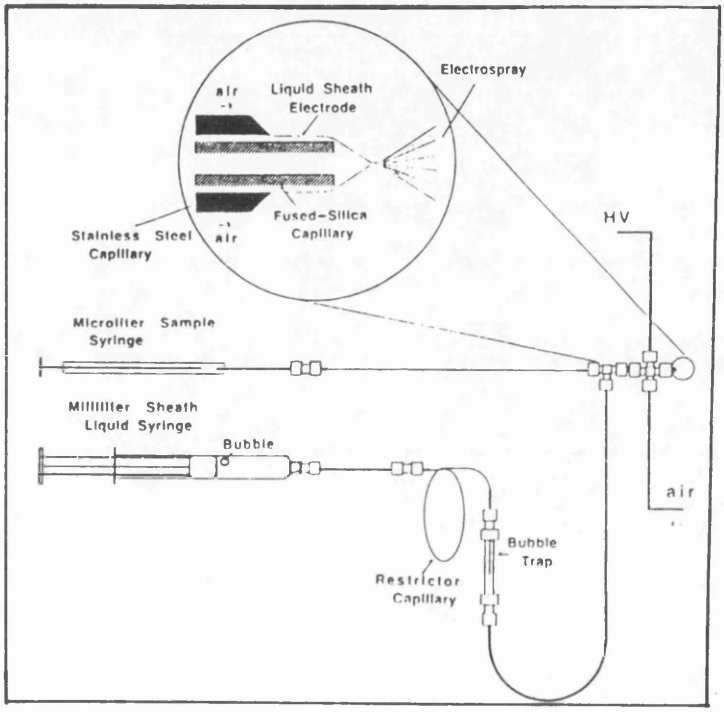

Figure 2.2. Schematic Diagram of the Sheath Flow Interface for Electrospray Mass Ionisation Mass Spectrometry showing the Arrangement for Direct Infusion of Analyte Solutions (From Edmonds and Smith, 1990).

2.16. Crystallisation of the B800–820 Peripheral Antenna Complex from *Rhodopseudomonas acidophila*

2.16.(i) Sample Preparation

The B800–820 complex from cells of *Rhodopseudomonas acidophila* strain 7750 was isolated and purified as detailed in sections **2.1** – **2.7.** The com-

plex was exchanged from LDAO into the detergent used for crystallisation. The absorption spectra of samples eluted from the column were recorded as were the purity indices. Samples with a purity index of 0.9-3.0 were used for crystallisation trials.

2.16. (ii) Crystallisation using the Method of Hanging Drop to achieve Vapour Phase Equilibration

This method of crystallisation relied upon the addition of a small amphiphilic molecule (Michel *et al.*, 1980, Garavito *et al.*, 1980). Protein crystallisation was performed using the vapour diffusion method (MacPherson, 1982). Disposable plastic culture plates (Corning) with 24 wells (16mm diameter), with a flat ground rim that permited airtight sealing by the application of silicon grease around the circumference were used. Microscope coverslides (18mm diameter) were siliconised using dimethylchlorosilane solution (Fisons). 1ml of inorganic salt solutions (5-50% concentration) at pH 9.0 and 9.5 were added to the well. A microdroplet of 3μl containing protein with 1% octyl glucoside in 20mM Tris-HCl buffer and the small amphiphile benzamidine hydrochloride at 5% (w/v), was added to 3μl of the well solution or to 3μl of 2M di-potassium hydrogen orthophosphate in Tris-HCl buffer. This 6μl droplet was suspended from the underside of a microscope coverslide(18mm diameter), which was placed over the well. Protein concentrations were in the range 4-8mg/ml with purity indexes of 0.9-3.0. These plates were incubated at temperatures of 6, 10, 15 and 20°C. All trials were conducted in duplicate and monitored at weekly intervals until either crystal growth or protein denaturation occurred.

2.16. (iii) Crystallisation using the Method of Sitting Drop to achieve Vapour Phase Equilibration

Two types of sitting drop apparatus were used: disposable plastic trays (Cryschem) and Petri dishes with a raised bridge containing a 20μl or 50μl depression. Protein crystallisation was performed using the vapour diffusion method (MacPherson, 1982).

A. Crystallisation using Cryschem Trays

Disposable plastic trays with 24 reservoirs (16mm diameter) each of 1ml volume were used. Each reservoir contained a raised bridge with a 20μl depression. Different inorganic salt solutions(1.8-3.0M) at pH in the range 8.5–10.0, were added to each reservoir. 450μl of protein sample was dispensed into a 1ml Eppendorf vial, containing the small amphiphile. 150μl of 4M di-potassium hydrogen orthophosphate was added. This gave a final concentration of 1M di-potassium hydrogen orthophosphate and amphiphile in the range 2.0-3.0% (v/v). The sample was mixed until the amphiphile dissolved. The pH of the protein preparation was then adjusted to pHs in the range 8.5-10.0 using a small volume of 1M sodium hydroxide. The protein preparation was then centrifuged at 13000rpm for 10min to pellet any denatured, unsolubilised material. 20μl of this solution was then dispensed into each depression. These reservoirs were then individually sealed using microscope coverslides (18mm) or by drawing clear sealing tape over the top of the plastic tray. All trials were conducted in duplicate over a range of temperatures: 6, 10, 15 and 20°C. The protein concentrations used were in the range 4–8mg/ml, with purity indexes of 0.9–3.0. All trials were conducted in duplicate and monitored at weekly intervals until either crystal growth or protein denaturation occured.

B. Crystallisation using Petri Dishes

A 20μl or a 50μl depression bridge was attached using acetone to a plastic Petri dish. 8ml of different inorganic salt solutions(1.8–3.0M) in the pH range 8.5–10.0 were added to each reservoir. The protein sample was dispensed into a 1ml Eppendorf vial, containing the small amphiphile and 4M di-potassium hydrogen orthophosphate was added. This procedure was used to give crystallisation trials with concentrations of di-potassium hydrogen orthophosphate in the range 0.8–1.2M and 2.5–3.0% (v/v) of small amphiphile. The sample was mixed until the amphiphile dissolved. The protein preparation was then adjusted to the required pH using a small volume of 1M sodium hydroxide. The protein preparation was then centrifuged at 13000rpm for 10min to pellet any denatured, unsolubilised material. 20μl or 50μl of mother liquor was then dispensed into each depression and the lid air-sealed using plastic tape. All trials were conducted in duplicate over a range of temperatures: 6, 10, 15 and 20°C. The protein concentrations used were in the range 4–8mg/ml, with purity indexes of 0.9–3.0. All trials were conducted in duplicate and monitored at weekly intervals until either crystal growth or protein denaturation occured.

2.17. Density Measurement using Aqueous Ficoll Solutions

A 60% (w/w) Ficoll solution (Sigma) was made by adding 75g of Ficoll to 50ml of distilled, deionised water at 50°C with gentle stirring by hand. The lumpy, white, viscous suspension was covered, kept warm (37°C) and allowed to stand overnight to yield a clear, slightly yellow solution, with a density of approximately 1.28g/ml (Westbrook, 1985). A 30% (w/w)

Ficoll solution, with a density of approximately 1.1g/ml, was made by mixing equal volumes of water and 60% Ficoll solution. Density gradients were formed in 27ml polycarbonate centrifuge tubes (Dupont), using a peristaltic pump. Calibration droplets were aliquots of solutions made by mixing carbon tetrachloride (density 1.594g/ml) and toluene (density 0.8669g/ml) in ratios necessary to give the desired densities. The density gradients were then calibrated using 5μl droplets of these mixtures of organic solvents. Single crystals were introduced into the gradients by capillary, and care was taken to transfer the minimum mother liquor volume. Equilibrium of the gradients was then reached via centrifugation at 10,000 rpm for 30min. The positions of the crystals and calibration droplets were then measured with a metric ruler to the nearest 0.5mm.

2.18. X-Ray Analysis of the B800–820 Peripheral Light-Harvesting Antenna Complex

2.18 (i) The Siemens Area Detector

A Siemens Area Detector mounted on a rotating anode source (5.4kW, 0.3mm focus, Cu $K\ \alpha$=1.54Å), with a Siemens P3 four circle goniometer (**Figure 2.3**) was used to collect X-ray diffraction data. The system was controlled by a frame buffer processor (networked as a VAXstation peripheral), using the *FRAMBO* (Frame Buffer Operation) program. The area detector was mounted on a sliding dovetail track permitting adjustment of the crystal to detector distance. The output signals of the detector were decoded by the Position Decoding Circuit (PDC) to create a digital position of each x-ray event measured by the detector. The frame buffer recieved data from the PDC and converted it into frame information. Each frame stored by the frame buffer comprised of all the X-ray events measured by the

detector for a designated time period. Data frames were then transferred to the second VAXstation via an Ethernet link. The program *SANTA* (SAXII Area- Detector Network Transfer Agent), accepted the frames generated by *FRAMBO* at the frame buffer.

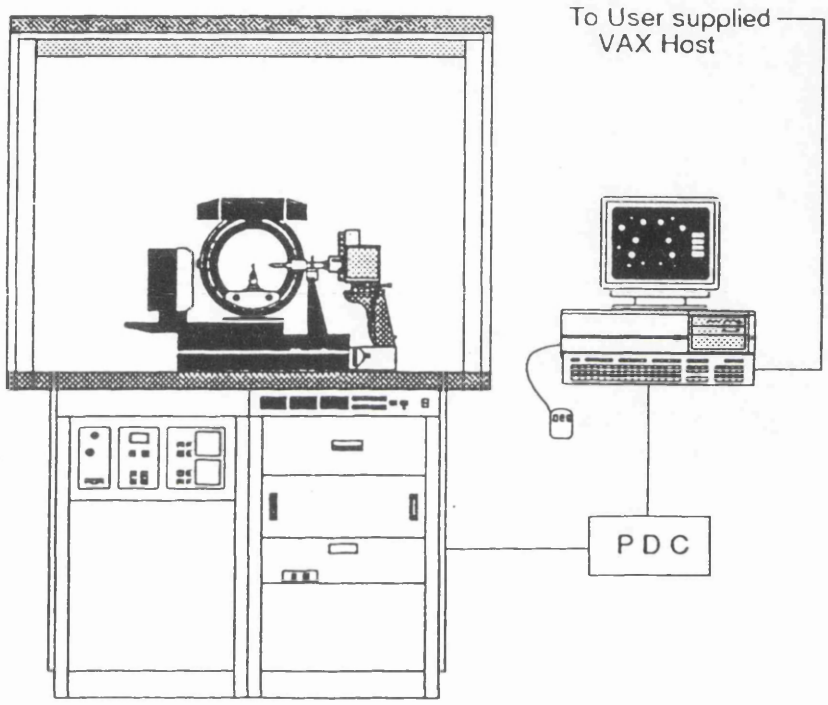

Figure 2.3. A Diagram of the Area Detector Set-up

2.18. (ii) Initial Set-up of the Area Detector for Data Collection

The area detector was adjusted to the desired detector to crystal distance for data collection. A radioactive Fe55 source was used to collect a flood-field image, to be used for the background radiation correction. A machined fiducial brassplate with drilled holes at known positions was placed over the detector face and exposed to the Fe55 source. The centre of the X-ray beam with respect to the detector face was determined. The data frame from the brassplate was later used to construct a mapping of detector pixels into actual distances in cm. The set-up parameters for data collection are shown in **Table 2.1.**

Crystal Form	Crystal to Detector distance	Floodfield Collection	Brassplate Collection	Beam centre X, 511-Y
1	15cm	2700sec•	4860sec	255, 244
2	20cm	5400sec•	9900sec	253, 243

• A further 300sec of Fe55 radiation was added to check that the flood-field image was free of lines and distortions

Table 2.1. Set-up parameters prior to data collection

2.18. (iii) Crystal Mounting

Protein crystals were mounted in thin-walled quartz capillaries (1mm diameter, Müller), as described by King (1954) and Holmes and Blow (1966). Excess mother liquor was carefully removed using thin strips of filter paper. A small volume of mother liquor was sealed into the end of the capillary using high vacuum wax and the remaining end also sealed with wax. An alternative mother liquor of di-potassium hydrogen orthophosphate (2M, pH 9.5) was used to compensate for the removal of mother liquor during crystal mounting. All crystals were mounted at 6°C.

2.18. (iv) X-Ray Data Collection

The capillary containing the crystal was attached to the goniometer head and mounted on the 4-circle goniometer. The crystal was then optically centred. A general strategy for data collection has been outlined by Xuong *et al.* (1985). Data were collected by scanning around the ϕ axis (**Figure 2.4**), with χ, 2θ and ω at 0°. An ω scan was employed (2θ=0° and χ=0°) to obtain data in the blind region close to the spindle axis. Data were collected on two forms of tabular plate crystals as shown in **Table 2.2.**

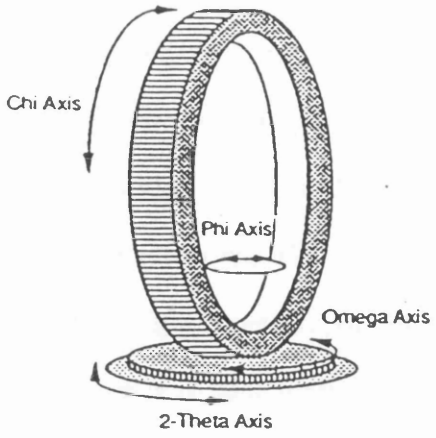

Figure 2.4. The 4-Circle Goniometer, showing the Rotation Axes.

Crystal Form	Run	Scan Type	Frame Width	Number of Frames	Angular Range	Time/Frame	Detector Voltage
1	#1	ϕ	0.3°	1-69*	0-20.40°	300sec	50kV 80mA
	#2	ϕ	0.25°	70-637	19.50-122.25*	300sec	50kV 80mA
	#3	ω	-0.25°	1-40	25.00-17.00°	300sec	50kV 70mA
2	#1	ϕ	0.25°	1-436	0-108.75°	360sec	40kV 70mA

* Crystal slippage at Frame 69

Table 2.2. Summary of collected x-ray diffraction data

2.18. (v) Data Processing

X-ray diffraction data were processed using the software packages *XDS* (Kabsch, 1988) and *XENGEN* (Howard *et al.*, 1987). Both of these packages automatically determine the unknown crystal orientation matrix using a similar auto-indexing procedure (Kabsch, 1988). This procedure uses a list of centroids of 'bright' spots ('bright' meaning one pixel N sigma greater than the background count, where N is user defined). These centroids are then sorted in order of increasing $sin\theta$. A set of difference scattering reciprocal space vectors are then constructed from this centroid list. Low resolution difference vectors are used and the first three vectors which are noncoplanar, (with an angular orientation of greater than 45°), are selected and used as a reference set. The indices to these vectors must be properly assigned if the correct orientation of the unit cell is to be found. Trial *hkl* values for these three vectors are obtained. Each ordered triplet of trial *hkl* vectors constitutes a 3x3 matrix of indices for the reference difference vectors and from it a 3x3 unit cell matrix is obtained . The procedure then compares each unit cell matrix against the entered unit cell parameters to see if any of the lengths and angles fall outside the allowed range. If any given triplet of trial vectors passes the test, the remaining difference vectors are locally indexed with the resulting matrix and checked to see if the resulting indices are integers. The method of least-squares is then used to refine a better estimate of the parameters.

XDS differs from *XENGEN* in the method used for determining the integrated intensities of reflections. *XDS* uses a pixel-labelling procedure as opposed to *XENGEN* which collects pixel counts falling into shoeboxes centred on precalculated spot positions. *XENGEN* divides the detector face into twelve regions and uses model profiles which were generated whilst

compiling the list of centroids of bright spots. The intensity is then computed as the scale factor between this normalised model profile and the observed profile. *XDS* overcomes the difficulty in distinguishing between signal and background points within each reflection, by estimating the reflection intensity using a two-pass integration procedure. This procedure assumes strong and weak reflections have the same normalised profile (Diamond, 1969). The first pass is deemed the 'learning' phase where the reference profiles are learned as a function of the detector and spindle angle. Nine detector positions are used (**Figure 2.5**).

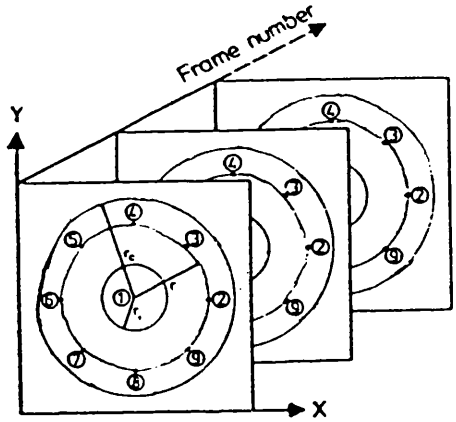

Figure 2.5. Positions of Reference Profiles on the Area Detector Face. The detector positions cover equal positions of the radius r_0 of the detector face. The central position no. 1 covers the circle of radius $r_i = r_0/3$.

A box of 9x9x9 grid points ($\alpha\beta\gamma$) is used for reflection profiles (the step sizes between points derived from the approximate values for beam divergence and crystal mosaic spread, as specified by the user). The strongest reflections in the profile boxes are normalised and added to the nearest reference profile boxes, the contributions weighted according to distance. Each gridpoint within the average profile box is classified as signal if it is 2% above that of the highest outputted peak. In the second pass intensities are estimated for each reflection, using the nearest reference profile. After profile fitting in both these programs the integrated intensities of each reflection are corrected for Lorentz, polarisation, absorption and crystal decay factors to yield the desired structural amplitudes.

Although X-ray diffraction data was processed using both *XENGEN* and *XDS*, *XDS* was more successful in distinguishing between weak signals and background intensity. Consequently this data was used in subsequent calculations (see **Chapter 5**). The CCP4 programs *ROTAVATA* and *AGROVATA* were used to calculate and apply scaling between batches of data.

2.18. (vi) Programs used in Data Processing

The following programs were used as part of the *CCP4* package :

ROTAVATA- was written by J.M Smith and A.J Wonacott . *ROTAVATA* calculates scale factors and/or temperature factors between overlapping batches of data using the method of G.C Fox and K.C Holmes (Fox and Holmes, 1966).

AGROVATA- was written by J.M Smith and A.J Wonacott. It was used to apply scale factors calculated by *ROTAVATA*. This program adds together partially recorded reflections, monitors and rejects bad agreements between repeated measurements or symmetry equivalents and then averages them for output.

FFT- This crystallographic fast Fourier transform (FFT) was written by L.F Ten Eyck (1973) and was used to calculate the Patterson function (Patterson, 1934).

EXTEND- The program *EXTEND* generates any part of a map from a map calculated using *FFT* which typically only contains one asymmetric unit (Evans and Dodson, 1985).

POLARRFN- This is a fast rotation function which works in polar angles (**Figure 2.6.**), written by W. Kabsch. *POLARRFN* was used to search for local symmetry. The program produces sections of constant rotation angle χ for different axis directions defined by ψ and ϕ. The direction cosines of the axis are given by :

$$\sin \omega \cos \phi$$

$$\sin \omega \sin \phi$$

$$\cos \omega$$

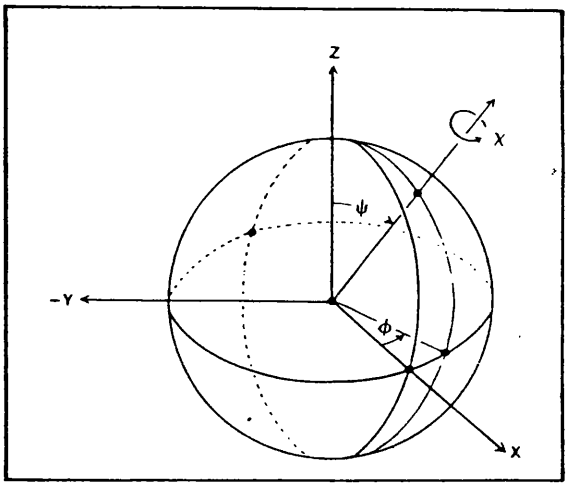

Figure 2.6. Definition of Spherical Polar Angles. The direction of the rotation axis is defined by the angles ψ, measured from the z axis, and by the angle ϕ measured in the x-y plane from the x axis. The rotation itself is given by the spin χ about the axis.

CHAPTER 3. Characterisation of the B800–820 Antenna Complex from *Rhodopseudomonas acidophila* 7750

3.1. Introduction

In purple photosynthetic bacteria the components required for the "light reactions" are localised in and on the intracytoplasmic membranes (Remsen, 1983, Drews, 1985). The pigment-protein complexes which make up the photosynthetic unit (the light-harvesting complexes and photochemical reaction centres) constitute the majority of the proteins in these membranes. Environmental stimuli such as light intensity and/or temperature can alter the photosynthetic unit by determining the amount and type of light-harvesting antenna complex or complexes which is/are produced. Depending on the wild type strain, *Rhodopseudomonas acidophila* can synthesise several different types of light-harvesting antenna complex. It is therefore important to gain a detailed understanding of the differences in both structure and function of these different light-harvesting antenna complexes. A prerequisite for this understanding is a full and comprehensive characterisation using different biochemical methods.

3.2. A Spectral Characterisation of 23°C and 30°C Grown *Rhodopseudomonas acidophila* strain 7750, and their Antenna Complexes

The major light-absorbing pigments of *Rhodopseudomonas acidophila* strain 7750 are bacteriochlorophyll *a* (Pfennig, 1969) and carotenoids of the "normal spirolloxanthin series" (Schmidt, 1971) (see **Table 3.2**), which are non-covalently bound to antenna apoproteins.

The spectral characteristics of the 7750 strain of *Rhodopseudomonas acidophila* were investigated by Cogdell *et al.* (1983a). They reported the isolation of a B800–850 antenna complex from cells grown under high light conditions, in addition to the core B880 complex. Brunisholz *et al.* (1987)

reported that when *Rhodopseudomonas acidophila* strain 7750 is cultured at a temperature of 23°C a B800–820 complex is synthesised. (Gardiner A.T., (1992), Personal Communication) has noted that production of the B800–820 complex is controlled by both low light intensity and low temperature.

Near infrared absorption spectra of 23°C grown cells and 30°C grown cells are compared in **Figure 3.1**. The spectrum of 30°C grown cells indicate the presence of B800–850 antenna and B880 core complexes. When the temperature is lowered to less than 24°C, absorption at 850nm is replaced by absorption at 820nm. On further lowering the temperature to less than 18°C the absorption due to the B800–850 complex reappears as a shoulder at 850nm. This emphasises that production of these antenna complexes, in response to different environmental stimuli is very much a dynamic process, with constant optimisation of the cells light-harvesting ability.

Membranes of *Rhodopseudomonas acidophila* strain 7750 cells grown at 23°C were prepared (see **Section 2.3**) (**Figure 3.2.(i)**). B880 and B800–820 complexes were isolated by DEAE-cellulose anion exchange chromatography and the B800–820 complex further purified by gel filtration. The B800–820 complex containing B880 core complex is eluted first from the anion exchange column. This mixture of complexes has a red/brown colour. When the B800–820 antenna complex is free of core complex it is deep red in colour.This is eluted next after addition of 150mM sodium chloride with 0.1% LDAO in 20mM Tris-HCl, pH 8.0. As the elution volume increases there is also a gradual decrease in the purity index of the complex. As mentioned in **Section 2.5** only fractions with a purity index of 2 or greater were retained for further purification. An absorption spectrum of the isolated B800–820 antenna complex is shown in **Figure 3.2.(ii)**. An elution

profile from the anion exchange column is shown in **Figure 3.3**.

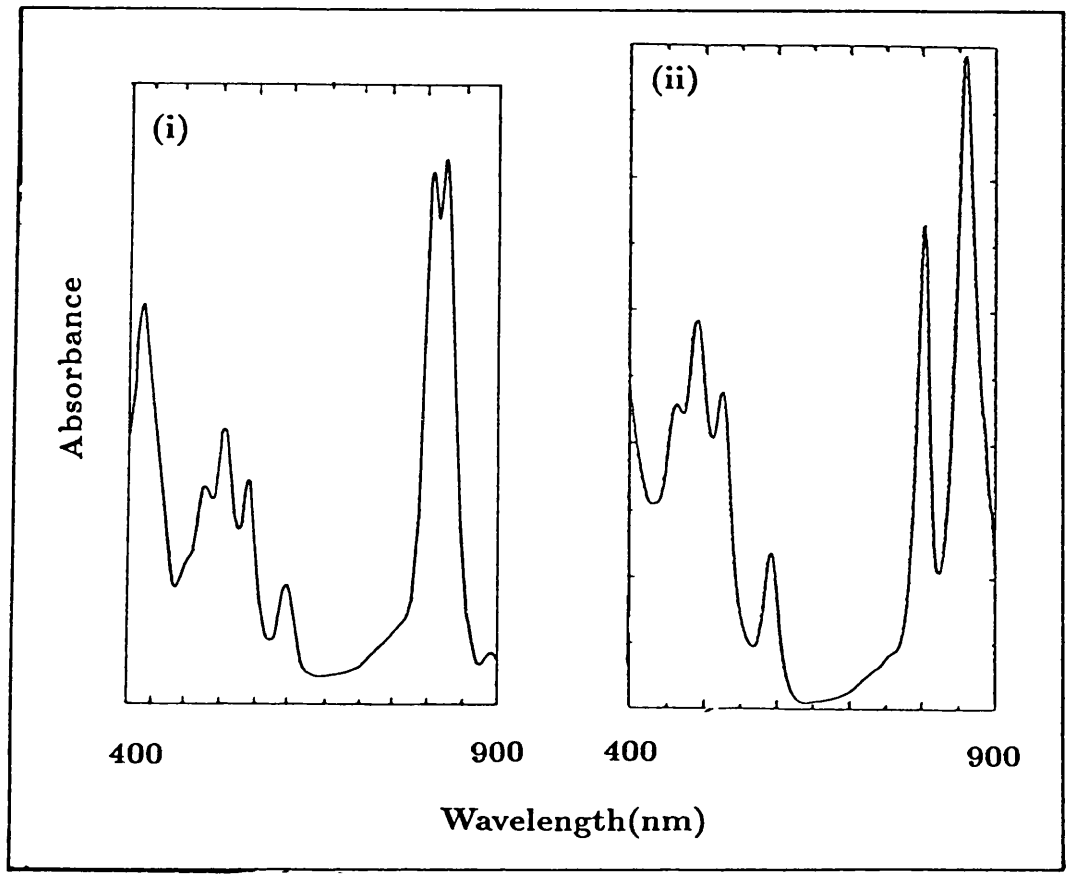

Figure 3.1. A Comparison of the Absorption Spectra of Cells from *Rps. acidophila* strain 7750: (i) grown at 23°C and (ii) grown at 30°C.

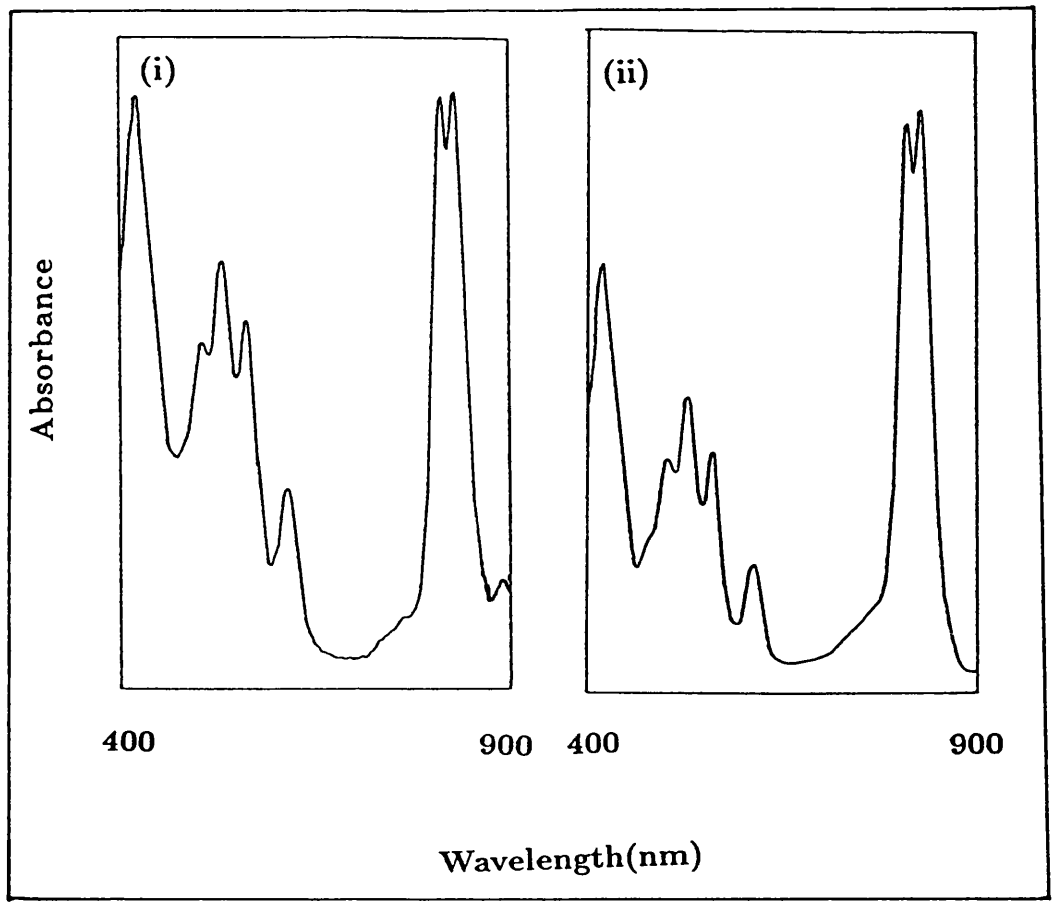

Figure 3.2. Absorption Spectra of: (i) Photosynthetic Membranes from *Rps. acidophila*, strain 7750, grown at 23°C and, (ii) their Isolated B800–820 Antenna Complexes.

Two points can be emphasised from the fractionation of these membranes. Firstly the near infrared absorption of the whole cells can be adequately accounted for in terms of the absorption spectra of the isolated complexes, and secondly the isolated B800-820 antenna complex retains its integrity during isolation and purification. Monomeric bacteriochlorophyll *a* in organic solvents absorbs maximally in the near infrared at approximately 772nm (Clayton, 1963), but in the B800–820 antenna complex its near infrared absorption bands are strongly red shifted. This red shift is

fully reversed if the antenna complexes are denatured (**Figure 3.4**). The position of the near infrared absorption bands is therefore a good indication of the correct pigment-protein interactions. The near infrared absorption maxima of the isolated complex is the same as that seen in the whole cells from which they were derived and thus it is clear that the isolated complex has retained its native structure.

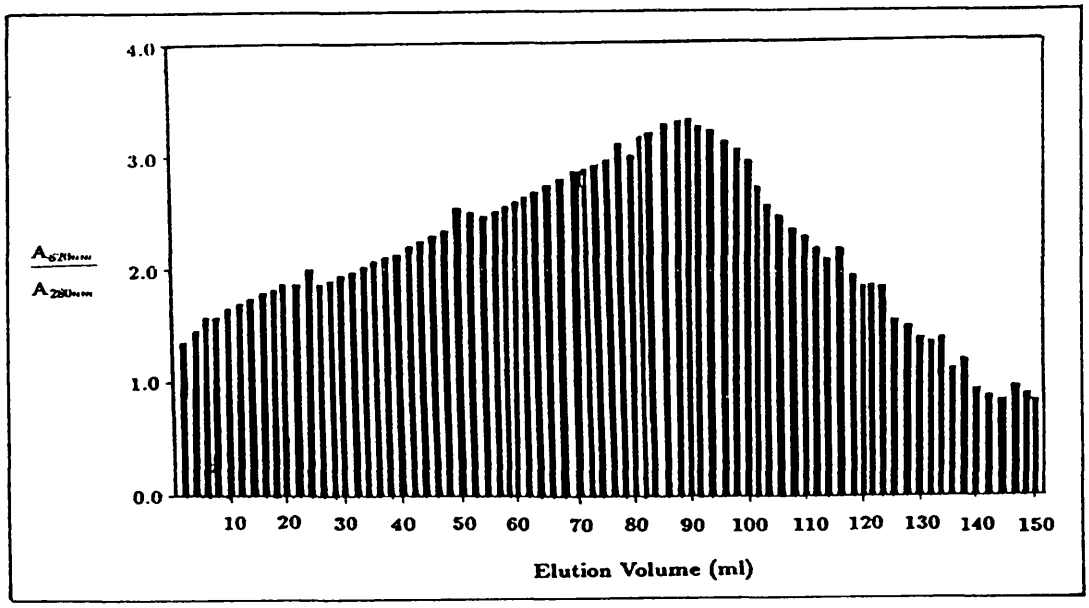

Figure 3.3 Elution Profile from the First DEAE Anion Exchange Column (Purity Index vs. Elution volume).

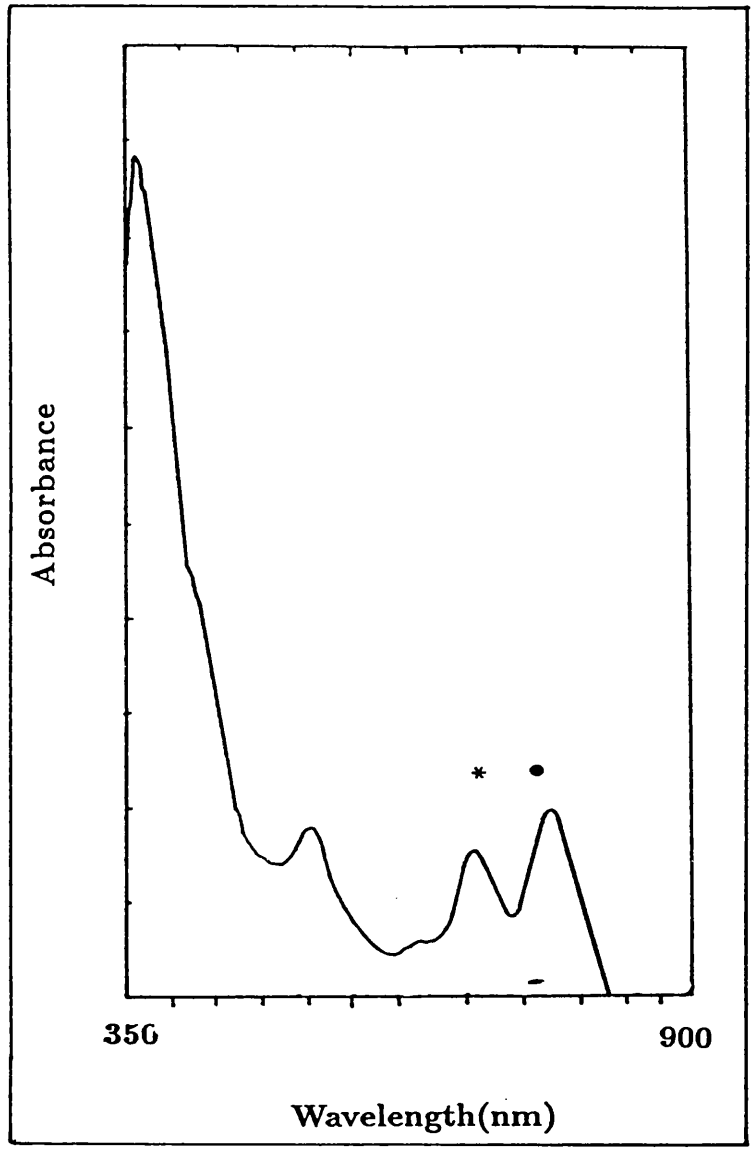

Figure 3.4 Absorption Spectrum of the Denatured Antenna Complex with free bacteriochlorophyll *a* removed from the apoproteins (772nm)•, which has partially oxidised (680nm)*.

3.3. Yield of the B800–820 Antenna Complex during Purification

A study of the yield of the antenna complex obtained during each stage of isolation and purification (**2.2–2.7**) was undertaken. The detergent used in the final exchange step was 1% β octyl-glucoside. The yield of antenna complex recovered at each stage was measured by calculating the OD_V.

$$OD_V = \frac{Absorbance_{820nm}}{\text{Volume(ml)}}$$

The results are taken from 5 different 10 litre cultures of cells each grown at 23°C for 5 days. The absorption at 820nm and the volume obtained, detailed in (**Table 3.1**), are average values taken from each preparation. The OD_V increases as the purity of the complex increases (**Figure 3.5**).

	Purification Stage	Abs_{820nm}	Volume(ml)	OD_V
☑	Harvested Cells	50.80	118	0.43
☐	Solubilised Membranes	52.10	82	0.63
☐	DEAE(1) Chromatography	22.97	100	0.23
☑	DEAE(2) Chromatography	85.30	15	5.69
☐	Gel Filtration	66.50	15	4.43
☐	Concentration/ Detergent exchange	81.00	8	10.13

Table 3.1. Yield of the Antenna Complex. These values are averages of both the absorbance and volume taken at each stage of purification of 5 different 10 litre cultures of cells.

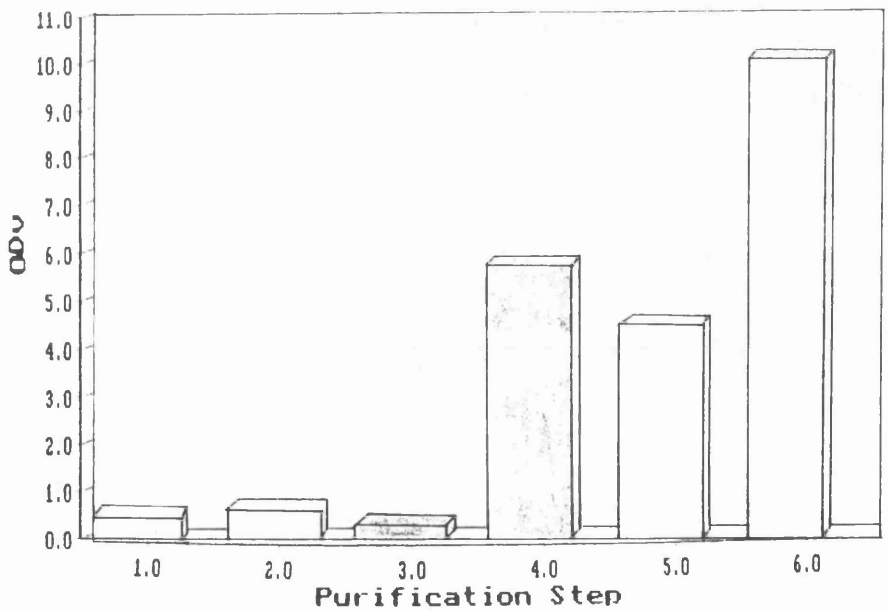

Figure 3.5. Bar Graph of OD_v at each Stage of Purification. This illustrates the changes in OD_V from initially harvesting *Rps. acidophila* strain 7750 to finally obtaining pure, detergent-exchanged B800–820 antenna complex.

3.4. Determination of the Bacteriochlorophyll *a*: Carotenoid Photosynthetic Pigment Ratio

The bacteriochlorophyll *a*: carotenoid ratio of the concentrated and detergent-exchanged B800–820 antenna complex was determined to complement studies on the polypeptide compositions presented in a later section of this chapter. The absorption spectrum of total pigment extracts of the B800–820 complex is shown in **Figure 3.6**. The concentration of bacteriochlorophyll *a* in an acetone/methanol pigment extract can be determined using the absorption coefficient of $76 mM^{-1}cm^{-1}$, at 772nm (Clayton, 1966). The carotenoids from the B800–820 antenna complex from the 7750 strain of *Rhodopseudomonas acidophila* have already been identified (Evans, 1989).

% rhodopin	65.4
% lycopene	30.2
% rhodopin glucoside	3.1
% anhydrorhodovibrin	≤ 1
% spirilloxanthin	≤ 1

Table 3.2. Carotenoid Composition of the B800–820 Antenna Complex from *Rhdopseudomonas acidophila* strain 7750 (Evans, 1989).

Evans (1989) reported an average absorption coefficient for the total carotenoid of the B800–820 complex to be $134 mM^{-1}cm^{-1}$. This value was used to calculate the concentration of carotenoid present. The ratios determined for the antenna complex preparations are shown in **Table 3.3**. These

ratios give an arithmetic mean of 1.91 and a sample standard deviation of 0.169. This data gives a bacteriochlorophyll *a*: carotenoid ratio of 2:1 and corroborates the result obtained by Evans using the simultaneous equation method.

1.72	1.73	1.74	1.75
1.77	1.78	1.79	1.83
1.83	1.84	1.85	1.85
1.87	1.88	1.89	1.89
1.90	1.90	1.90	1.91
1.91	1.91	1.94	1.99
2.11	2.29	2.31	2.38

Table 3.3. Ratios of Bacteriochlorophyll: Carotenoid for 24 Different Samples of Concentrated and Detergent-Exchanged (β-octyl glucoside) B800–820 Antenna Complex. These results give an arithmetic mean of 1.91, with a sample standard deviation of 0.169.

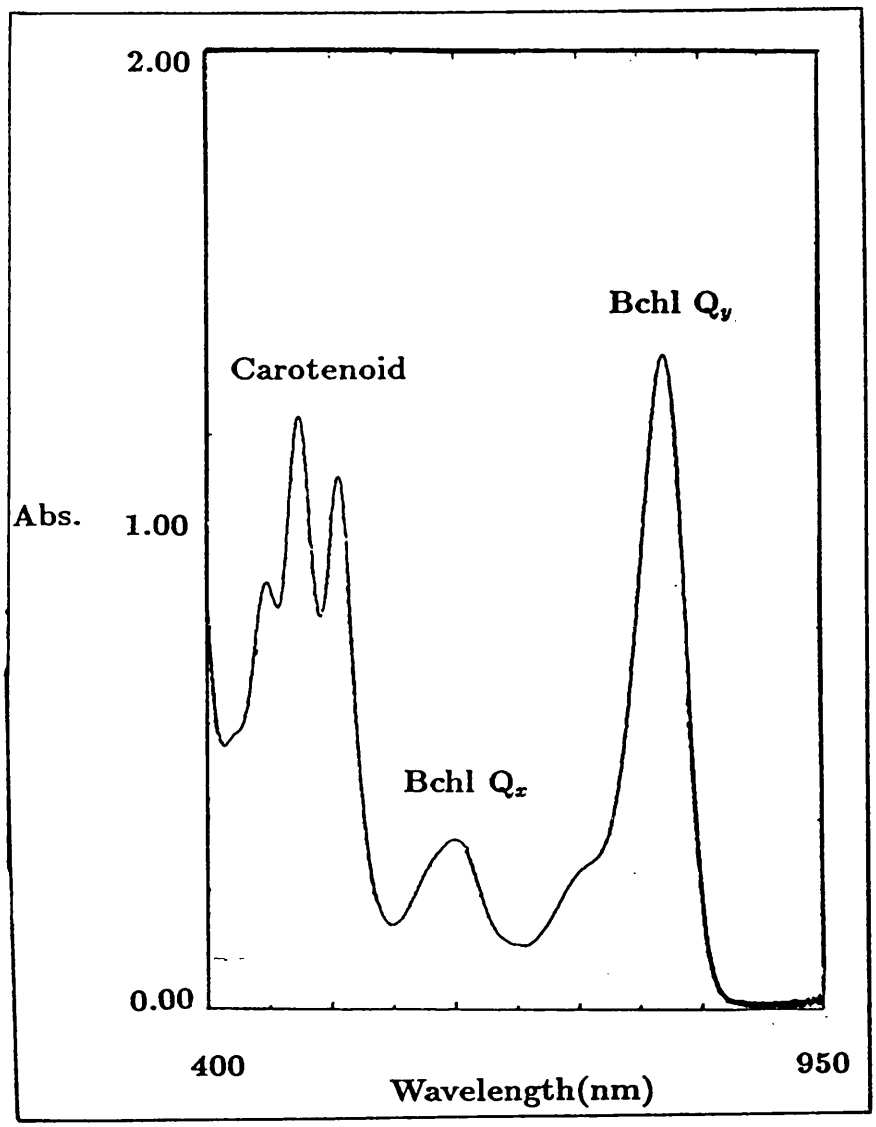

Figure 3.6. Absorption spectrum of total pigment extract of the B800–820 complex from *Rhodopseudomonas acidophila* strain 7750

3.5. Circular Dichroism Studies

A molecule is optically active if it interacts differently with left- and right-handed circularly polarised light. The differential absorption of each beam is known as circular dichroism (CD). Very few chromophores are intrinsically optically active; those that are active include peptide and disulphide cystine bonds. Most optical activity of chromophores is induced by interactions with asymmetrically placed neighbouring groups.

Although CD spectroscopy has been recognised for its utility and simplicity for conformational studies, interpretation of the spectra is not trivial. The CD spectrum of each secondary conformation may be obtained on the basis of the CD spectrum either obtained from model polypeptides (Greenfield *et al.*, 1969) or extracted from a set of spectra of proteins whose X-ray structural data are available. In one approach, the references are the pure component spectra extracted from a set of CD spectra of proteins (fixed reference method) (Saxena *et al.*, 1971, Bolotina *et al.*, 1981). In the other approach a set of the CD spectra of proteins are used as references (variable reference methods) (Provencher *et al.*, 1981). On the basis of the results of these investigations, the CD spectrum of the α helix consists of a positive peak around 190 to 195nm (π-π^* transition) and two negative peaks at 208 (π-π^* transition) and 222nm (n-π^* transition) (Greenfield *et al.*, 1969). The CD spectrum of β sheet has the π-π^* transition around 195 to 200nm and the n-π^* at about 215 to 220nm (Greenfield *et al.*, 1969), while the spectra correlated with the "random" conformation has a large negative band around 200nm and a small positive peak or a shoulder with a small negative value at 220nm (Greenfield *et al.*, 1969). The most recent development in the deconvolution of circular dichroism spectra has been in the use of a Convex Constraint Analysis algorithm (Perczel *et al.*, 1991). This has been

used in the analysis of several membrane proteins, differentiating between the estimated amount of transmembrane and peripheral helices (Park *et al.*, 1992).

Measurements were carried out in the ultraviolet (190–260nm) and infrared (400–950nm) regions, allowing investigation of both the polypeptide conformation and the structural arrangement of the chromophores in each different detergent-exchanged B800–820 antenna complex.

The spectra of the ultraviolet region (190–260nm) is shown in **Figure 3.7**. The dominating feature of the spectra is that of α helix with a positive peak at 190-195nm and negative peaks at 208 and 222nm. These spectra are similar in shape to those obtained for the B800–850 antenna complex from *Rhodobacter sphaeroides* (Breton *et al.*, 1984) and also the B800-850 antenna complex from the 10050 strain of *Rhodopseudomonas acidophila* (Park *et al.*, 1992).

The relative amounts of α helix, β sheet and random structure were estimated using the procedure of Provencher & Glöckner (1981), with fitting based on eleven polypeptides of known secondary structure. The results of these secondary structure estimations are shown in **Table 3.4**. The estimated amount of α helix in each different detergent exchanged sample of antenna complex was 40-56%. The results agree well with those recorded by Breton *et al.* (1984) for the B800–850 antenna complex from *Rhodobacter sphaeroides* (46% α helix, 12% β sheet and 42% "others"), but are slightly lower than those reported for the B800–850 complex from *Rhodopseudomonas acidophila* strain 10050 by Park *et al.* (1992) using the Convex Constraint Analysis Method (65% α helix). However they still corroborate secondary structure predictions of a central α-helical stretch of 20-23 amino acid residues spanning the membrane based on primary struc-

ture data (Bissig, 1990).

There are several factors whose contributions can only be estimated semi-quantitatively. The basis set used in the fitting procedure of the CD spectrum does not include any membrane proteins, as there are still not enough structural data on membrane proteins. A second uncertainty concerns the relative magnitudes of the CD bands related to the chromophores and those of the peptides in the far UV region. Cogdell *et al.* (1985) reported that the contribution of the chromophores to the CD spectrum below 230nm was relatively minor.

Despite these limitations which restrict its exactness, this analysis clearly demonstrates that exchanging the antenna complex into different detergents had little effect on the conformation of its polypeptides.

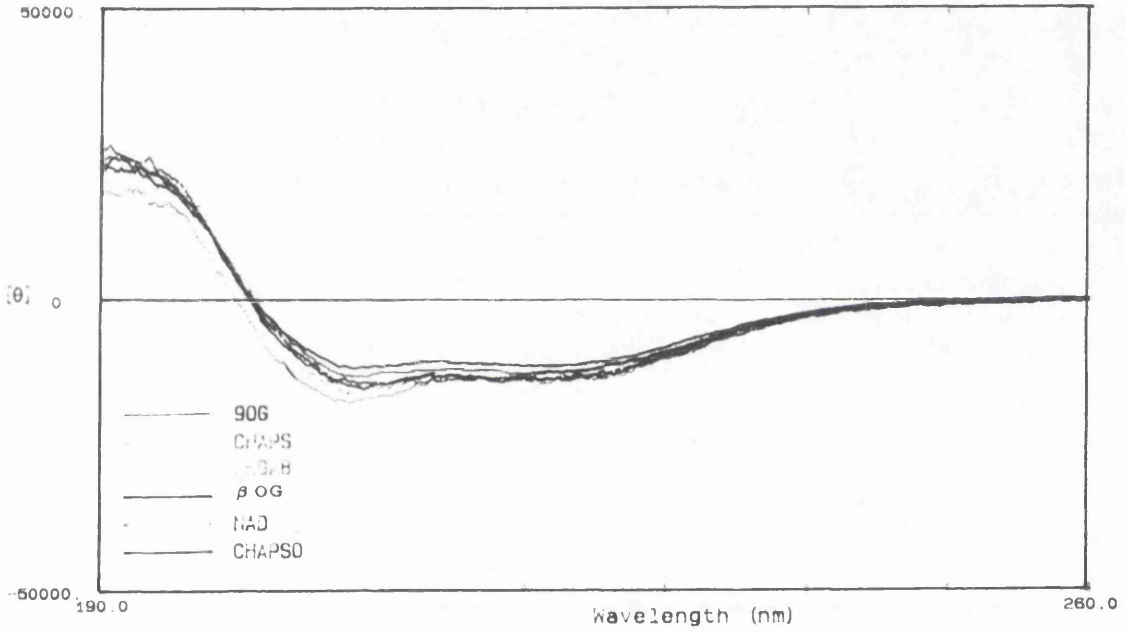

Figure 3.7. Ultra Violet CD Spectra of the B800–820 Antenna complex Exchanged into Different Detergents (Wavelength Scan Range 190–260nm), (See **Section 4.2.** for Abbreviations of Detergents).

Detergent	α-helix	β-sheet	remainder
Nonyl Glucoside	49±1.20%	6±1.40%	44±2.30%
CHAPS	45±0.97%	24±1.10%	31±1.80%
MEGA8	53±0.74%	9±1.10%	38±1.30%
β Octyl Glucoside	56±1.20%	0±1.80%	44±2.20%
NDA	40±0.94%	24±1.10%	36±1.80%
CHAPSO	41±1.40%	4±1.6%	55±2.60%

Table 3.4. Estimated secondary structure of the B800–820 Antenna Complex after Exchange into Different Detergents (Calculated using the method of Provencher *et al.*, 1981). (See **Section 4.2.** for Abbreviations of Detergents).

The CD spectra of the wavelength range 400-950nm are presented in **Figure 3.8.** By comparison with the absorption spectrum of the antenna complex, bands in the near infrared can be seen which are attributable to bacteriochlorophyll *a*. Bacteriochlorophylls are themselves asymmetrical, but the CD spectra of the antenna complex differs from that of bacteriochlorophyll *a* in organic solvent (Sauer *et al.*, 1978). The reasons for this change in the CD spectra must be due to either the environment in which the bacteriochlorophyll *a* is situated or interactions between bacteriochlorophylls or a combination of both factors. The CD spectra of the B800–820 antenna complex in the near infrared region (at 820nm corresponding to the bacteriochlorophyll *a* Q_y band) is similar in shape to that of the B800–820 antenna complex from *Rhodopseudomonas acidophila* strain 7050 (Cogdell *et al.*, 1985). The CD spectrum of the B800–820 complex from the 7050

strain was rationalised by assuming that there were two overlapping and intense exciton couplets centred in the two absorption bands. The spectra differ in the size of the bacteriochlorophyll Q_x band, with that of the B800–820 antenna complex resembling the Q_x of the B800–850 antenna complex from the 7750 strain of *Rhodopseudomonas acidophila.*

CD signals arising from the carotenoid absorption bands in the 500-560nm region also show strong optical activity with positive signals. Cogdell *et al.* (1976) have shown that carotenoids in petroleum ether show no CD spectrum. This induced CD possibly arises from binding of the carotenoid to the protein or via exciton coupling with other pigments. The CD spectra of the B800–820 antenna complex exchanged into different detergents are again similar showing that exchanging detergent had no effect on the environment of the pigments.

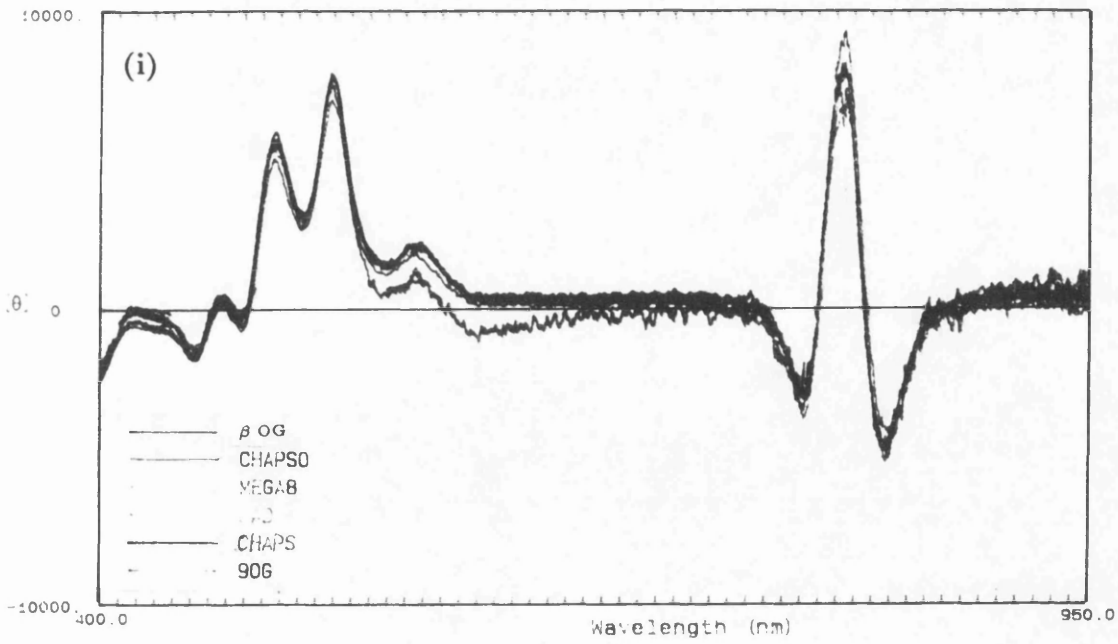

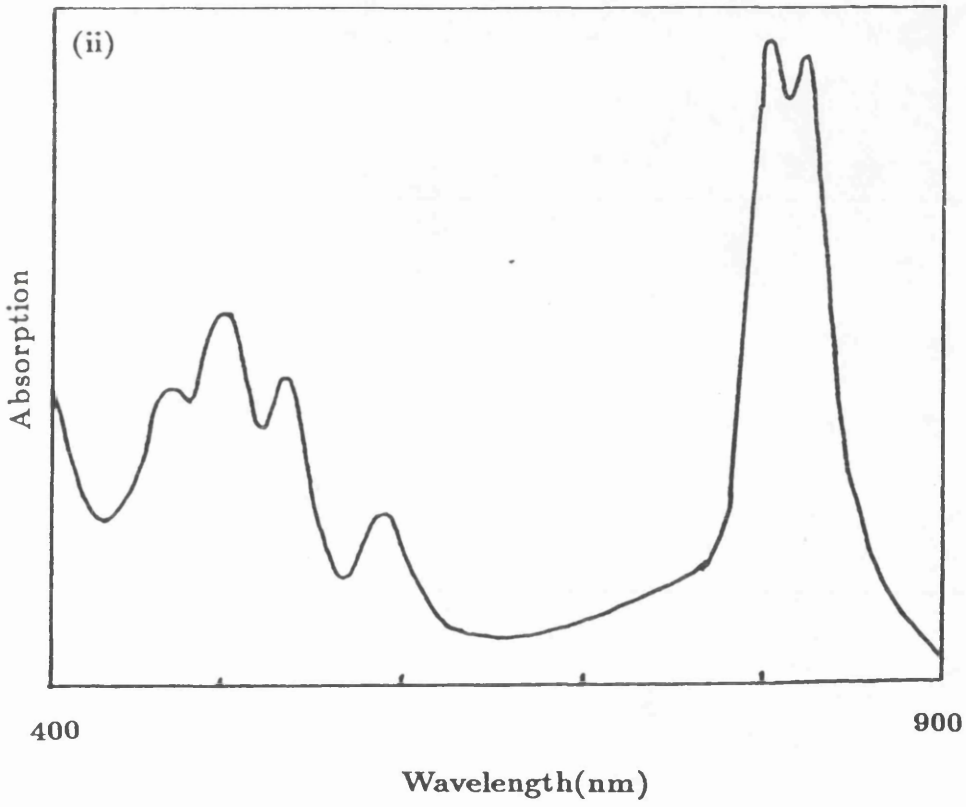

Figure 3.8 (i)Near Infrared CD Spectrum of the B800-820 Antenna Complex after Exchange into Different Detergents (Wavelength Scan Range 400–950nm). (ii)An absorption spectrum of the antenna complex in β octyl glucoside is shown for comparison.

3.6. Analysis of Low Molecular Weight Apoproteins

Most antenna complexes so far studied have been shown to be composed of two types of antenna apoprotein, the α- and β- apoprotein (Zuber *et al.*, 1991). Some species, such as *Rhodopseudomonas acidophila* or *Rhodopseudomonas palustris*, can synthesise antenna complexes which contain more than single α, β types. This is the case in the B800–820 antenna complex from *Rhodopseudomonas acidophila* strain 7750. Three low molecular weight apoproteins designated α_1, β_1, and β_2 have been sequenced (Bissig, 1990). The molecular weights of these are 5567, 4721 and 4520 Da respectively.

Tricine SDS polyacrylamide gel electrophoresis was used to examine the apoprotein composition because it allows resolution of small proteins in the molecular weight range 5000-20000 Da. Proteins with a molecular weight of greater than 30,000 Da are retained within the spacer gel. A calibration curve of protein mobility vs. ln molecular weight is presented in **Figure 3.9.** A photograph of a tricine-SDS polyacrylamide gel of the denatured antenna complex in 1% β octyl-glucoside is shown in **Figure 3.10.** Two distinct sets of two bands corresponding to α and β apoproteins are observed in track 5. The first set of two bands have an M_{APP} of 6600 Da and 6300 Da, while the second set have an M_{APP} of 3350 and 2550 Da. Comparison of the B800–820 complex with the B800–850 complex from strain 10050 (Tracks 6,7), demonstrates the differences in polypeptide composition. Two apoproteins from the B800–850 antenna complex have been sequenced (Zuber *et al.*, 1991). During electrophoresis a green coloured band due to denatured pigment ran ahead of the dye front. This is observed as a faint band in several of the tracks with an apparent molecular weight lower than the smallest marker.

Differences in the true molecular weight (M_r) deduced from the amino acid sequences and apparent molecular weights obtained from SDS-PAGE (M_{APP}) have been reported for many different species of purple phototrophic bacteria (Zuber *et al.*, 1991). This makes it impossible to state which is the α_1, β_1, or β_2 apoprotein obtained from sequence analysis for the B800–820 antenna complex or the α_1 or β_1 for the B800–850 antenna complex. The polypeptide composition of the B800–820 antenna complex has also been examined using reverse phase HPLC and has α_1, α_2, β_1 and β_2 polypeptides present (Zuber H., (1992), personal communication).

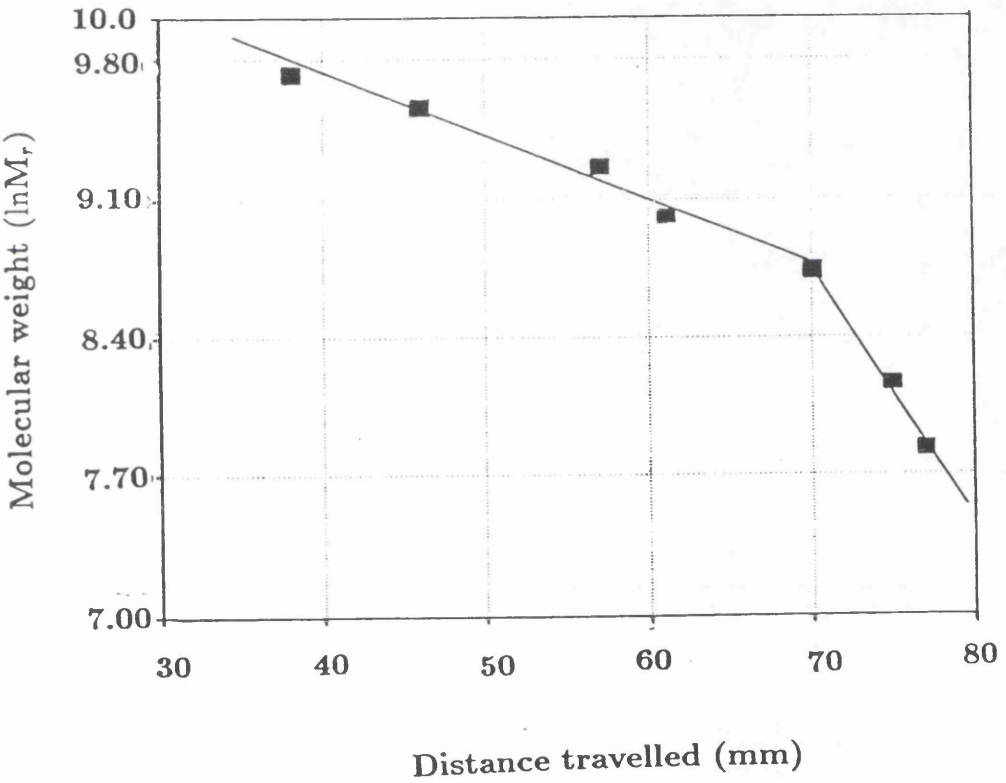

Figure 3.9. A Calibration Curve of $\ln M_r$ vs. Distance travelled by the Marker Proteins.

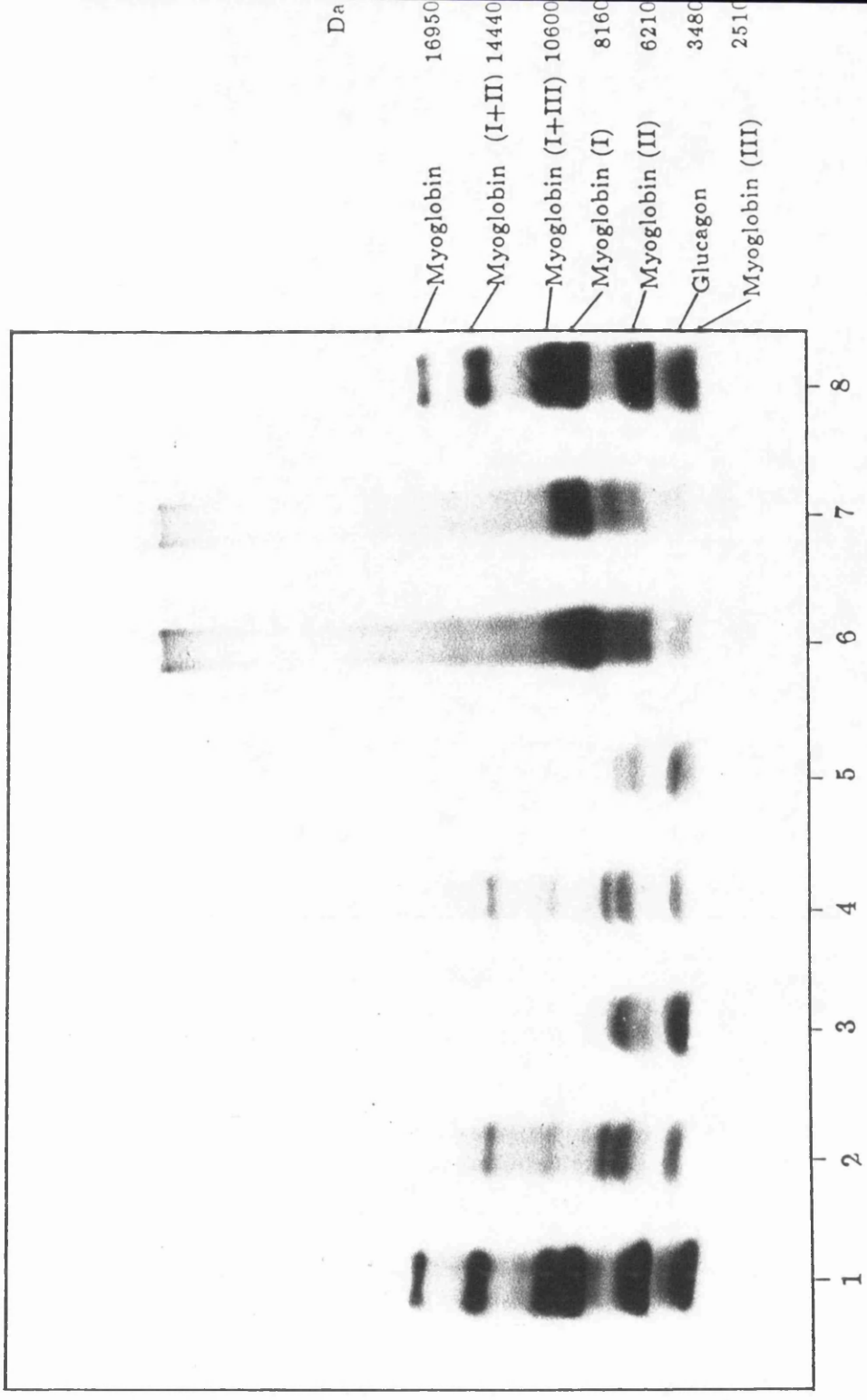

Figure 3.10. Tricine-SDS Polyacrylamide Gel of the B800–820 Antenna Complex. Tracks **1, 8**–marker proteins. Tracks **2, 4**–B800–820 complex prior to gel filtration chromatography. Tracks **3, 5**–purified B800–820 complex. Tracks **6, 7**–B800–850 antenna complex from *Rps. acidophila* strain 10050. A description of the low molecular weight markers is detailed in **Appendix D.**

3.7. Isolation of α– and β–Apoproteins using the Sephadex LH60 Gel Filtration Column.

A trace from the monitored eluate from the Sephadex LH60 column is presented in **Figure 3.11.**

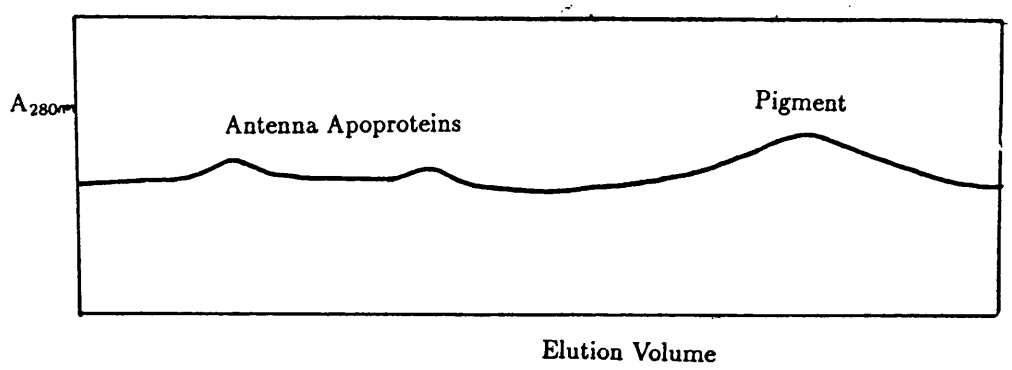

Figure 3.11. Elution Profile of an Organic Solvent Extract of B800–820 Antenna Complex, Separated on a Sephadex LH60 gel permeation column.

3.8 Electrospray Mass Spectrometry

3.8 (i) Introduction

Electrospray mass spectrometry is a new and highly sensitive technique for the determination of the molecular weight of proteins. Electrospray ionisation occurs when highly charged droplets shrink in a large electrostatic field, which leads to the production of molecular ions from a liquid solution. These positive ions arise by attachment of protons, alkali cations or ammonium ions (Iribarne and Thompson, 1976).

Electrospray ionisation was originally described by Dole *et al.* in 1968, in studies of the intact ions from synthetic and natural polymers of molecular mass in excess of 100,000 Da based on gaseous ion mobility measurements.

The multiple protonation of basic residues in oligopeptides and proteins enabled this technique to be used, in conjunction with a quadrupole mass spectrometer, for an analysis range of molecular masses up to 40,000 Da (Loo *et al.*, 1989). This range has subsequently been extended to masses of 130000 Da and permits the measurement of relative mass in the range of 5 to 40 kDa with a precision of better than 0.01% (Mann *et al.*, 1989).

3.8 (ii). Results of Electrospray Mass Spectrometry

The deconvoluted mass spectra of different samples of concentrated and detergent-exchanged B800–820 antenna complex are compared in **Figure 3.12 (i)**, **Figure 3.12 (ii)** and **Figure 3.12 (iii)**. Examination of these spectra shows two distinct sets of peaks corresponding to α– and β–apoproteins. The most prominent peak, consistent in all three spectra, has a molecular mass of 5906 $\pm$0.59 Da. This molecular weight is greater than that of any reported from primary structure analysis (using automated sequential Edman degradation, α_1– 5567 Da, β_1– 4721 Da and β_2– 4520 Da) and may possibly correspond to the α_2–apoprotein which has not yet been sequenced. Of the remaining peaks, the peak at 4861 $\pm$0.49 Da also appears consistently in all three samples. This molecular mass is different to that reported for any of the apoproteins, but corresponds most closely to molecular mass of the β–apoproteins.

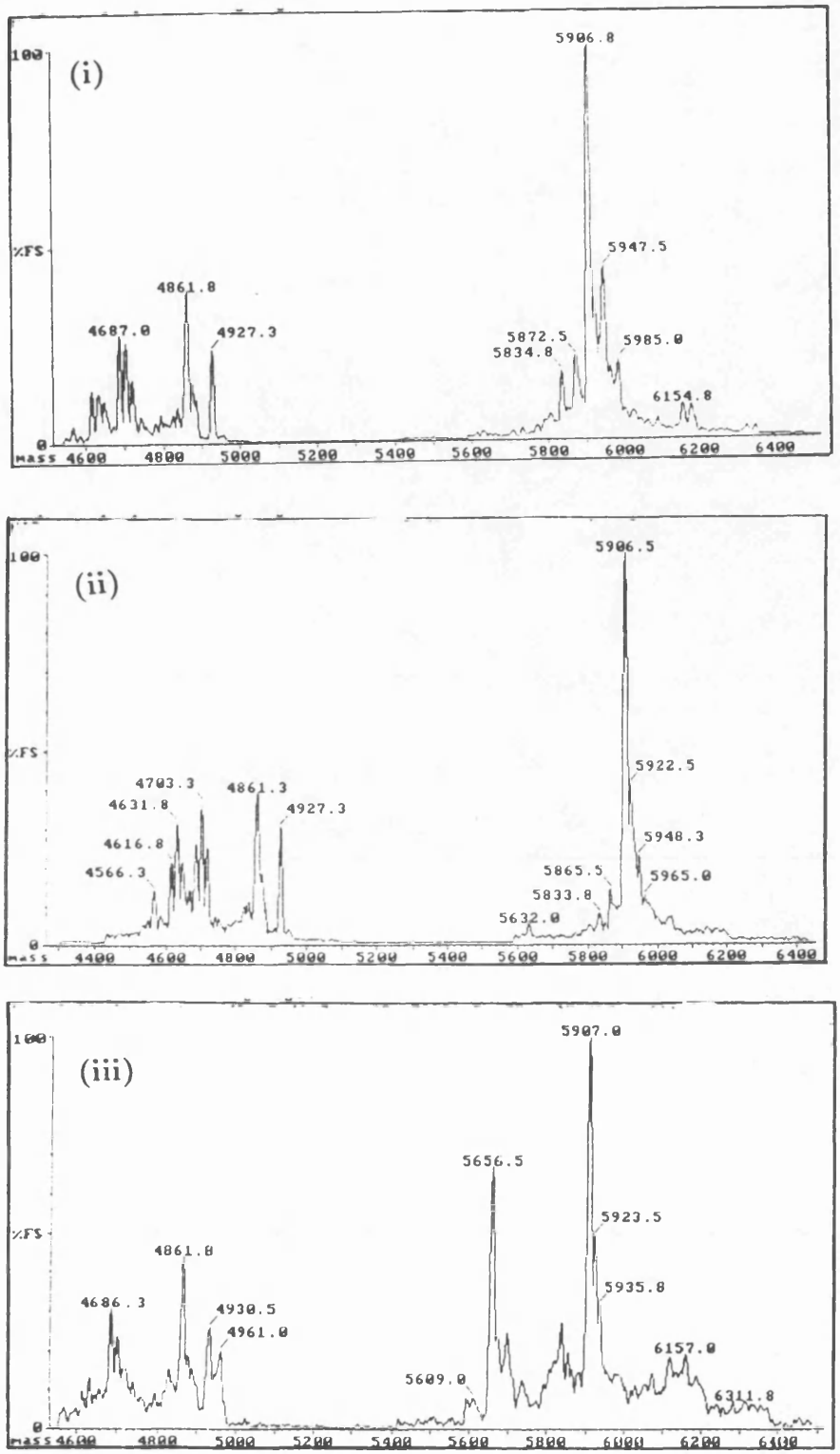

Figure 3.12. **(i), (ii) & (iii)** Electrospray Ionisation Spectra of Different Samples of Antenna Complex.

So far only a relatively small number of proteins have been analysed using electrospray ionisation mass spectrometry. In general these have been exploratory experiments where the protein is relatively pure and quite soluble in convient electrospray ionisation solvent systems (Jardine, 1990). There have been no documented examples of experiments using membrane proteins.

Sodium chloride (350mM) was used to elute the antenna complex from the small column in the final concentration and detergent exchange step (see **Section 2.7**). It has been reported that salts may well interfere with the analysis (Jardine, 1990). The Sephadex LH60 column was used as a further purification step to isolate the polypeptides into α– and β–apoproteins. The solvent system was changed from dichloromethane/methanol to formic acid/methanol because the electrospray method requires the use of polar solvents. Although sodium chloride is removed during this further purification step, it is necessary to add ammonium acetate to prevent aggregation of these membrane apoproteins. The minimum amount of ammonium acetate required to prevent aggregation was determined to be 50mM and this was added to the sample in the formic acid/methanol solution. The protein sample in this solvent system precipitated out of solution during injection.

Due to time constraints this approach had to be abandoned. This method merits a further thorough investigation by optimising different solvent systems to overcome the problem of precipitation.

3.9. Determination of the Molecular Weight of the Antenna Complex using SDS-PAGE

Electrophoresis of the isolated and undenatured antenna complex on a polyacrylamide gel showed that the coloured pigments co-migrate with pro-

tein as a purple band. Analysis of the absorption spectrum (wavelength range 250–900nm) of the pigments band after electrophoresis showed no change compared with the native absorption spectrum of the antenna complex.

An SDS polyacrylamide gel of the isolated and undenatured antenna complex is shown in **Figure 3.13 (i)**. This has a molecular weight greater than that of the largest molecular weight marker (BSA 68kDa), which means the intact complex must be an aggregate of the low molecular weight apoproteins and pigments. An estimate of the M_r of the intact complex was obtained from the calibration curve of protein mobility vs. molecular weight is presented in **Figure 3.13 (ii)**. This calibration curve was constructed using known molecular weight markers. Electrophoresis was then repeated using different gel concentrations (15%, 17% and 18%T)and confirmed the apparent M_r as 92kDa. This M_r is in the range of molecular weights reported for other intact antenna complexes (80-100kDa) (Cogdell *et al.*, 1983, Zuber, 1985).

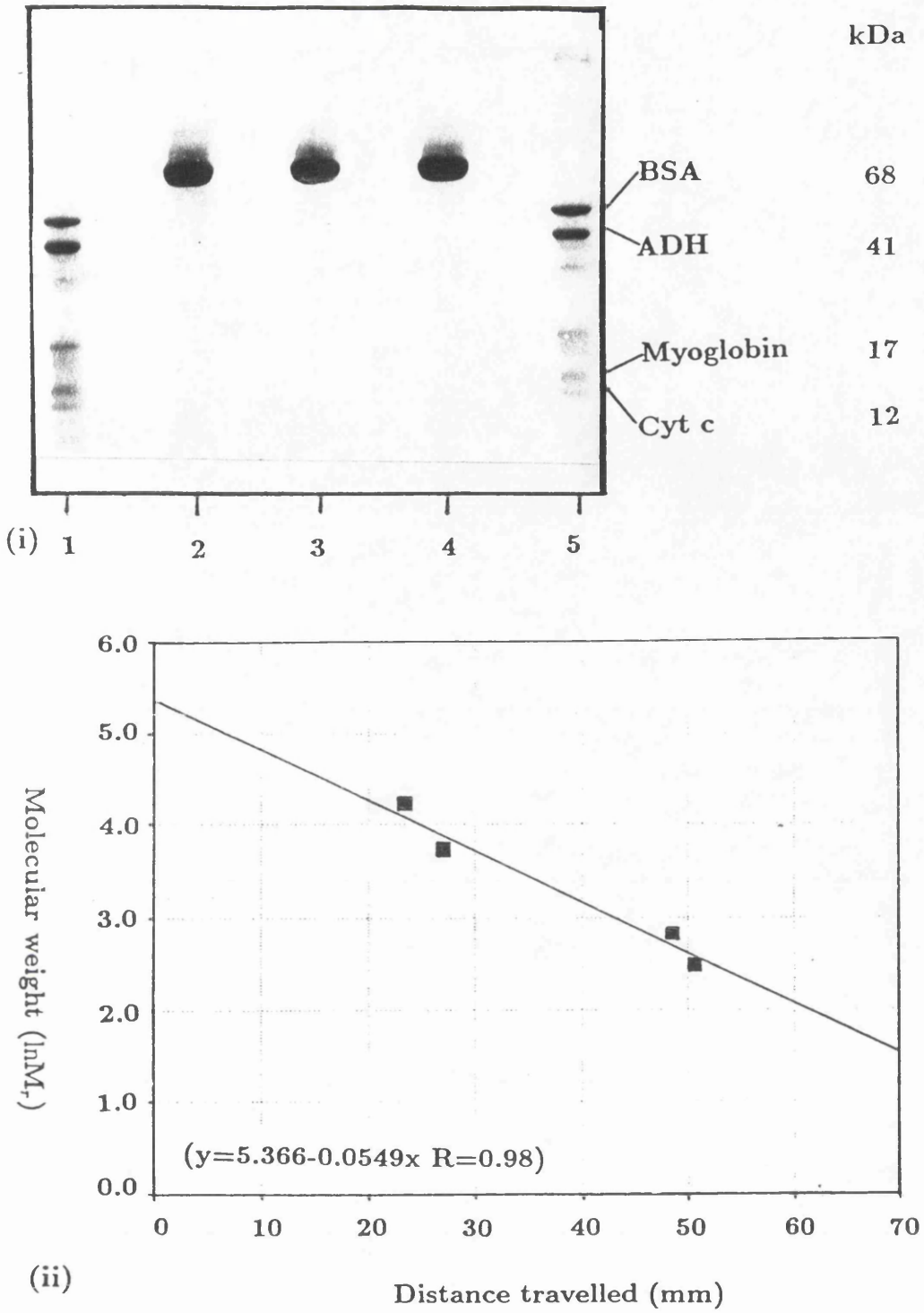

Figure 3.13. (i) SDS polyacrylamide gel (13.5%T) showing the isolated and undenatured B800–820 antenna complex. Lanes 1,5: markers, lanes 2,3,4: antenna complex. (ii) A Calibration Curve of $\ln M_r$ vs. distance travelled by the Marker Proteins.

3.10. Summary

The isolated B800–820 antenna complex from *Rhodopseudomonas acidophila* displays the same absorption maxima as the whole cells from which they are derived. This is a clear indicator that the native structure has been retained during isolation and purification. Secondary structure analysis of the native antenna complex by ultraviolet circular dichroism confirmed the presence of α helix which has been suggested from sequencing (Brunisholz *et al.*, 1989). Infrared circular dichroism spectroscopy shows that the carotenoid pigments in the antenna complex are influenced by their environment and show strong, induced optical activity. The bacteriochlorophyll *a* pigments show a strong Q_y absorption in the near infrared region and a different spectra to that found for bacteriochlorophyll in organic solvent. This may be due the environment in which the bacteriochlorophylls are situated or interactions between them (exciton coupling). Both ultra violet and infra red CD spectra demonstrate that exchanging the antenna complex into different detergents has no effect on conformation.

The B800–820 antenna complex from *Rhodopseudomonas acidophila* is formed from the aggregation of four low molecular weight, pigment-binding apoproteins (B800–820α_1, B800–820α_2, B800–820β_1 and B800–820β_2). These have M_{APP} of 2550, 3350, 6300 and 6500 Da determined by tricine SDS polyacrylamide gel electrophoresis. Electrospray ionisation mass spectrometry showed distinct sets of peaks corresponding to α– and β–apoproteins. The largest peak may be consistent with the unsequenced α_2 apoprotein. Reverse phase HPLC confirmed the presence of two sets of closely related α and β apoproteins. The stoichiometric ratio of bacteriochlorophyll *a*: carotenoids in the detergent-exchanged antenna complex is 2:1. The molecular weight of the isolated antenna complex was determined

by SDS polyacrylamide gel electrophoresis to be approximately 92kDa. This is in the range of molecular weights reported for native antenna complexes and similar to that reported for the B800-850 antenna complex from the 10050 strain of *Rhodopseudomonas acidophila*. The smallest possible structural unit is an $\alpha_1\alpha_2\beta_1\ \beta_2$ which binds six bacteriochlorophyll *a* molecules and three carotenoid molecules (Evans, 1989). The smallest oligomeric assembly, consistent with the molecular weight of 92kDa is a trimer of this smallest possible structural unit.

CHAPTER 4. Crystallisation of the B800–820 Antenna Complex from *Rhodopseudomonas acidophila* 7750

4.1. Introduction

In order to understand how the process of light capture occurs in purple photosynthetic bacteria at a molecular level, it is necessary to obtain the three-dimensional structure of a light-harvesting antenna complex. To determine a protein structure to atomic resolution, the technique of X-ray diffraction is used. The first step in such a structural analysis is the formation of single, well-ordered protein crystals. These must be large (between 0.3-1.0mm in all dimensions), because the intensity of the x-ray diffraction pattern of a crystal is roughly proportional to the volume of the crystal and inversely proportional to the volume of the crystallographic unit cell volume (Blundell & Johnson, 1976). Crystallisation is usually accomplished by a trial and error approach that is guided by a large body of empirically determined procedures and conditions (MacPherson, 1982). Although a systematic approach to investigate the mechanisms of crystallisaton of water soluble proteins has been developed (Feher *et al.*, 1985), these investigations have so far not been extended to membrane proteins. The principles and methods for crystallising water soluble proteins will be discussed, followed by a discussion of the problems which arise in membrane protein crystallisation due to the amphiphilic nature of these proteins.

The change in state between the solute and the solid during the formation of a crystal is an equilibrium process. This is not spontaneous because a fully solvated molecule lies at a potential energy minimum. For the formation of solid from a saturated solution there has to be a change in this state of equilibrium. These changes must be initiated and maintained by gradually altering the characteristics of the concentrated protein solution, so that the protein becomes less soluble. When the solution has more solute present than the solubility allows, it is said to be "supersaturated".

Supersaturation can be divided into labile and metastable regions. Crystal nuclei spontaneously form and dissolve in the labile region. Some of these nuclei continue to develop and become "stable" nuclei as long as the system is supersaturated. They will accumulate molecules and thus deplete the liquid phase until the system returns to the metastable region of supersaturation. The metastable region differs from the labile region in that it can only support growth of the stable crystal nuclei, it cannot spontaneously form nuclei. Crystal growth occurs much more slowly in the metastable region, so the best strategy is to quickly return to the metastable region for slow and controlled growth of a few large nuclei.

The process of crystallisation occurs because the crystalline state represents a minimum potential energy of the system. Sometimes, however, disordered aggregates or precipitates are formed. These represent false energy minima and are not the state of lowest free energy. Amorphous precipitate is formed when supersaturation has proceeded too extensively or too rapidly. The condition of limited supersaturation necessary for crystallisation, may be achieved by modifying some physical property such as pH or temperature, or through equilibration with precipitating agents. The precipitating agent may be a salt such as ammonium sulphate, a highly soluble synthetic polymer such as polyethylene glycol or an organic solvent such as ethanol. The first two are most commonly used in the crystallisation of proteins.

Precipitation using salt or "salting out" as it is known, is due to solvation of salt by water molecules in preference to solvation of the protein (Green *et al.*, 1955). By slowly increasing the level of saturation of a salt, the protein can be induced to separate from solution and enter the solid state. Polymers such as polyethylene glycol serve to dehydrate proteins in solutions and alter the solvents dielectric constant. Polyethylene glycol also

perturbs the natural structure of the the solvent and creates a complex network having both water and itself as structural elements. A consequence of the solvent restructuring is that macromolecules, particularly proteins tend to be excluded and phase separation is promoted (Lee *et al.*, 1981, Hermans, 1982).

Vapour diffusion is one of the most widely used techniques to achieve supersaturation. One method which allows control of crystallisation parameters is that of the "sitting drop". The starting material is pipetted into a well on a depression slide which is suspended above a reservoir of solution containing the precipitant. The crystallisation apparatus is then sealed to provide an isolated environment. Through the vapour phase the concentration of the precipitant in the reservoir equilibrates with that in the sample. The droplet of mother liquor must contain a level of precipitant lower than the reservoir and equilibration proceeds by distillation of water out of the drop and into the reservoir. As the concentration of salt in the sample gradually increases protein precipitation is induced.

The "hanging drop" method also uses vapour phase equilibration, but with a microdroplet of mother liquor suspended from the underside of a microscope coverslip. This is then placed over a small well containing 1ml of the precipitating solution.

While the principles of equilibration with both sitting and hanging drop are essentially the same, they frequently do not give the same results even though the protein and reservoir solutions in both methods are identical. The path taken to equilibrium is presumably different in the two cases even though the end point is the same (Mikol *et al.*, 1989, Mikol *et al.*, 1990).

The problem with crystallising integral membrane proteins is that they are amphipathic. This means that they require the use of detergents to pre-

vent their non-specific aggregation in aqueous media (Tanford *et al.*, 1976). Detergents are lipids which contain polar and non-polar regions (Helenius *et al.*, 1975). When detergents are present above a certain concentration (critical micellar concentration) they form micelles. During detergent solubilisation, the membrane proteins hydrophobic region is incorporated into the detergent micelle where it is shielded from aqueous media. These micelles are known as protein-detergent complexes (PDC). It is these PDC which are the basis for crystallisation. However when these mixed micelles come into contact with high concentrations of precipitants, a phase separation is induced and the detergent comes out of solution. This results in a detergent-rich and an aqueous detergent-poor phase. The hydrophobic membrane protein moves into the detergent-rich region where, in the case of the antenna complex, it becomes denatured. This process occurs at salt concentrations well below that required to cause true precipitation. By addition of a small amphiphilic compound to the mixed micelle, phase separation occurs at a higher salt concentration. Thus this shift in the phase separation boundary allows crystallisation to take place. These small amphiphilic compounds are also thought to have an effect on the radius of the PDC and might replace detergent molecules at positions critical for the formation of the crystal lattice (Michel, 1983). The shape of detergent molecules are important for the packing of the proteins into ordered crystals. Protein crystals are mainly stabilised by polar interactions so if the detergent molecules are too large they will obscure the polar regions of the protein and impede crystal formation. The type of protein detergent packing thought to occur in three-dimensional crystals is shown in **Figure 4.1.**

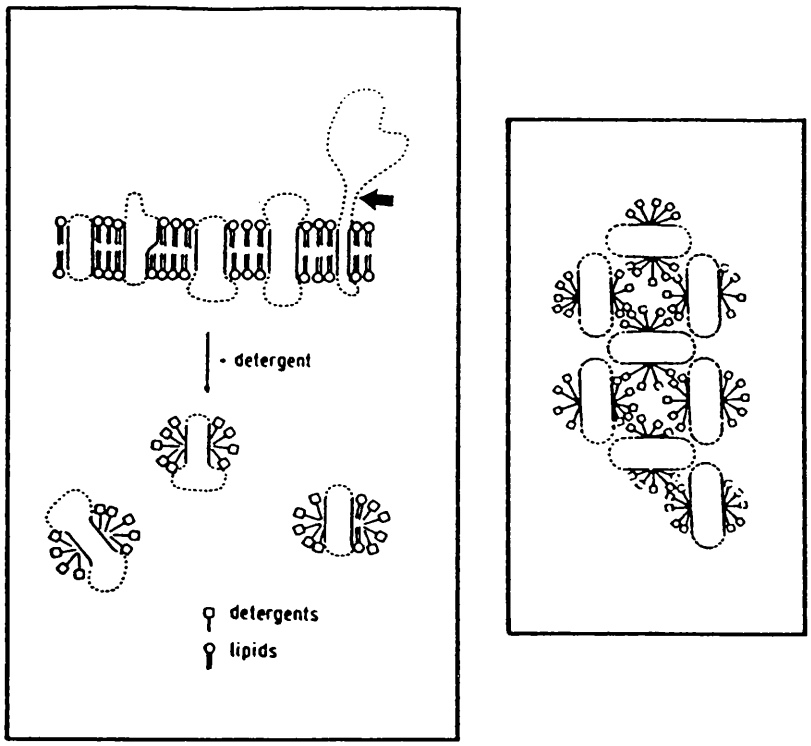

Figure 4.1. Left: Diagram depicting proposed arrangements of detergent-solvated membrane proteins. The hydrophobic tails of the detergents associate with membrane spanning hydrophobic regions of the proteins.
Right: Proposed packing of protein-detergent micelles during crystal formation. (From Michel, 1983).

The production of well-ordered three-dimensional membrane protein crystals has only recently been achieved. Crystals which diffract X-rays to high resolution have been obtained for matrix porin of *Escheria coli* (Garavito *et al.*, 1983) and for the photosynthetic reaction centres from *Rhodopseudomonas viridis* (Michel *et al.*, 1986) and *Rhodobacter sphaeroides* (Allen *et al.*, 1987a,b).

4.2. Determination of the Stability Range of the Antenna Complex

Before crystallisation trials were carried out, the stability of the antenna complex was determined with respect to changes in pH, temperature, detergent and small amphiphile. The electronic absorption spectra in the wavelength range 250-900nm was used to monitor the integrity of the complex during stability tests. When the pigments are correctly bound to their antenna apoproteins their absorption spectra are red-shifted with respect to their spectra in organic solvents. Denaturation reverses this red-shift.

The most important parameters were found to be temperature and pH. An increase in the absorbance at 680nm was noted when the antenna complex was subjected to temperatures of 25°C for 24hr. This was due to the presence of oxidised bacteriochlorophyll indicating the antenna complex had begun to denature. It was found that long term stability of the antenna complex required the pH to be greater than 8.5. The effect of exchanging the antenna complex into different detergents was also monitored by examination of the absorption spectra. When the detergent lauryl dimethyl N-amine oxide (LDAO), used during the purification process, was exchanged for any of the nonionic alkyl glucoside detergents (lauryl maltoside, heptyl thioglucoside, heptyl, octyl or nonyl glucoside), a change in the relative heights of the two bacteriochlorophyll Q_y bands at 800 and 820nm occurred. This effect occurred to the same extent on exchanging the complex into any of these detergents. The wavelength of absorption remained unchanged and gel electrophoresis showed no evidence of denaturation. It was possible to reverse this effect by exchanging the complex back into LDAO. The absorption spectra of the antenna complex in 1% LDAO and 1% β octyl glucoside are shown in **Figure 4.2.**

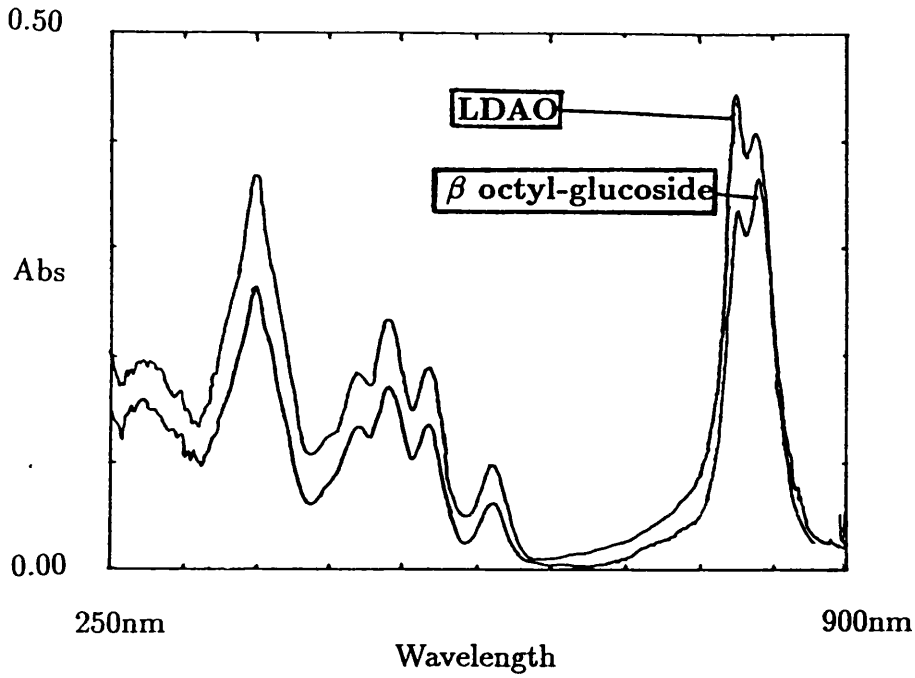

Figure 4.2. Absorption spectra illustrating the change in the relative heights of absorbance of the two bacteriochlorophyll Q_y bands at 800 and 820nm after detergent exchange into β octyl-glucoside. Samples of the protein in the two detergents are present in different dilutions hence the overall difference in absorption height.

There was no change in the near-infra spectra when the complex was exchanged into MEGA8 (octanoyl-N-methylglucamide) or the zwitterionic detergents CHAPS (3-[(3-cholamidopropyl)dimethylammonio]-1-propane-sulfonate), CHAPSO (3-[(3-cholamidopropyl)dimethylammonio]-2-hydroxy-1-propane-sulfonate) and NDA (N-dodecyl-N,N-dimethyl-3-ammonio-1-propane-sulfonate). The small amphiphiles heptane-1, 2, 3-triol, piperidine 2-carboxylic acid and benzamidine hydrochloride were added to

the antenna complex at 2.5% (w/v) concentration, without causing any denaturation. It has been reported that organic solvents have successfully been used as small amphiphiles (Garavito *et al.*, 1986). Addition of either 5% methanol or ethanol caused denaturation of the antenna complex with the appearance of green denatured bacteriochlorophyll. This precluded the use of these organic solvents in later crystallisation trials.

4.3. Preliminary Crystallisation Trials

Once the conditions under which the protein was stable had been determined, the next step was to begin crystallisation trials. Because of the intricacy of the interactions between solute and solvent, these trials must be applied over a broad set of conditions with the objective of discovering the particular minima which yield crystals.

A wide range of conditions were varied in sitting drop trials, initially using the larger sandwich boxes. These were very time consuming to set up and also required a large amount of space for incubator storage. Similar results were achieved using Cryschem disposable trays, with a reduction in both set-up time and space needed for storage.

4.3. (i) Crystallisation Trials using Sitting Drop

The first parameter to be determined was the precipitation point of the antenna complex using the salt di-potassium hydrogen orthophosphate and the organic polymer PEG 6000. It was found that addition of the small amphiphile benzamidine hydrochloride, (2.5% (w/v)), raised the concentration of salt required to precipitate the protein from 1M to 2.6M at 20°C. A similar increase in the concentration of PEG was also required (10% to 22.2%). Initial trials were set up using the same salt in the drop at 1M concentration, and the reservoir over a greater range of concentrations (1.8-3.0M). The salts used were ammonium sulphate, di-potassium hydrogen

orthophosphate, sodium sulphate, sodium citrate and magnesium sulphate. The reservoir pH ranged from 8.5–10.0. In all cases the small amphiphile benzamidine hydrochloride was present in the drop at 2.5% concentration. The pH of the drop was adjusted to that of the reservoir unless ammonium sulphate was used in the reservoir. There was no need to alter the drop of the pH in this case because its pH is changed to that of the reservoir due to equlibration of free ammonia (Mikol, 1989). Trials were also setup using PEG 6000 at 10% concentration in the drop over a range of concentrations of PEG 6000 in the reservoir (15-100%). The results of successful trials using salt as the precipitant are shown in **Table 4.1**.

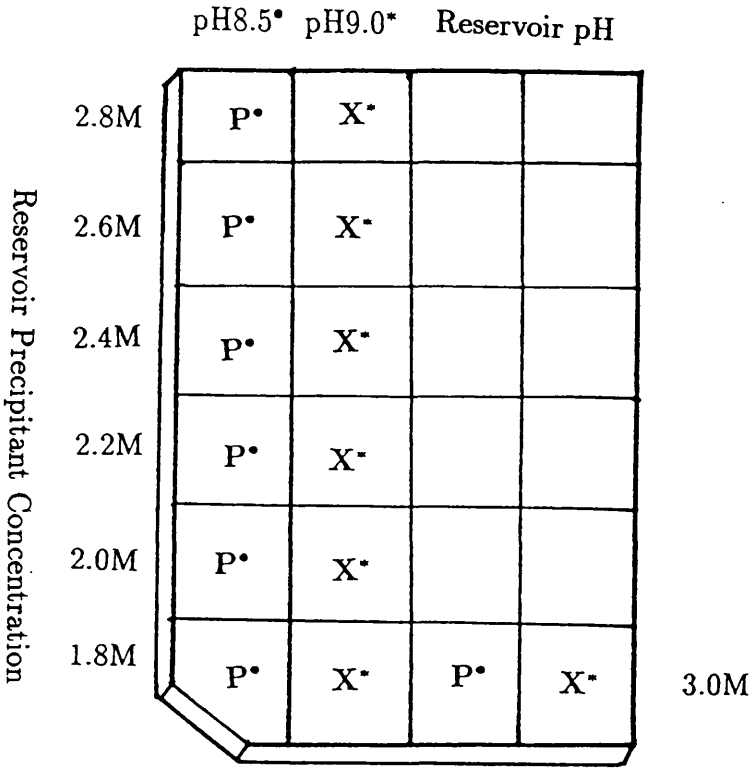

X – Crystal formation

P – Precipitate

Drop

Protein concn – 4mg/ml (Purity Index 3.0) in 20mM Tris-HCl, pH8.0

Detergent – 1% β octyl-glucoside

Precipitant – 1M di-potassium hydrogen orthophosphate

Amphiphile – 2.5% (w/v) benzamidine hydrochloride

Reservoir

Precipitant – ammonium sulphate, pH8.5•, pH9.0*

Incubation Temperature

15°C

Table 4.1. Sitting Drop Trial Illustrating the Influence of Reservoir pH on Crystallisation (Sandwich Box).

Crystal formation was only found in the boxes containing di-potassium hydrogen orthophosphate in the drop concentrated against ammonium sulphate in the reservoir at pHs 9.0 and 9.5. Precipitation of the protein occurred in all trials on either side of these values. Crystallisation resulted in a change in the colour of the mother liquor from dark red to clear. The crystal habit and speed of crystallisation varied depending on the concentration of ammonium sulphate used. Needle shaped crystals were observed at 3.0M ammonium sulphate, changing to rod shaped crystals at 2.6M ammonium sulphate and finally to tabular plates at 2.0-2.4M ammonium sulphate (**Figure 4.3**).

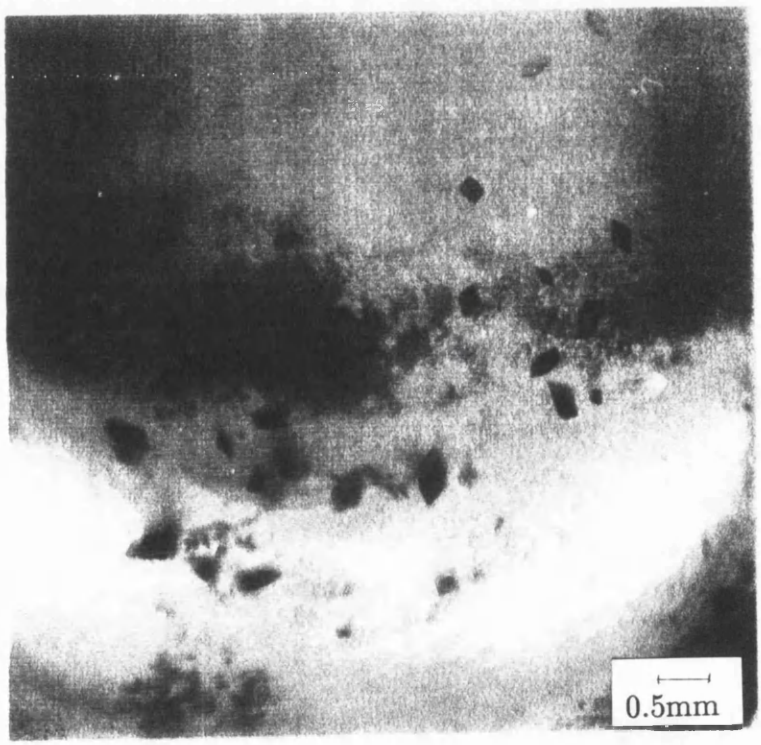

Figure 4.3. Small Tabular Plate Crystals grown using a Reservoir Concentration of 2.4M ammonium sulphate, pH 9.0.

Needle shaped crystals grew in 17 days whilst the rod shaped crystals took 25 days. Formation of small diamond shaped tabular plates took between 45-80 days, with decreasing salt concentration. These small tabular plates diffracted X-rays to 10Å resolution. The use of PEG 6000 resulted in complete phase separation in all trials, even in the presence of benzamidine hydrochloride (**Figure 4.4.**).

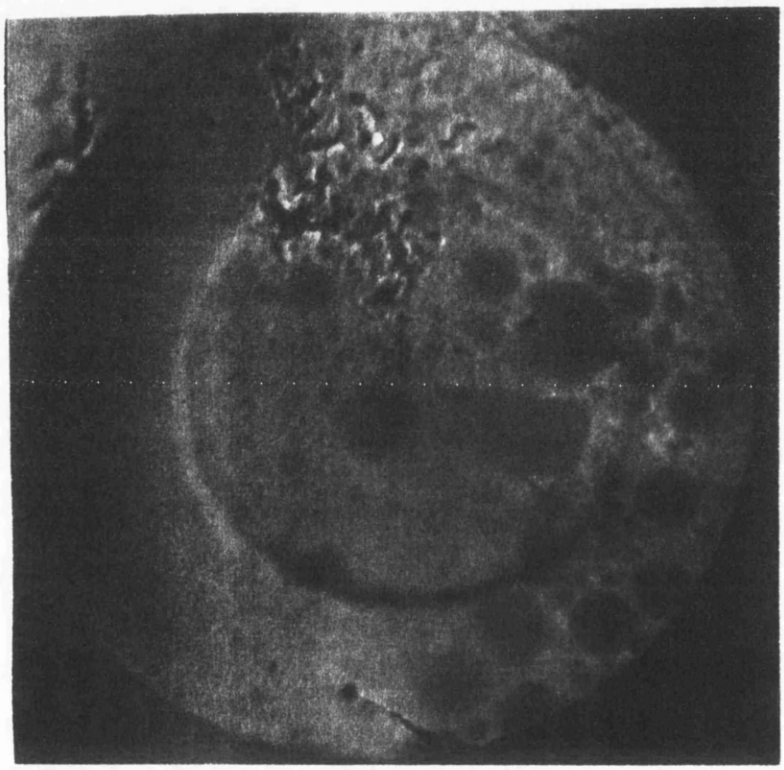

Figure 4.4. Phase Separation into Detergent Rich and Poor Regions using 10% PEG 6000 in the Drop Concentrated against 25% PEG 6000 in the Reservoir. This was followed by the appearance of green bacteriochlorophyll.

After obtaining crystals using β octyl-glucoside, the next step was to assess the effect of changing detergent. A range of trials were setup using each of the detergents in which the complex was stable. Each detergent was present at 1% (w/v) concentration, with 1M di-potassium hydrogen orthophosphate in the drop and a range of concentrations of ammonium sulphate in the reservoir (1.8-3.0M). In conjunction with the small amphiphile benzamidine hydrochloride it proved possible to obtain small crystals in all detergents used except two.

Phase separation into a detergent rich and detergent poor aqueous phase occured in all trials using the detergents CHAPS (**Figure 4.5.**) and CHAPSO. When the antenna complex entered the detergent rich phase it quickly became denatured over a period of 2hr.

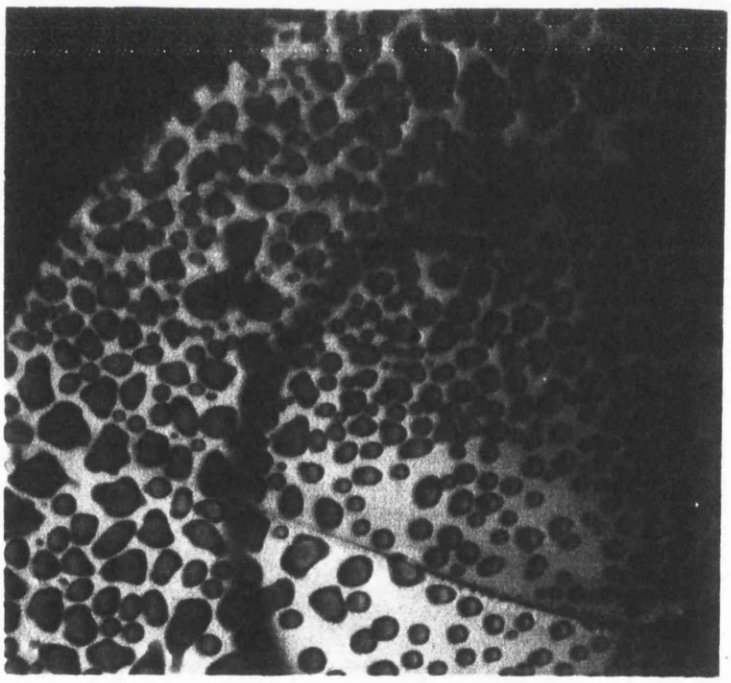

Figure 4.5. Attempted Crystallisation with the Antenna Complex in 1% CHAPS. This Photograph shows the resulting Phase Separation with Denaturation of the Purple Antenna Complex as it enters the Detergent Rich Micelles.

Trials were conducted using the detergent MEGA-8 (**Table 4.2**). A reservoir concentration of 2.2M ammonium sulphate gave small bar shaped crystals of the complex after 3 weeks (**Figure 4.6**). Deterioration of these crystals occured approximately 1 week after the mother liquor turned clear. This was due to a partial phase separation of the detergent from the aqueous phase (**Figure 4.7**).

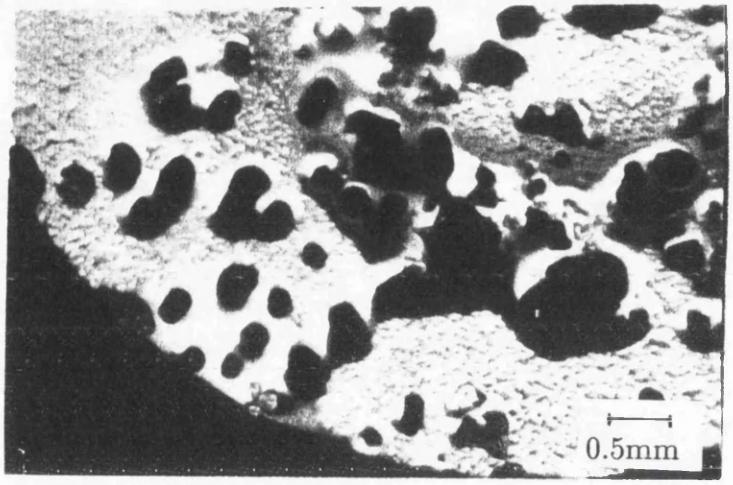

Figure 4.6. Small Bar Shaped Crystals of the Antenna Complex in the detergent MEGA8.

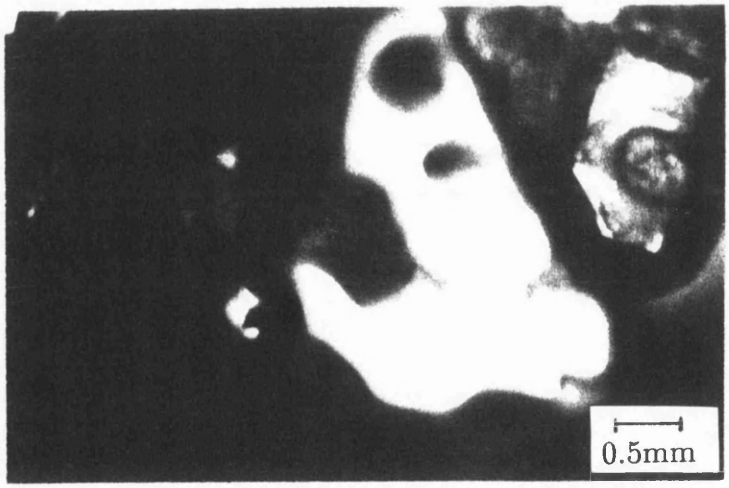

Figure 4.7. Deterioration of these crystals due to phase separation of the detergent MEGA8.

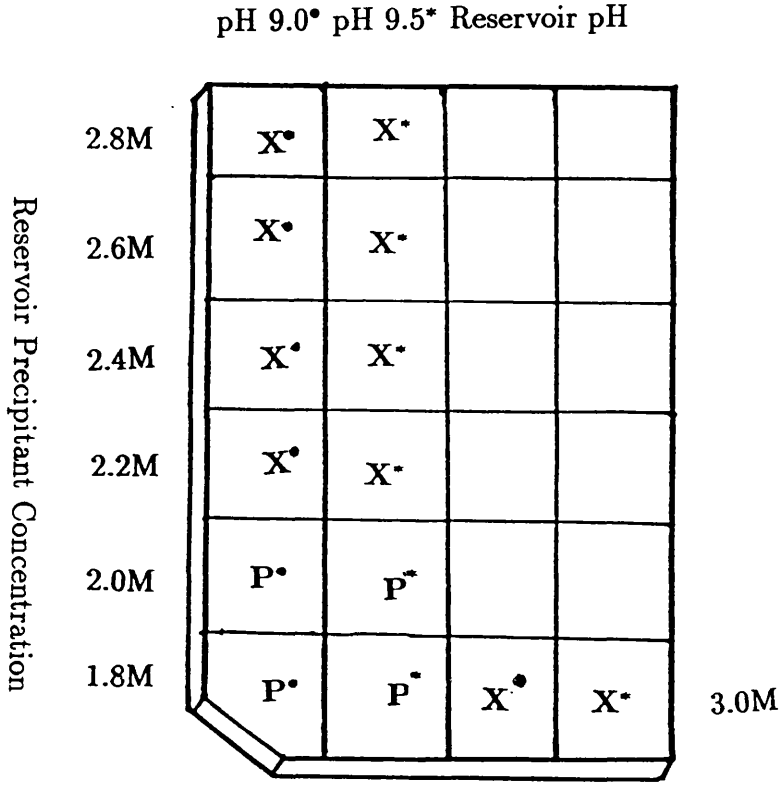

X – Crystal formation

P – Precipitate

Drop

Protein concn – 4mg/ml (Purity Index 2.2) in 20mM Tris-HCl, pH8.0

Detergent – 1% MEGA8

Precipitant – 1M di-potassium hydrogen orthophosphate

Amphiphile – 2.5% (w/v) benzamidine hydrochloride

Reservoir

Precipitant – ammonium sulphate, pH9.0• , pH 9.5*

Incubation Temperature

15°C

Table 4.2. Sitting Drop Trial using the Detergent MEGA8 (Sandwich Box).

Trials conducted using NDA gave different crystal forms depending on the concentration of ammonium sulphate used (**Table 4.3**). These different crystal forms are shown in **Figure 4.8**, **Figure 4.9** and **Figure 4.10**. The differences in crystal morphology ranged from needle shaped crystals at 2.6M ammonium sulphate, bar shaped crystals and larger plate crystals at 2.4M ammonium sulphate and tabular plates at 2.2M ammonium sulphate. In all trays crystallisation occured following the presence of precipitate. The largest of these tabular plate crystals were of a size suitable for X-ray analysis (0.4mm x 0.3mm x 0.2mm), but proved not to be well ordered and weakly diffracted X-rays to only 15Å.

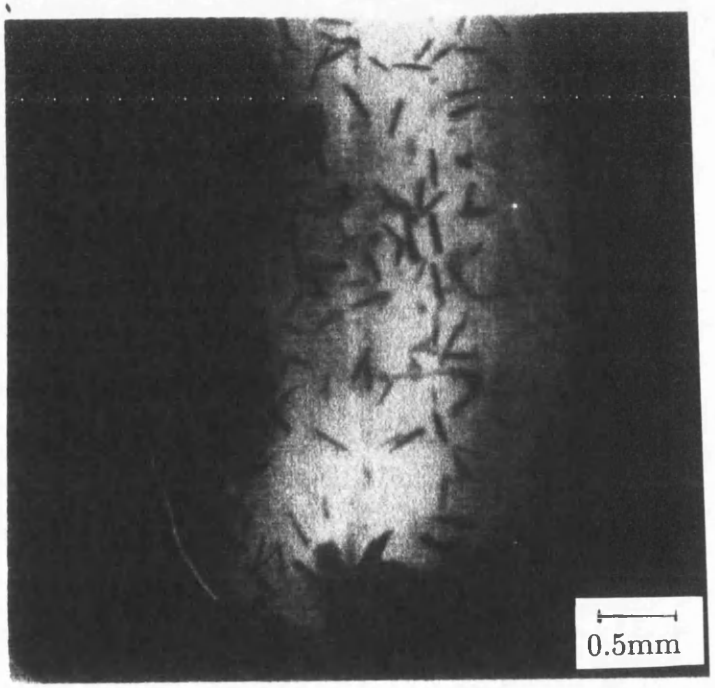

Figure 4.8. Needle Shaped Crystals of the Antenna Complex in the Detergent NDA grown using a Reservoir Concentration of 2.6M ammonium sulphate, pH 9.5.

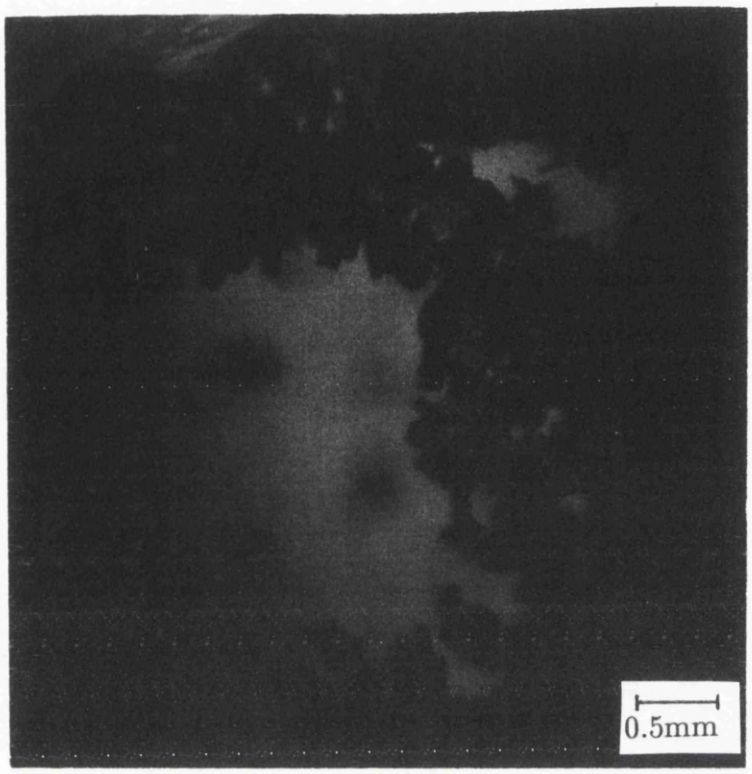

Figure 4.9. Bar and Tabular Plate Crystals of the Antenna Complex in the Detergent NDA grown using a Reservoir Concentration of 2.4M ammonium sulphate, pH 9.5.

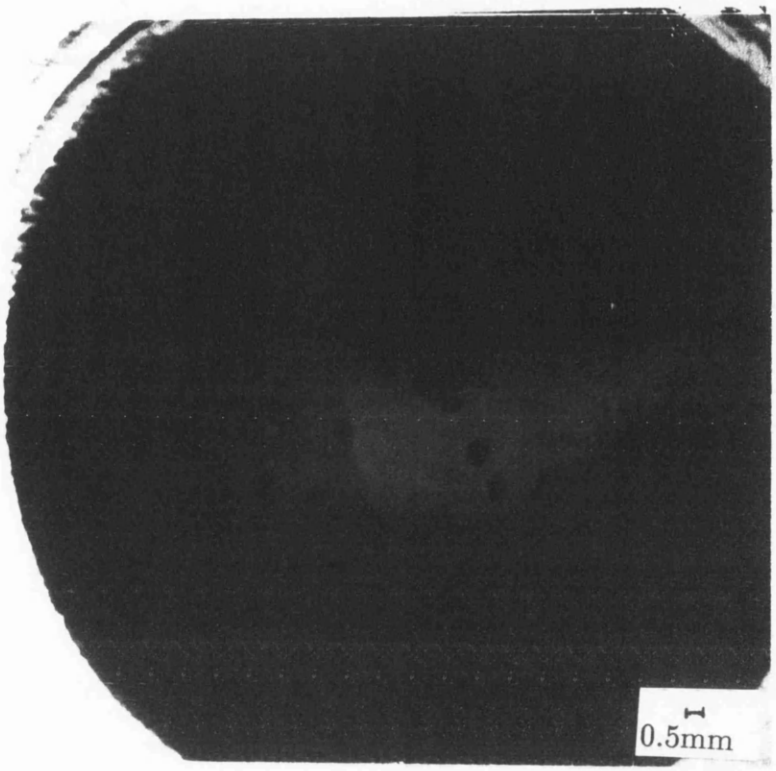

Figure 4.10. Tabular Plate Crystals of the Antenna Complex in the Detergent NDA grown using a Reservoir Concentration of 2.2M ammonium sulphate, pH 9.0. These weakly diffracted x-rays to 15Å resolution

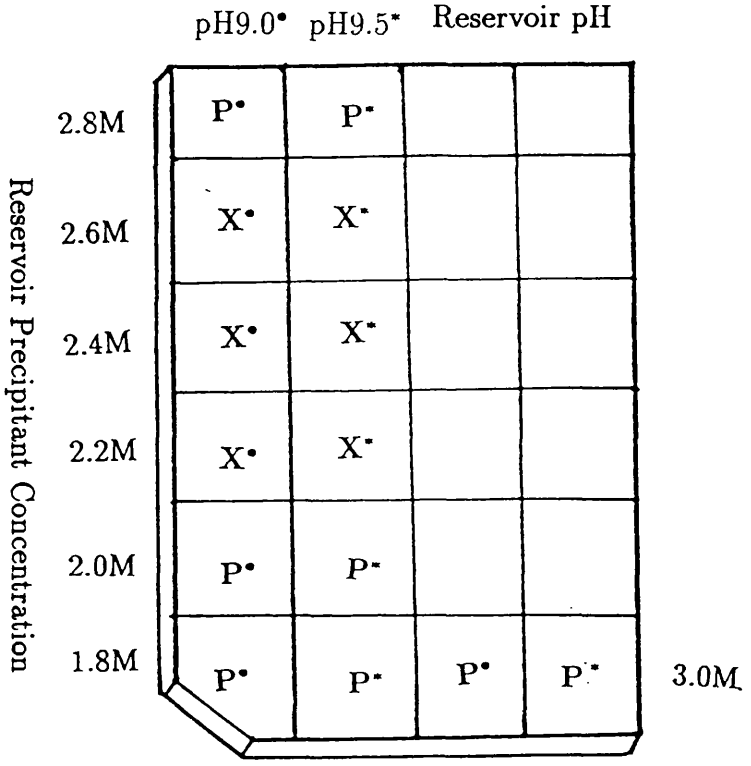

X – Crystal formation

P – Precipitate

Drop

Protein concn – 4mg/ml (Purity Index 3.0) in 20mM Tris-HCl, pH8.0

Detergent – 1% NDA

Precipitant – 1M di-potassium hydrogen orthophosphate

Amphiphile – 2.5% (w/v) benzamidine hydrochloride

Reservoir

Precipitant – ammonium sulphate, pH9.0•, pH9.5*.

Incubation Temperature

15°C

Table 4.3. Sitting Drop Trial using the Detergent NDA (Sandwich Box).

Trials were set up using a range of glucoside detergents with different alkyl chain lengths. Nonyl glucoside yielded only precipitate across the entire range of ammonium sulphate concentrations. Bar shaped crystals were obtained using heptyl glucoside (**Figure 4.11**) and heptyl thioglucoside. The rate at which these crystals appeared varied from 1-3 weeks depending on the rate of vapour diffusion (**Table 4.4**).

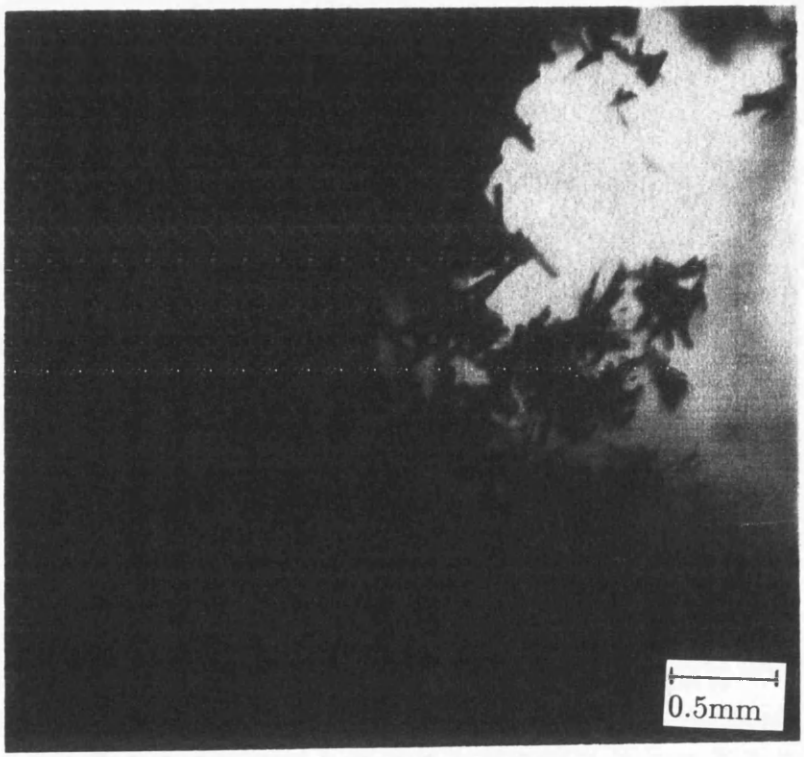

Figure 4.11. Bar Shaped Crystals of the Antenna Complex in the Detergent Heptyl Glucoside grown using a Reservoir Concentration of 2.2M ammonium sulphate, pH 9.0. The size and morphology of the crystals was always the same and too small for X-ray analysis.

The small amphiphile was changed to 2.5% (w/v) heptane-1, 2, 3-triol and trials in each of the detergents repeated. Crystallisation failed to occur in all trials. Trials were also conducted using 2.5% (w/v) Piperidine 2-carboxylic acid as a small amphiphile. This was only successful in aiding crystallisation in the presence of the detergent LDAO yielding small cube and needle shaped crystals after approximately 6 months (**Figure 4.12.**) (**Table 4.5**). These crystals were too small to use for X-ray diffraction studies.

Figure 4.12. Crystals of the Antenna Complex in the Detergent LDAO grown using the small amphiphile Piperidine 2-carboxylic acid and a Reservoir Concentration of 2.2M ammonium sulphate, pH 9.0.

Detergent – 1% heptyl glucoside*, 1% heptyl thioglucoside*

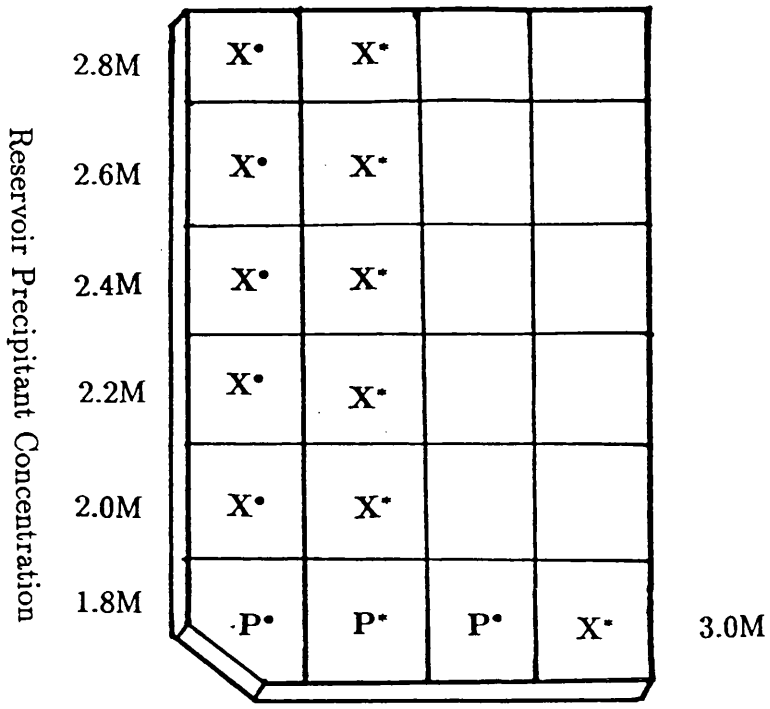

X – Crystal formation

P – Precipitate

Drop

Protein concn – 4mg/ml (Purity Index 2.3) in 20mM Tris-HCl, pH8.0

Detergent – 1% heptyl glucoside*, 1% heptyl thioglucoside*

Precipitant – 1M di-potassium hydrogen orthophosphate

Amphiphile – 2.5% (w/v) benzamidine hydrochloride

Reservoir

Precipitant – ammonium sulphate, pH9.0.

Incubation Temperature

15°C

Table 4.4. Sitting Drop Trials using the Detergents Heptyl Glucoside and Heptyl Thioglucoside (Sandwich Box).

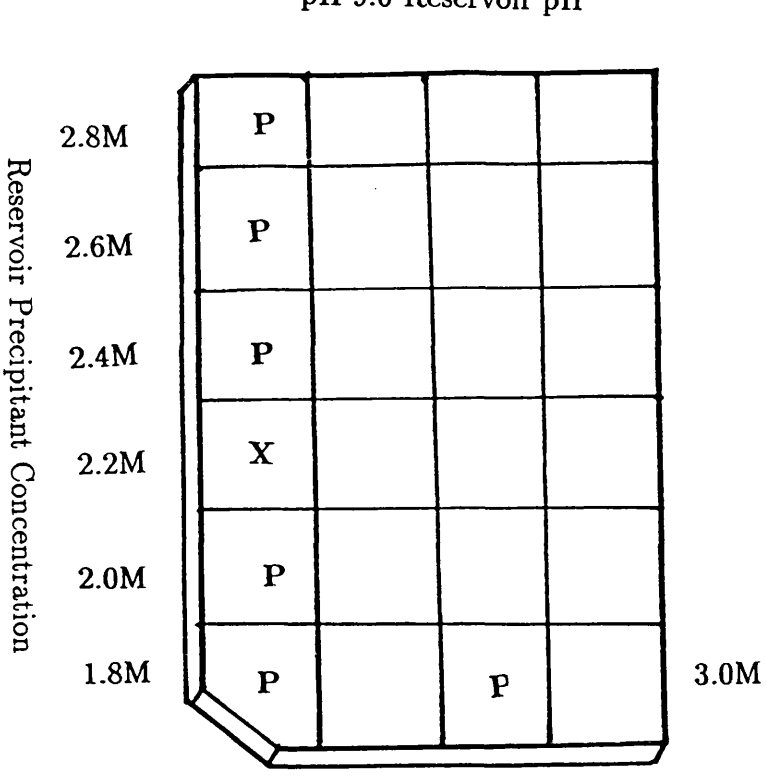

X – Crystal formation

P – Precipitate

Drop

Protein concn – 4mg/ml (Purity Index 2.7) in 20mM Tris-HCl, pH8.0

Detergent – 1% LDAO

Precipitant – 1M di-potassium hydrogen orthophosphate

Amphiphile – 2.5% (w/v) piperidine 2-carboxylic acid

Reservoir

Precipitant – ammonium sulphate, pH9.0.

Incubation Temperature

15°C

Table 4.5. Sitting Drop Trials using the Detergent LDAO and the Small Amphiphile Piperidine 2-carboxylic acid (Sandwich Box).

4.3. (ii) Crystallisation using Hanging Drop

It is desirable to conduct trials using hanging drop because a large number of crystallisation conditions can be quickly screened using only minimal amounts of protein. The presence of detergent necessitated both siliconisation of the microscope coverslide and also placed a limitation on the size of the drop due to the reduction in surface tension (Garavito *et al.*, 1986). The maximum effective microdroplet of mother liquor which could be used was 6μl.

The only successful trials were those using 1M potassium phosphate in the drop concentrated against a 1ml reservoir of 25% ammonium sulphate at pH9.0 (**Table 4.6**). Small rod shaped protein crystals (0.1mm x 0.05mm x 0.02mm) grew over a period of 2 weeks at 15°C. The small size of the microdroplet, proved to be very susceptible to local fluctuations in incubator temperature, and any crystals which formed subsequently redissolved without crystallisation recurring. Using these conditions the concentration of protein in the trial was elevated to 8mg/ml, but there was no increase in either the size or stability of the crystals. An increase in the size of droplet led to it falling off the the coverslip into the reservoir. Consequently trials using this technique were abandoned.

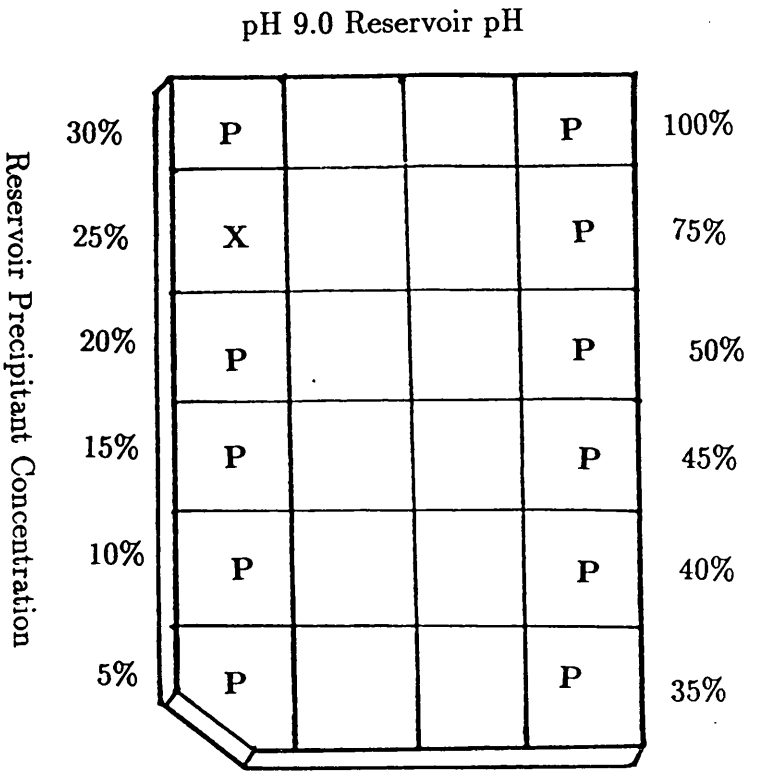

X – Crystal formation

P – Precipitate

Drop

Protein concn – 4mg/ml (Purity Index 2.9) in 20mM Tris-HCl, pH8.0

Detergent – 1% β octyl-glucoside

Precipitant – 1M di-potassium hydrogen orthophosphate

Amphiphile – 2.5% (w/v) benzamidine hydrochloride

Reservoir

Precipitant – ammonium sulphate, pH9.0.

Incubation Temperature

15°C

Table 4.6. Crystallisation Trials using the Method of Hanging Drop

4.3. (iii) Review of Results of Preliminary Trials

It was initially found that crystallisation occurred within a pH range of 9.0-9.5 and using a combination of di-potassium hydrogen orthophosphate in the drop concentrated against a reservoir of ammonium sulphate. Crystal formation was possible in almost all of the detergents tried, but only in the presence of the small amphiphile benzamidine hydrochloride. The only other combination of detergent and amphiphile which gave crystals was that of LDAO and piperidine 2-carboxylic acid. These crystals were too small for X-ray diffraction studies. The precipitation point of the antenna complex in the presence of either 2.5% (w/v) heptane-1, 2, 3-triol or 2.5% (w/v) piperidine 2-carboxylic acid with potassium phosphate was identical to that with 2.5% (w/v) benzamidine hydrochloride. The results of these trials show the small amphiphile may have a more significant effect than merely perturbing the phase equilibrium of the detergent. It it is possible that benzamidine hydrochloride specifically interacts with the antenna complex, during crystal formation. Both Michel (Michel *et al.*, 1980) and Garavito (Garavito *et al.*, 1980) have emphasised a second role of the small amphiphile in the actual process of crystal formation. They view these small amphiphiles as agents which enter the crystal lattice and act to balance the hydrophillic and hydrophobic surfaces of the membrane protein. In this fashion they may affect the packing of the protein monomers within the crystal. Using SANS (small angle neutron scattering) it has been demonstrated that the overall diameter of the LDAO micelle was reduced with increasing concentration of heptane-1, 2, 3-triol (Timmins *et al.*, 1991). A similar effect may occur during crystallisation of the antenna complex. The size of the detergent micelle is significant for the alkyl glucoside detergents because larger crystals could only be obtained using the 8 carbon alkyl chain. It is possible

that the detergent micelle is compacted in the presence of benzamidine hydrochloride allowing the formation of better crystal contacts. The effect of slightly changing the concentration of benzamidine hydrochloride was one of the factors studied in the next stage, which was to obtain more highly ordered crystals.

4.4. Optimisation of Crystallisation Conditions using β-octyl glucoside

The next step was optimisation of crystallisation parameters to obtain larger and better ordered crystals. One of the major problems was the time taken for crystal nucleation to occur and it was hoped that this could be reduced to weeks instead of months.

The first of these parameters to be optimised was protein concentration. Trials were set up over a range of protein concentrations containing 1-10 mg/ml, using 1M di-potassium hydrogen orthophosphate in the drop and ammonium sulphate in the reservoir at 2.0-2.3M (**Table 4.7**). It was found when the concentration of protein was very dilute ie 1mg/ml or less the solution was depleted of protein and remained very small. Large tabular plate crystals could only be grown in the range of 6-8mg/ml with the biggest crystals occuring at 8mg/ml protein in the presence of a reservoir concentration of 2.1M ammonium sulphate at pH9.0 (**Figure 4.13**). Using a protein concentration of greater than 8mg/ml resulted in the formation of precipitate. It was found that varying the purity index over a range of values 0.9, 1.5, 2.0, 2.5 and 3.0 had no effect on crystal size or quality of X-ray diffraction.

pH 9.0 Reservoir pH

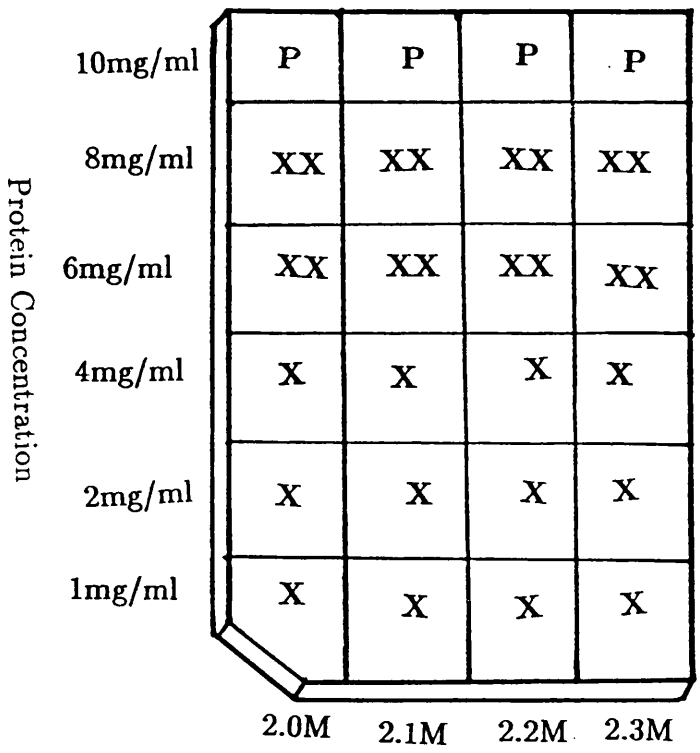

XX – Larger crystal formation

X – Small crystal formation

P – Precipitate

Drop

Protein concn – 1-10mg/ml (Purity Index 2.5) in 20mM Tris-HCl, pH8.0

Detergent – 1% β octyl-glucoside

Precipitant – 1M di-potassium hydrogen orthophosphate

Amphiphile – 2.5% (w/v) benzamidine hydrochloride

Reservoir

Precipitant – ammonium sulphate, pH9.0.

Incubation Temperature

15°C

Table 4.7. Crystallisation Trials showing the effect of varying the Protein Concentration. The morphology of all crystals was tabular plates.

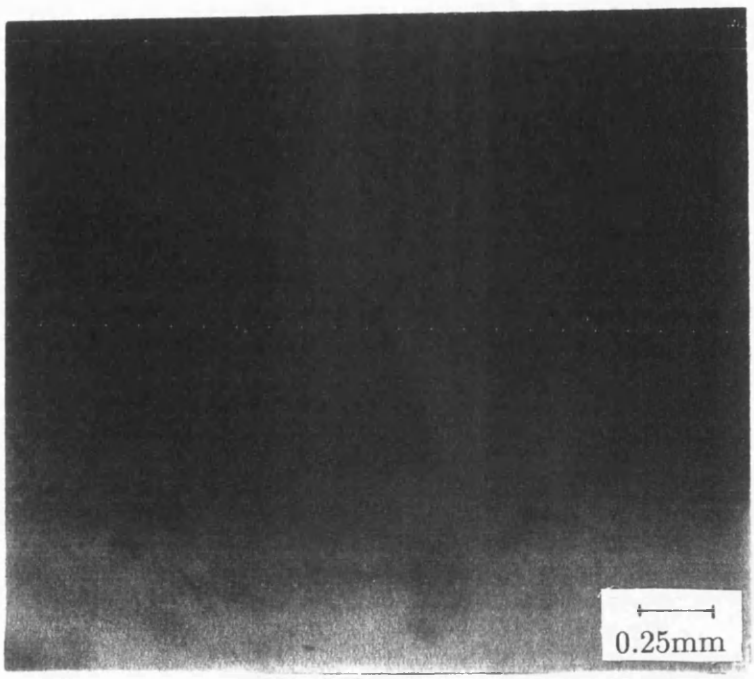

Figure 4.13. A Large Tabular Plate Crystal which grew using a protein concentration of 8mg/ml. This crystal diffracted X-rays to a resolution limit of 5Å.

The next set of trials concerned the effect of temperature on the speed of crystal formation (**Table 4.8**). Trials were set up at 6, 10, 15 and 20°C. At 20°C the time required for crystallisation was reduced from 3 months to approximately 6 weeks. Experiments by Mikol *et al.* (1989) have shown that the time taken for vapour diffusion to occur during crystallisation trials, was 1-3 days depending on the crystallisation system and temperature at which the experiments were performed. An increase in the rate of vapour diffusion is therefore not the cause of the decrease in crystallisation time.

At 20°C it is possible that the protein is less soluble than at lower temperatures hence it more quickly reaches the supersaturated state. It was not possible to use temperatures greater than 20°C because of the breakdown in stability of the antenna complex.

Trials were set up using finer increments of reservoir pH (9.0, 9.1, 9.2, 9.3, 9.4 and 9.5). This was found to have no effect on the size, shape or diffraction quality of crystals of the antenna complex.

The final two sets of crystallisation trials concerned changing the concentration of the small amphiphile and the concentration of di-potassium hydrogen orthophosphate in the drop. Trials were set up using 1M potassium phosphate, with different concentrations of benzamidine hydrochloride in the drop and a range of concentrations of ammonium sulphate in the reservoir (2.0–2.4M) (**Table 4.9**). Precipitation occured in all trials using 2% benzamidine hydrochloride.Raising the concentration to 3.0% meant that crystals of benzamidine hydrochloride began to form beside those of the antenna complex (**Figure 4.14**). Trials set up over a finer range of concentrations (2.1, 2.2, 2.3 and 2.4%) of benzamidine hydrochloride yielded no improvement in crystal diffraction.

The concentration of di-potassium hydrogen orthophosphate in the drop was varied between 0.8–1.2M (**Table 4.10**). This gave large tabular plate crystals in all trials. Changing the concentration of di-potassium hydrogen orthophosphate in the drop from 0.9M to 1.0M led to a decrease in the dimension of the *c* axis of the crystal (see **Section 5.2**). Crystal form #1 grew in the presence of 0.9M di-potassium hydrogen orthophosphate and crystal form #2 grew in the presence of 1.0M di-potassium hydrogen orthophosphate.

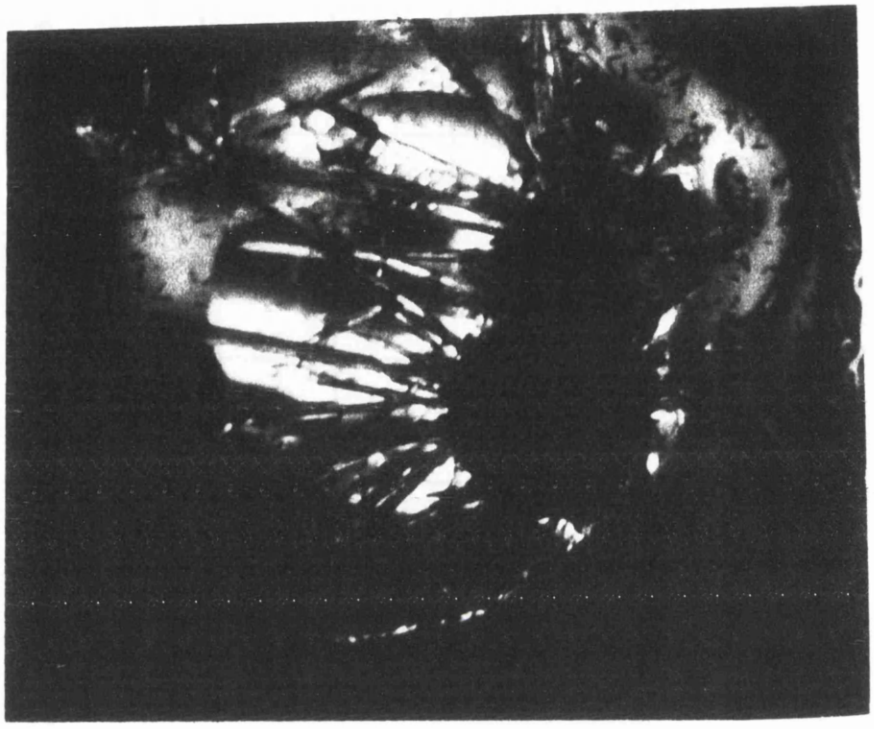

Figure 4.14. A photograph showing the formation of spike shaped crystals of benzamidine hydrochloride. These occured when the concentration of benzamidine hydrochloride was increased from 2.5 to 3.0%, and meant that only small microcrystals of the antenna complex were formed.

pH 9.0 Reservoir pH

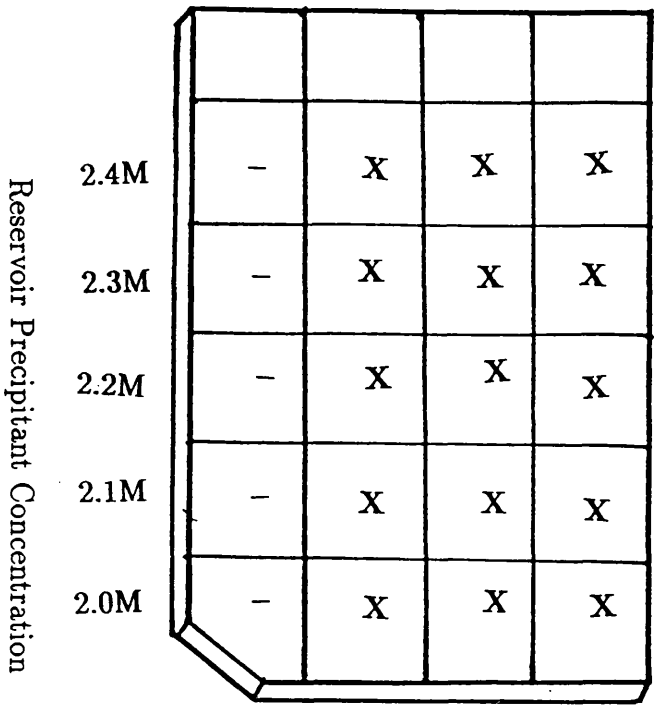

X – Crystal formation

– – No crystallisation after 1 year

Drop

Protein concn – 8mg/ml (Purity Index 3.0) in 20mM Tris-HCl, pH8.0

Detergent – 1% β octyl-glucoside

Precipitant – 1M di-potassium hydrogen orthophosphate

Amphiphile – 2.5% (w/v) benzamidine hydrochloride

Reservoir

Precipitant – ammonium sulphate, pH9.0.

Incubation Temperature

6, 10, 15, 20°C

Table 4.8. Trials set up to assess the effect of temperature on crystallisation.

pH 9.0 Reservoir pH

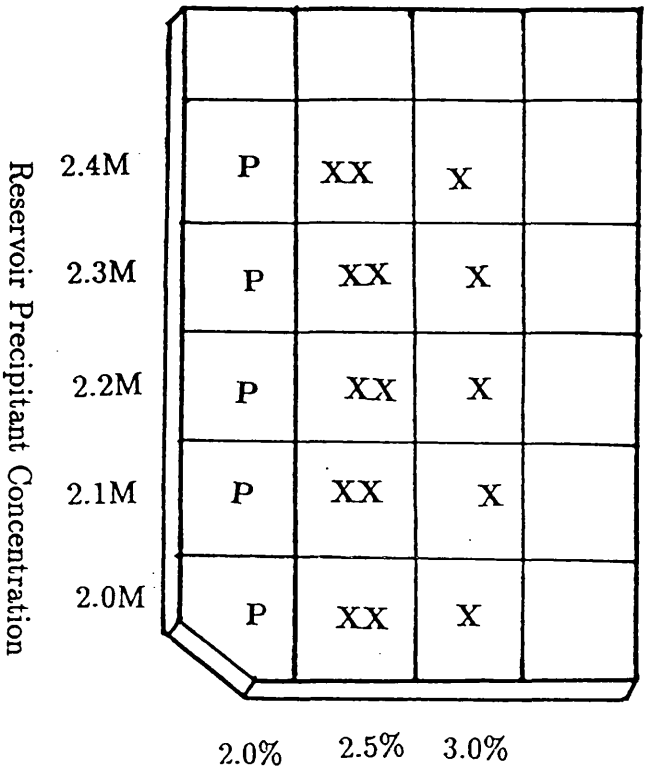

P – Precipitate

XX – Large crystal formation

X – Microcrystals of antenna complex

Drop

Protein concn – 8mg/ml (Purity Index 2.8) in 20mM Tris-HCl, pH8.0

Detergent – 1% β octyl-glucoside

Precipitant – 1M di-potassium hydrogen orthophosphate

Amphiphile – 2.0, 2.5, 3.0% (w/v) benzamidine hydrochloride

Reservoir

Precipitant – ammonium sulphate, pH9.0.

Incubation Temperature

20°C

Table 4.9. Variation in the concentration of benzamidine hydrochloride used as the small amphiphile.

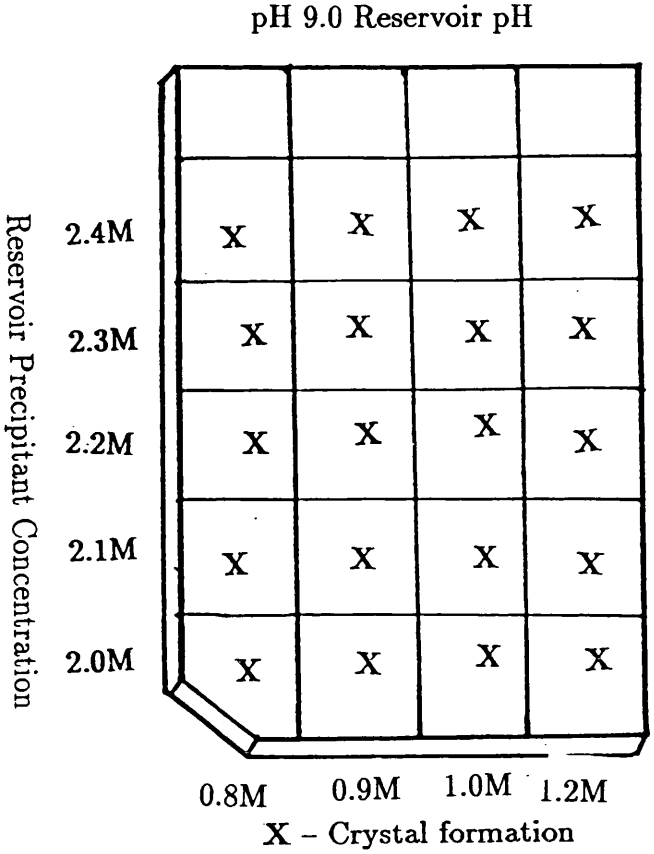

Drop

Protein concn – 8mg/ml (Purity Index 3.0) in 20mM Tris-HCl, pH8.0

Detergent – 1% β octyl-glucoside

Precipitant – 0.8M–1.2M di-potassium hydrogen orthophosphate

Amphiphile – 2.5% (w/v) benzamidine hydrochloride

Reservoir

Precipitant – ammonium sulphate, pH9.0.

Incubation Temperature

20°C

Table 4.10. Trials set up to assess the effect of changing the concentration of di-potassium hydrogen orthophosphate on crystallisation.

4.5. Review of Optimised Crystallisation Parameters and their Effect on X-ray Diffraction

The first parameters to be optimised were the protein purity index and protein concentration used in trials. It was found that a protein concentration of 8mg/ml gave the biggest tabular plate crystals with dimensions of 0.9mm x 0.4mm x 0.2mm. These crystals diffracted X-rays to 5Å resolution and were used in subsequent structural studies. The purity index of the protein was determined from the last detergent exchange step in the purification protocol and had no bearing on the X-ray diffraction quality of the crystals. The time taken for the formation of these large crystals was improved by slightly increasing the temperature of incubation from 15°C to 20°C, giving crystals in 6 weeks. Using reservoir ammonium sulphate concentrations of greater than 2.4M tabular plate crystals could be obtained more quickly than 6 weeks, but these were too small to be of any use in X-ray structural studies. This would be explained by the system quickly reaching the labile phase of supersaturation with the removal of protein from solution to form many nuclei. When the system returns to the metastable phase any remaining protein in solution is depleted during the growth of these nuclei. As a result of the numbers of nuclei, the growth of each is limited and the crystals remain very small. The longer period necessary for formation of fewer, larger crystals is due to the fact that the system only briefly enters the labile phase before it returns to the metastable phase. This would seem to occur using lower concentrations of ammonium sulphate in the reservoir. Attempts at "fine tuning" the reservoir pH made no difference to crystal size, shape or most importantly X-ray diffraction quality. It was also possible that LDAO (the detergent used to isolate the antenna complex) was

present and this was exerting a deterimental effect on crystallisation. In the final detergent exchange step of purification, the complex was washed with an increased volume of detergent free buffer (12ml) and also 1.5ml of buffer containing 0.5mM sodium dithionite which removes any traces of LDAO. Again this yielded no further improvement in the resolution of X-ray diffraction.

A slight change in the concentration of di-potassium hydrogen orthophosphate in the crystallisation drop from 0.9M to 1.0M, led to a decrease in the length of the c axis from 291.71Å to 283.1Å, suggesting tighter packing in the crystal.

In conclusion, the detergent β octyl-glucoside in conjunction with the small amphiphile benzamidine hydrochloride possesses the optimal micelle size for the B800–820 antenna complex. The time taken for crystal formation was decreased, and crystal size increased by optimisation of different physical parameters. This also led to a significant improvement in the resolution of X-ray diffraction from 10Å to 5Å.

CHAPTER 5. Preliminary X-ray Studies of the B800-820 Antenna Complex from *Rhodopseudomonas acidophila* 7750

5.1. Introduction

Although the three–dimensional structures of two types of bacterial reaction centre have been determined (Deisenhofer *et al.*, 1985, Michel *et al.*, 1986 and Allen *et al.*, 1987 (a) (b)), similar structural information is not yet available for antenna complexes. Crystallisations of several different antenna complexes have been documented (Cogdell *et al.*, 1985, Welte *et al.*, 1985, Wacker *et al.*, 1986 and Woolley *et al.*, 1986), but it is only recently that crystals which diffract X-rays to a resolution sufficient for the determination of a three-dimensional structure have been reported. Crystals of B800–850 antenna complexes from *Rhodopseudomonas acidophila* strain 10050 (Papiz *et al.*, 1989) and *Rhodospirillum molischianum* (Michel, 1991) diffract X-rays to a resolution of 3.5Å and 2.8Å respectively. A core antenna complex from a reaction centre deficient mutant strain of *Rb. Sphaeroides* (Nunn *et al.*, in press) also diffracts X-rays to 2.8Å resolution.

5.2. X-ray Diffraction Data from Crystal Form #1

X-ray diffraction data were collected on form #1 of tabular plate crystal as detailed in **Section 2.15 (iv)** (Crystallisation conditions **Section 4.4**). Using the *XENGEN* package (Howard *et al.*, 1987), this diffraction data indexed as a tetragonal cell with dimensions a=b=120.01Å and c=169.71Å. Statistical analysis of the integrated and scaled data gave an R factor;

$$\text{R factor} = \frac{\sum_i \mid I_{h,i} - \overline{I}_h \mid}{\sum_i I_{h,i}}$$

of 21.3%, which suggested this was not the correct cell. After re–examination of the list of trial vectors, a hexagonal cell similar to the cell

obtained for the B800–850 antenna complex from *Rhodopseudomonas acidophila* strain 10050 (Papiz *et al.*, 1989) was identified. This hexagonal cell had dimensions a=b=120.01Å and c=293.91Å, (cf. a=b=121.1Å and c=296.7Å, for the B800–850 antenna complex), and like the B800-850 antenna complex could be indexed as a rhombohedral cell with dimensions a=120.01Å, α=60°. Papiz *et al.* (1989) reported that this hexagonal crystal form of the B800–850 antenna complex exhibited pseudocubic symmetry and could also be indexed on a cubic face centred lattice of dimensions a=171.3Å. Following this approach a cubic face centred lattice of dimensions a=169.71Åwas constructed (**Figure 5.1**). In terms of a matrix transformation this conversion from a tetragonal to a cubic face centred cell is represented by the matrix in **Figure 5.2**.

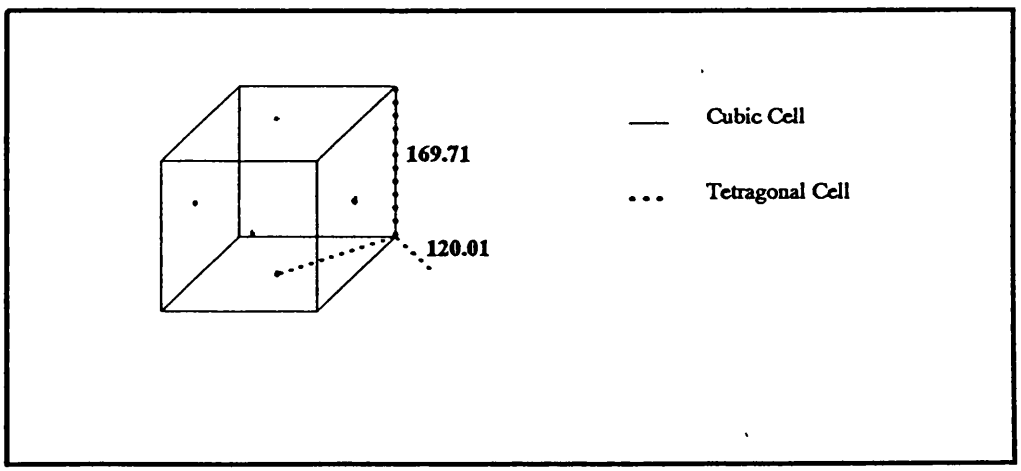

Figure 5.1 A cubic face centred cell of dimensions a=169.71Å, showing the tetragonal cell

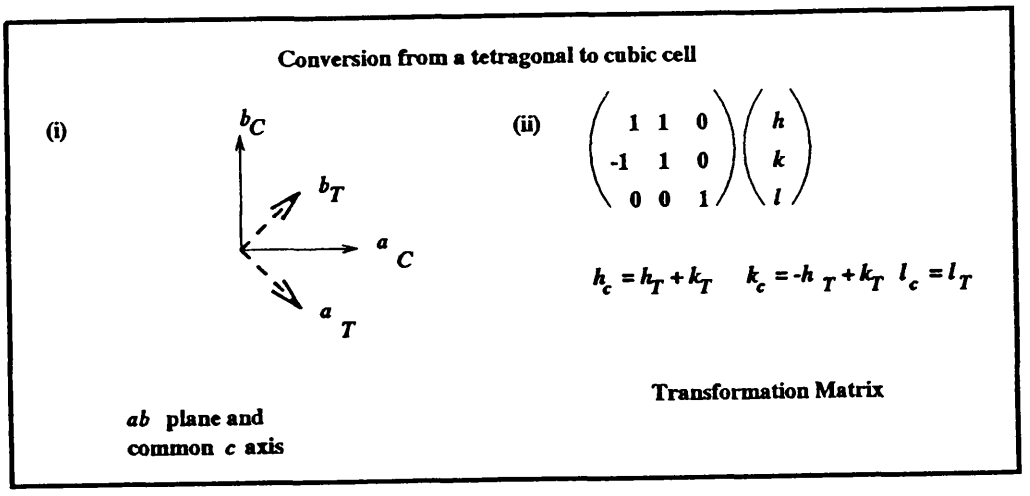

Figure 5.2 (i) Face Centred Cubic Lattice showing Tetragonal Axes. (ii) The matrix transformation for the conversion from a tetragonal (h_T k_T l_T)to a cubic cell (h_c k_c l_c).

The next step is to transform from the cubic to the rhombohedral cell (**Figure 5.3**).

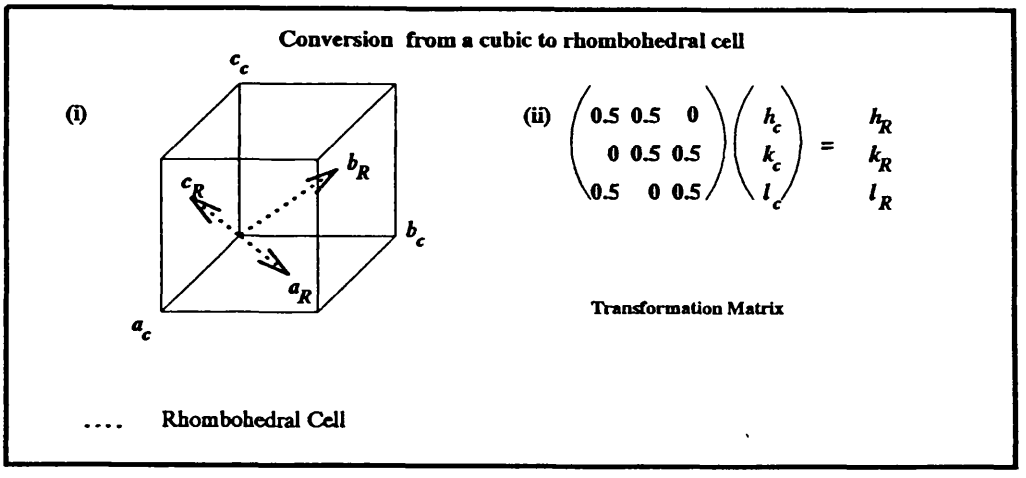

Figure 5.3 (i) Rhombohedral Cell Axes within the Cubic Cell. (ii) The transformation matrix for the conversion from a cubic (h_c k_c l_c) to rhombohedral (h_R k_R l_R) cell.

The final transformation is from a rhombohedral to a hexagonal cell using the matrix in Figure 5.4.

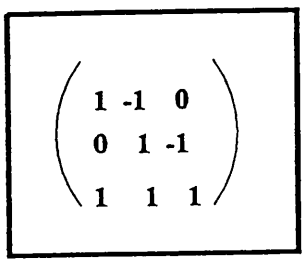

Figure 5.4 The Matrix for the Transformation from a Rhombohedral to a Hexagonal cell (from International Tables I, p21).

A summary of the matrice transformations for the conversion of a tetragonal to a hexagonal cell is shown in Figure 5.5.

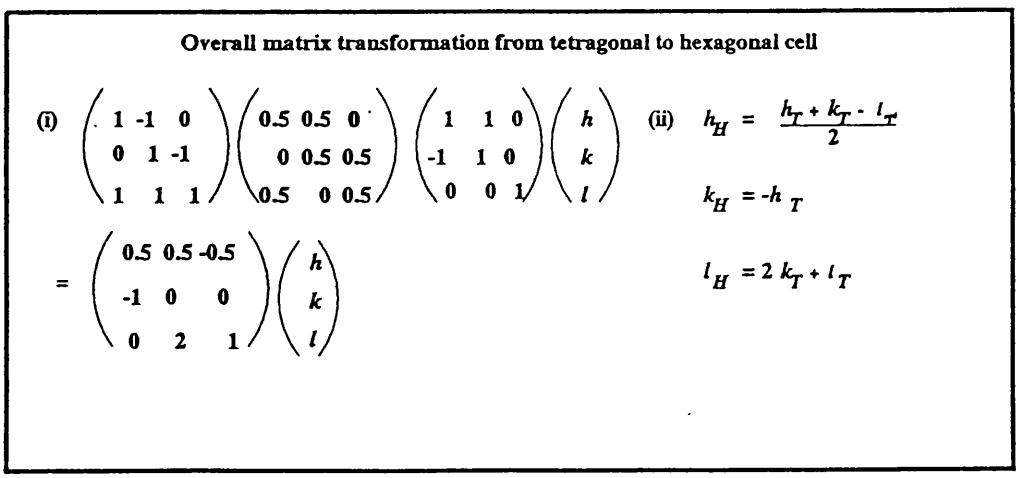

Figure 5.5 (i) A Summary of the Matrix Transformations required to convert from a Tetragonal to a Hexagonal Cell. **(ii)** This transformation in terms of indices.

REFINE, the autoindexing procedure in *XENGEN*, constructed an orthogonal trial vector set based on the halves of two face diagonals (a=b=120.01Å) and one cell edge (c=169.71Å) of this cubic lattice. This explains the initial misindexing of diffraction data. The correct hexagonal cell consists of halves of the two face diagonals (a=b=120.01Å) and a body diagonal (c=293.91Å).

A statistical analysis of X-ray diffraction data from crystal form #1 processed using *XENGEN* is presented in **Table 5.1.**

Dmin(Å)	AvI	σ_{mean}	R	No. Measurements	No. Reflections
7.76	58.25	19.35	7.13	2918	525
6.16	9.78	3.21	26.61	3120	432
5.38	9.41	1.83	38.29	3056	560
4.89	12.41	1.52	37.36	2714	482
4.54	11.53	1.11	41.26	1664	375
4.27	12.90	1.07	52.16	496	151
Total	19.85	5.20	18.89	14168	2525

AvI - Average intensity for all observations.

R- $\frac{\sum_i \mid I_{h,i} - \overline{I}_h \mid}{\sum_i I_{h,i}} * 100$

Table 5.1 Statistical Analysis of X-ray Diffraction Data from Tabular Plate Crystal #1 processed using *XENGEN*.

In view of the weakness of the intensity of diffraction data, the software package *XDS* was used to re–determine the integrated intensities of reflections. *XDS* uses a different procedure for determining the integrated intensities of reflections, which overcomes the difficulties in distinguishing between weak signal and background points within each reflection (**Section 2.16.**) (Kabsch, 1988). *XDS* chose a cell of a=b=120.8Å and c=293.1Å, with an R_{symm} of 9.9.

$$R_{symm} = \frac{\sum_i | I_{h,i} - \overline{I}_h |}{\sum_i I_{h,i}}$$

ROTAVATA was used to calculate scale and temperature factors between overlapping batches of data (Fox and Holmes, 1966). *AGROVATA* was then used to apply scale factors by *ROTAVATA*. A summary of *XDS* data scaled using *ROTAVATA/ AGROVATA* is presented in **Table 5.2.**

Dmin(Å)	AvI	σ_{mean}	R_{cum}	No. Measurements	No. Reflections
7.98	1615	121.8	0.046	1637	881
5.65	273	98.9	0.90	2360	1172
4.62	346	153.6	0.120	1427	710
4.00	162	65.2	0.120	8	4
Total	696	122.2	0.120	5432	2697

R_{cum} – R_{symm} up to each resolution range listed

Table 5.2 Summary of *XDS* Data Scaled using *ROTAVATA* and *AGROVATA* for Tabular Plate Crystal #1.

The trigonal space groups which can be indexed using rhombohedral axes are *R3*, *R$\bar{3}$*, *R32*, *R3m*, *R$\bar{3}$m*, *R3c* and *R$\bar{3}$c*. It is possible to determine the space group using equivalences in *|F(hkl)|* (symmetry of the reciprocal lattice). For the space groups *R3* and *R32*, these equivalences are the same as those for *P3*, and *P321* respectively. The equivalence *$\overline{h}$$\overline{k}$l=khl* is present in *P321*, but not in *P3*. Using this distinction it should be possible to discriminate between *R3* and *R32*, however this was not possible due to merging during processing of the diffraction data using *AGROVATA*. The data was assigned the space group *R3* and reprocessed using *ROTAVATA* and *AGROVATA*. Twice as many reflections were present in the output file of structure factors (**Table 5.3**). The equivalence *$\overline{h}$$\overline{k}$l=khl* is present in these extra reflections. R_{symm} was to be close to zero for each pair of reflections. This confirmed the space group as *R32*, which is the same space group as that obtained for the B800–850 antenna complex from *Rhodopseudomonas acidophila* strain 10050.

$\overline{hkl}$	Intensity	σ	khl	Intensity	σ
$\bar{1}$ 0 32	4408	90	0 1 32	4591	95
$\bar{1}$ 0 14	3518	63	0 1 14	3488	63
$\bar{2}$ 1 21	1530	40	$\bar{1}$ 2 21	1650	47
$\bar{3}$ 2 28	1700	64	$\bar{2}$ 3 28	1716	60
$\bar{1}$ 3 38	351	162	$\bar{3}$ 1 38	367	165
$\bar{1}$ 2 45	423	176	$\bar{2}$ 1 45	440	178

Table 5.3. A table showing the equivalence $\overline{hkl}$=khl which is present in the output file of structure factors.

5.3. X-ray Diffraction Data from Tabular Plate Crystal Form #2

X-ray diffraction data were collected on a second form of tabular plate crystal (see **Section 4.4**). A hexagonal lattice with cell dimensions a=b=122.97Å and c=284.95Å was observed. A statistical analysis of the data collected from crystal form #2 and processed using *XENGEN* is shown in **Table 5.4**. The intensities of this data were also reintegrated using *XDS*, which gave a hexagonal cell with dimensions a=b=121.8Å and c=283.1Å. This data was scaled using *ROTAVATA/AGROVATA*. A statistical analysis of these results is presented in **Table 5.5**. The space group for this second tabular plate form of crystal was also determined to be *R32*, by the same method used for crystal form #1.

Dmin($\AA$)	AvI	σ_{mean}	R	No. Measurements	No. Reflections
10.09	165.38	47.43	3.14	2432	465
8.01	20.71	9.12	13.29	2759	435
7.00	5.79	2.69	35.33	2776	525
6.36	1.52	0.79	63.67	2785	480
5.90	0.93	0.31	62.33	1535	432
5.55	1.22	0.46	43.41	463	200
Total	35.89	11.22	7.61	12750	2537

$$\text{R - R factor} = \left(\frac{\sum_i \mid I_{h,i} - \overline{I}_h \mid}{\sum_i I_{h,i}}\right) * 100$$

Table 5.4 A Statistical Summary of Diffraction Data from Crystal Form #2 Processed using *XENGEN*.

Dmin($\AA$)	AvI	σ_{mean}	R_{cum}	No. Measurements	No. Reflections
11.94	471	35.1	0.031	1402	772
8.47	108	12.1	0.042	2841	534
6.92	17	7.1	0.059	3651	800
6.00	8	6.9	0.069	2184	750
Total	104	15.5	0.069	10078	2856

R_{cum} - R_{symm} up to each resolution range listed

Table 5.5. Summary of Scaling using *ROTAVATA* and *AGROVATA* of Crystal Form #2.

5.4. A Comparison of Processed Diffraction Data from the Two Forms of Tabular Plate Crystal

There was a difference of approximately 10Å in the cell dimensions of crystal forms #1 and #2 and a slight difference in the lengths of the *a* and *b* axes. There was no tetragonal cell, similar to the lattice obtained for crystal form #1, present in the list of trial vectors generated using the *XENGEN* package for crystal form #2. Attempts to refine the cell a=b=120.01Å and c=293.91Å using diffraction data from crystal form #2 were unsuccessful. Given that the crystallisation conditions are slightly different, these two forms would seem to be distinct.

A comparison of the statistics from processing of the two crystal forms using *XENGEN* and *XDS/ROTAVATA/ AGROVATA* is shown in **Table 5.6.**

Crystal form	AvI	σ_{mean}	R	No. Measurements	No. Reflections	%Complete at 6Å
#1 Xen	19.85	5.20	18.89	14168	2525	87%
#1 XDS	696	122	12.00	5432	2697	93%
#2 Xen	35.89	11.22	7.61	12750	2537	87.5%
#2 XDS	104	15.5	6.9	10078	2856	98.5%

Table 5.6 Summary of diffraction data collected from the two crystal forms (#1 and #2).

Reprocessing the data from both crystal forms using *XDS* resulted in an increase in the average intensity and a decrease in the total R factor the

two data from the two crystal forms. Examination of the normalised three-dimensional reflection profiles produced by *XDS* showed that reflections lay centrally in each profile box. This was the case in both crystal forms. In view of the lower R factor, data processed using *XDS* was used in subsequent calculations.

5.5. Crystal Density Measurement

The densities of the two crystal forms were measured using aqueous Ficoll solutions (see **Section 2.17**) (Westbrook, 1985). The densities of both crystal forms were determined to be 1.17g/cm^3. A plot of results is presented in **Figure 5.6.**

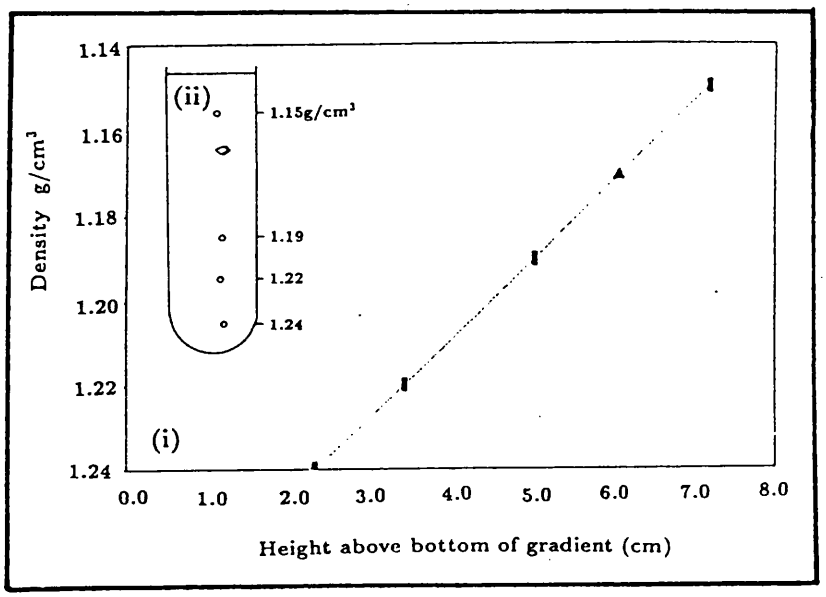

△ –Crystal Density

Figure 5.6. (i) Calibration Curve for Density Measurement using an Aqueous Ficoll solution. (ii) Schematic diagram of the centrifuge tube illustrating the relative height of the crystal (not shown to scale).

In a survey of different crystalline proteins whose molecular weights were known from other methods, it was found that the fraction of crystal volume occupied by solvent is usually near 43%, but may vary between 27% and

65% (Matthews, 1968). These values correspond to an average crystal volume per unit molecular weight (V_m= volume of asymmetric unit/molecular weight) of 2.4Å^3/Da with a variation of 1.68Å^3/Da to 3.53Å^3/Da. The computed V_m is 2.47Å^3/Da for crystal form #1 and 2.42Å^3/Da for crystal form #2, assuming a molecular mass of 83535 Da in the asymmetric unit with Z=18 (**Table 5.7**). These values fall within the range of values (1.7-5.5Å^3/Da) reported by Matthews (1977) and give solvent compositions of 49.8% for crystal form #1 and 50.2% for crystal form #2, using:

$$\%\text{solvent} = \frac{1.23}{V_m} X100 \qquad (Matthews, 1968)$$

	Apoprotein	Bchl	Carotenoid
Molecular Weight	α_1-5567Da*	911.5Da	554Da†
	α_2-5906Da*		
	β_1- 4721Da*		
	β_2- 4520Da*		
Per assembly of α_1 α_2 β_1 β_2 + 6BChl + 3 carotenoids			
27845Da			
Per trimer of this assembly			
83535Da			

*Determined from structure analysis (Brunisholz *et al.*, 1987)

*Determined from electrospray mass spectrometry

†Assume approximate molecular weight of carotenoid as lycopene (554 Da)

Table 5.7 The Molecular Weight of a Trimer of Apoproteins and Associated Pigments.

The equation shown below was used to calculate the density (ρ_{calc}) of the two crystal forms (Colman and Matthews, 1971, Matthews, 1985), in conjunction with the percentage solvent calculated above.

$$\rho_{calc} = \rho_{solvent}\ \ \phi_p\ (\bar{}^{1}\nu_p - \rho_{solvent})$$

ρ_{calc} - calculated density

$\rho_{solvent}$ - solvated density (assumed as 1.0g/cm^3 for H_2O)

$\bar{}^{1}\nu_p$ - partial specific volume of unsolvated protein (0.74g/cm^3)

ϕ_p - $(1-\frac{\%solvent}{100})$

Taking the solvent content as 0.498 for crystal #1 and 0.502 for crystal form #2 and substituting these into the equation above, gives a density (ρ_{calc}) for both crystal forms of 1.17g/cm^3. This is same density measured for each crystal form using the Ficoll method. These independent calculations of density indicate that the asymmetric unit of the B800–820 antenna complex is a trimer of molecular assemblies, with each assembly consisting of $\alpha_1\alpha_2\beta_1\beta_2$ apoproteins, six bacteriochlorophyll *a* and 3 carotenoid molecules. This is consistent with the stoichiometric ratio for bacteriochlorophyll *a*: carotenoid pigments of 2:1 derived in **Chapter 3.** The close similarity in the unit cell and space group of these protein crystals and crystals of the B800–850 antenna complex suggests a similar asymmetric unit in both cases. Papiz *et al.* (1989) propose an asymmetric unit containing six α/β–subunits, 18 bacteriochlorophyll *a* and nine carotenoid molecules.

There is a difference of 8465Da between the molecular weight of the trimer of molecular assemblies (83535Da) and the apparent molecular weight of the intact antenna complex determined from gel electrophoresis (M_{APP} of 92000Da). A difference was also reported in the molecular weights of the isolated *Rhodopseudomonas viridis* reaction centre complex (160–190000Da)(Clayton *et al.*, 1972, Thornber *et al.*, 1980) and the molecular weight of the complex determined using X-ray crystallography (145000 Da) (Deisenhofer *et al.*, 1989).

5.6. Introduction to the Patterson and Rotation Functions

5.6. (i) Introduction to the Patterson Function

The Patterson function (Patterson, 1934) is a convolution function which may always be calculated from a set of X-ray diffraction data.The expression used to calculate the Patterson function is shown below.

$$P(uvw)=\frac{2}{V}\sum_{h=\infty}^{\infty}\sum_{k=\infty}^{\infty}\sum_{l=0}^{\infty}F(hkl)^2\cos 2\pi(hu+kv+lw)$$

The Patterson function represents a map not of the individual atomic positions, but of the interatomic vectors. The Patterson summation always contains a large peak at the origin due to the superposition of all the self–self vectors $P(000)=\sum_{j=1}^{N} Z_j^2$.

In general if an atom i contains Z_i electrons and an atom j contains Z_j electrons then the peak in the Patterson summations which represents the vector between atoms i and j will have a weight proportional to Z_iZ_j.

The Patterson summation also contains a centre of symmetry at the origin although the structure itself may not be centrosymmetric. The value of the Patterson function at a position $\mathbf{u}_{12}$, which represents the vector from atom 1 to atom 2 is equal to the value of the function at -$\mathbf{u}_{12}$ which corresponds to the vector from atom 2 to atom 1. The centrosymmetric nature

of the Patterson synthesis implies that the space group of the synthesis is different from that of the real structure. The space group of the Patterson synthesis may be derived from the space group of the real structure by addition of a centre of symmetry, and the loss of the translational symmetry elements along screw axes or across glide planes. The corresponding Patterson symmetry for the space group *R32* is $R\bar{3}m$.

It is not possible to solve the structure of a protein from the Patterson function due to the complexity of the structure and because Patterson space is very much more crowded than Fourier space. If a structure contains N atoms per unit cell, then the numbers of vectors in the Patterson map is N^2, N of which are self–self vectors and superimpose at the origin. The remaining $N(N\text{-}1)$ vectors are distributed throughout the volume of the unit cell, which in a Fourier synthesis contains only N peaks. The possibility of recognising any detailed structural features in a protein Patterson is therefore unlikely. However some information can be extracted by means of the function which can be used to determine the relative orientations of subunits in an oligomeric protein.

The Patterson function forms the basis for the location of heavy atoms in the isomorphous replacement method.

5.6. (ii) Introduction to the Rotation Function

As the antenna complex exists as an oligomeric assembly it is useful to know the symmetrical relationship between sub-units in the asymmetric unit. This relationship is described in terms of non-crystallographic or local symmetry between these subunits. This information can be used later during interpretation of an electron density map or used in symmetry averaging procedures for the enhancement of available phases. The orientation of these local symmetry elements within the asymmetric unit is deduced

metry elements within the asymmetric unit is deduced using the Rotation function, originally developed by Rossmann and Blow, 1962.

$$R=\int_U P_2(X_2)P_1(X_1)\ dX_1$$

R – Rotation function

P_1 – Patterson function

P_2 – Rotated Patterson function

U – Volume of integration

The Patterson function contains sets of peaks representing intramolecular vectors (the self–vector sets) and also intermolecular vectors (the cross–vector sets). By rotating the Patterson function on top of a copy of itself, it is possible to determine the amount of overlap of one set of self vectors onto the other set. A maximum overlap of these sets will occur when they have the same orientation by means of a local symmetry axis.

POLARRFN, a fast Rotation function, which works in polar angles (**Figure 5.7**), was used to search for non-crystallographic symmetry within the asymmetric unit. Although slower in calculation than the Crowther fast Rotation function, *POLARRFN* is easier to interpret.

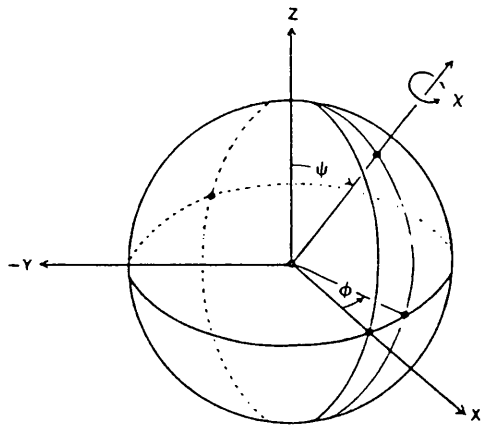

Figure 5.7. Definition of the Spherical Polar Angles used in the Program *POLARRFN*. The direction of the rotation axis is defined by the angle ψ, measured from the z axis, and by the angle ϕ measured in the xy plane from the x axis. The rotation itself is given by the spin χ about the axis.

5.7 The Search for Non-Crystallographic Axes of Symmetry

A search for local two fold axes was conducted for both crystal forms #1 and #2 keeping χ constant at 180° and altering ψ and ϕ. The initial resolution of data used was 10.0-6.0Å, with an integration radius of 4.2–30.0Å. This radius of integration was used to obtain only the self Patterson vectors. By taking the smallest integration radius as 4.2Å, the large peak corresponding to the origin is removed. The results for both crystal forms were identical. Eighteen peaks corresponding to crystallographic two fold symmetry axes were observed at ψ=90° and every 20° in ϕ (0°, 20° etc) with χ=180°. A peak corresponding to a non-crystallographic two-fold axis is present at ψ=0° ϕ=90° χ= 180°. This axis is parallel to the crystallographic c axis. As a check of the solutions integrity, the resolution range of data used was altered from 10.0–6.0Å to 15.0Å–6.0Å, with the same radius

of integration (4.2–30.0Å). There was no change in the number of observed peaks. Similarly there was no change on altering the integration radius range from 4.2–30.0Å to 4.2–25.0Å. A stereogram of the self rotation function illustrating section χ=180° is presented in **Figure 5.8** for crystal form #2.

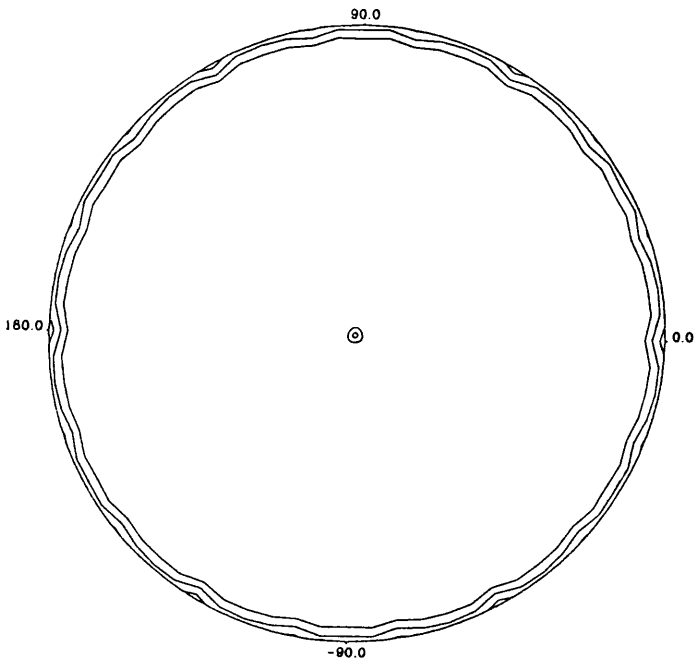

Figure 5.8. A Stereogram of the Self Rotation Function of Section χ=180° for Crystal Form #2. This section has ψ=0° at the centre, ψ=90° around the edge and ϕ around the periphery. The plot is contoured from a start level of 60, with a contour interval of 10.

A second search for local three fold symmetry was conducted keeping χ constant at 120° and altering ψ and ϕ. A stereogram plot of the self rotation function of section χ =120° is presented for crystal form #2 in **Figure 5.9.** Only a peak at ψ=0° ϕ=0° χ=120° corresponding to the crystallographic threefold axis is observed. It is possible that local threefold symmetry is present, but is obscured by the peak corresponding to the crystallographic

axis.

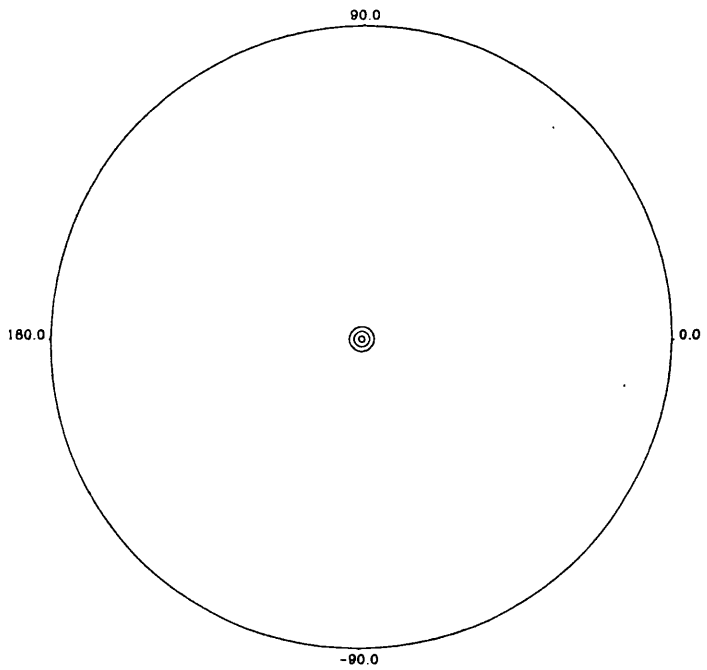

Figure 5.9. A Stereogram of the Self Rotation Function of Section χ=120° for Crystal Form #2. This section has ψ=0° at the centre, ψ=90° around the edge and ϕ around the periphery. The plot is contoured from a start level of 60, with a contour interval of 10.

5.8. A Model of the Asymmetric Unit of the B800–850 Antenna Complex

5.8 (i) Description of the Model

Papiz (unpublished results, 1990) has proposed a tentative model for the arrangement of the α–helices in the asymmetric unit of the B800–850 antenna complex from the 10050 strain of *Rhodopseudomonas acidophila.* This model is shown in **Figure 5.10.** A tetramer in this model consists of four parallel α-helices related by a local two fold symmetry axis parallel to the z axis. The asymmetric unit is composed of a trimer of these tetramers. These tetramers are related by a local three fold axis which is also parallel to the z axis. The distance between the centres of adjacent helices in the four helice bundle is 10.1Å. The distance between the centres of diagonally opposing α-helices in this four helice bundle is 16Å and the distance between the centres of each bundle equal to 24.5Å.

5.8 (ii) Consequences of this Model

An α-helix is a regularly repeating structure. If helices are aligned in parallel, as suggested in the model, then it is possible that peaks corresonding to interatomic vectors between these helices may appear in a Patterson map. α helices aligned in parallel along the z axis would give peaks which would be observed in the Patterson map at section z=0. In view of the number of subunits in the asymmetric unit of this model, non-crystallographic symmetry should be observed in plots of the rotation function. This symmetry may relate the positions of helices within bundles and/or between helice bundles.

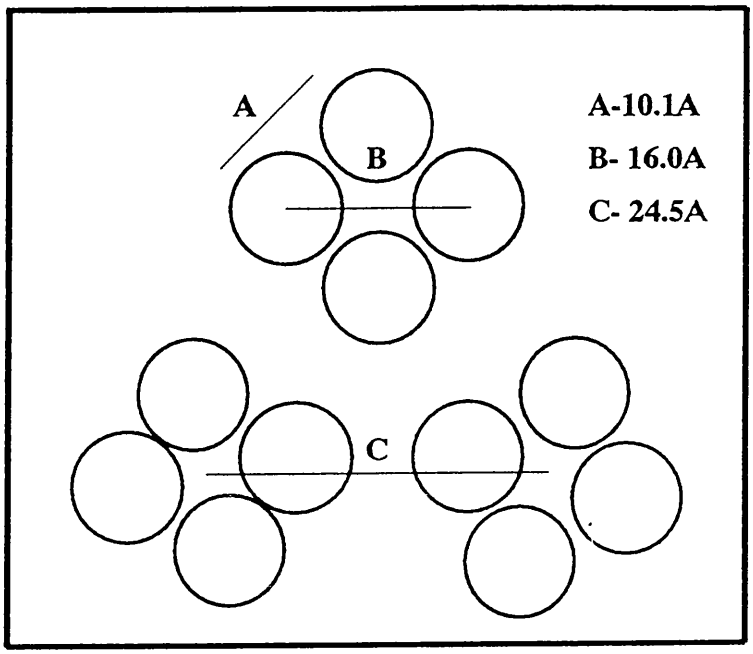

Figure 5.10 A Model for the Arrangement of α Helices in the Asymmetric Unit of the B800–850 Light-Harvesting Antenna Complex from *Rhodopseudomonas acidophila* Strain 10050. An α helix with its longest axis perpendicular to the plane of the paper, parallel to the membrane normal and the z axis is represented by a circle. The figure is not shown to scale.

5.9 Interpretation of Collected X-ray Diffraction Data for the B800–820 antenna complex

Earlier calculations show that the asymmetric unit of the B800–820 antenna complex is a trimer of tetramers related by local two-fold symmetry parallel to the z axis. Two possible arrangements of this trimer of tetramers are shown in **Figure 5.11.**

A map of the Patterson function was calculated at section z=0 using *FFT*. The number of sampling divisions (grid size) along the whole cell edge were taken as $\frac{1}{3}$ of the maximum resolution of X-ray diffraction data (6Å). The range of cell calculated was represented in terms of the asymmetric unit for the Patterson space group $R\bar{3}m$ ($0 \leq x \leq \frac{2}{3}$, $0 \leq y \leq \frac{2}{3}$, $0 \leq z \leq \frac{1}{6}$). The Patterson map was calculated using $P\bar{1}$ because of restrictions in calculating the map in the Patterson space group $R\bar{3}m$. The program *EXTEND* was used to generate more of the map calculated by *FFT*. The map was extended around the three fold axis using the symmetry operators $x\ y\ z$, $\bar{y}\ x\text{-}y\ z$ and $\bar{x}+y\ \bar{x}\ z$. An extended map of the z=0 section of the Patterson function of X-ray diffraction data from crystal form #2 is presented in **Figure 5.12.**

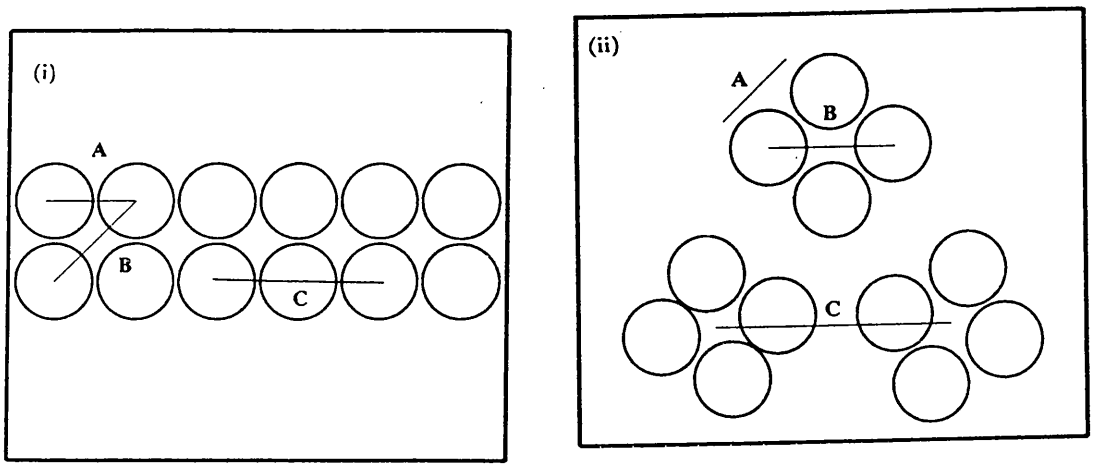

Figure5.11 Two possible arrangements of the trimer of tetramers of helices which display local two-fold symmetry parallel to the z axis. A circle represents an α helix with its longest axis perpendicular to the plane of the paper. **A** represents the distance between the centres of adjacent helices, **B** the distance between the centres of diagonally opposing helices and **C** the distance between the centre of each four helix bundle.

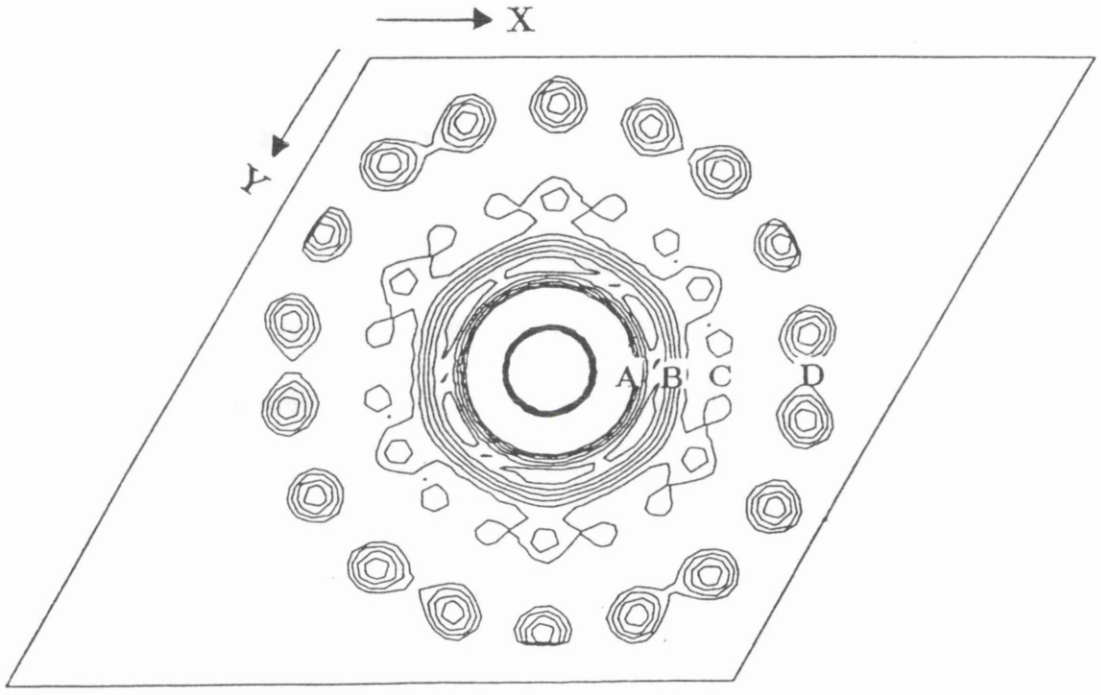

Figure 5.12. A map of the z=0 section of the Patterson function for Crystal Form #2. The map is contoured from 70 to 140 with intervals of 10 (Standard deviation 35.3). This map was calculated using data to a resolution of 6.0Å. The peaks at **D** have not been interpretated. Scale 1mm/Å.

By measuring the distance from the origin to each set of peaks it is possible to calculate the length of interatomic vectors. The first set of peaks is observed in the Patterson map at 11Å(**A**. The approximate distance between α helices was measured from a helix bundle in Phospholipase A_2 (Brunie *et al.*, 1985), as 10.8Å. Peaks corresponding to interatomic vectors between the centres of adjacent helices would appear at this distance (see **A** in **Figure 5.11**). The distance between diagonally opposing helices in this tetramer (see **B** in **Figure 5.11**) is 15.2Å. This is reflected in the Patterson map with a set of peaks at 15Å. Interatomic vectors between the centre of tetramers arranged as shown in the model in **Figure 5.11 (i)** would have a length of 21.6Å. These peaks are not observed in the Patterson map, but a third set of peaks is observed at 23Å. It is possible that this set of peaks is consistent with the interatomic vector lengths between the centres of tetramers arranged as in the model in **Figure 5.11 (ii)**. This is a more likely arrangement for the asymmetric unit, given the overall similarity between the B800–820 and the B800–850 antenna complexes and the stoichiometry of the chromophores. A Patterson map of the z=0 section of the B800–850 antenna complex is compared with the z=0 section of the Patterson map calculated for the B800–820 antenna complex in **Figure 5.13.** The map for the B800–850 antenna complex was calculated using data to a resolution of 4.5Å, with the map for the B800–820 antenna complex calculated using 6Å resolution data. Peaks corresponding to vectors between tetramers of helices are found at a distance of 24.5Å from the origin (c.f 23Å for the B800–820 antenna complex. This suggests that the B800-820 antenna complex may be slightly more closely packed.

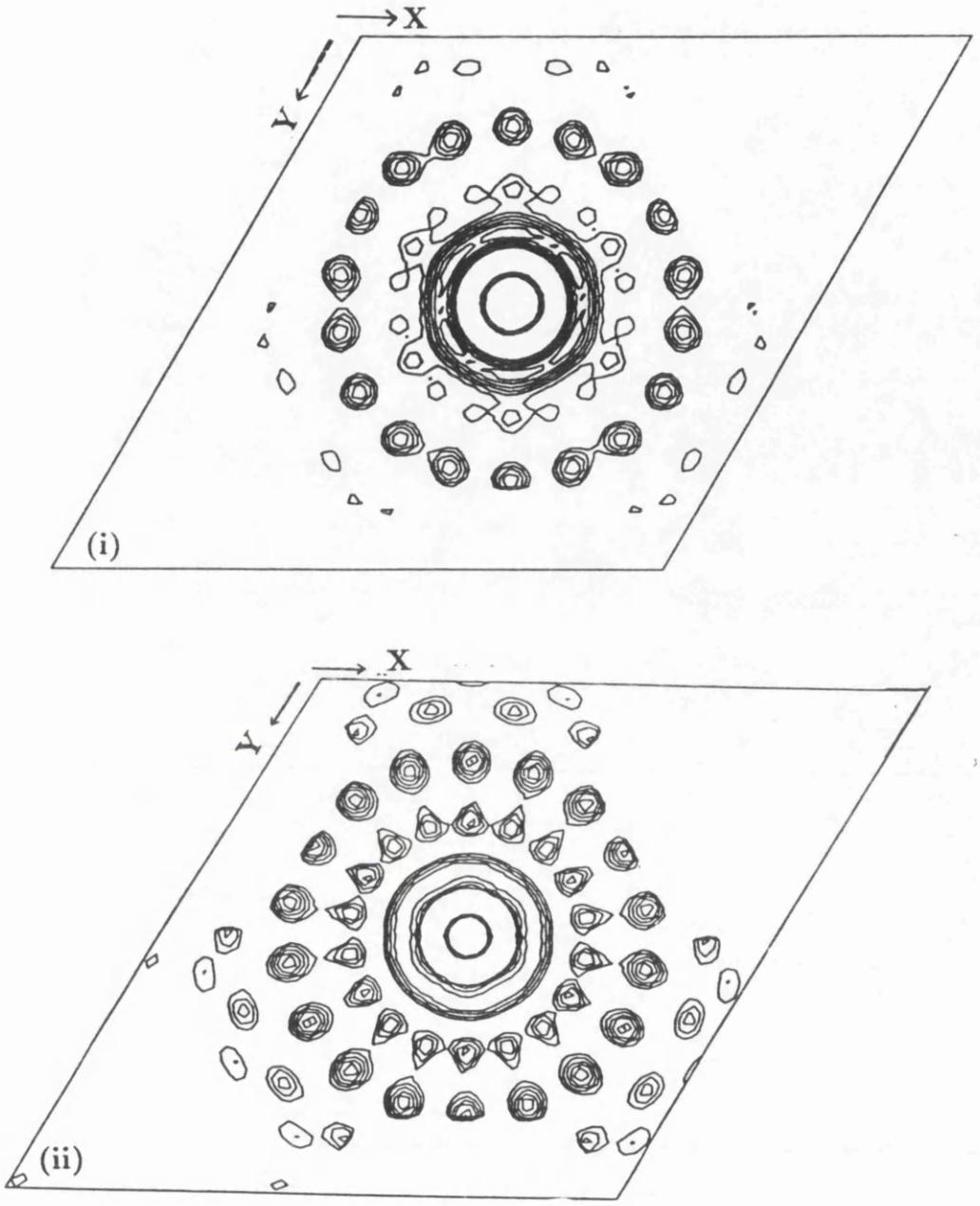

Figure 5.13 **(i)** A map of the z=0 section of the Patterson map for crystal form #2. The map is contoured from 70 to 140 with intervals of 10 (Standard deviation 35.3). **(ii)** A map of the z=0 section of the Patterson map for the B800–850 antenna complex from *Rhodopseudomonas acidophila* strain 100050. The scale of both maps is 0.7mmÅ.

5.10 Summary

X-ray diffraction data were collected on two forms of tabular plate crystal (#1 and #2). Crystal form #1 was initially indexed as a tetragonal cell. Statistical analysis of the integrated and scaled data gave a high R factor which suggested this was not the correct cell. Re–examination of the list of trial vectors gave a hexagonal cell with similar dimensions to the B800–850 antenna complex from *Rhodopseudomonas* strain 10050. This cell could also be indexed as a rhombohedral lattice with α=60°. Like the B800–850 antenna complex, crystal form #1 of the B800–820 antenna complex exhibited pseudo–cubic symmetry. It was possible to transform from the tetragonal lattice to a hexagonal lattice via a cubic intermediate. This pseudosymmetry led to the initial misindexing of the cell.

Crystal form #2 also had a hexagonal cell, but the *c* axis of this cell was 10Å shorter than the *c* axis in crystal form #1. Cubic pseudosymmetry was not present in this second crystal form.

It was not possible to determine the space group of both crystal forms by examination of the systematic absences because these are equivalent for the trigonal space groups in question. The equivalence $\overline{h}\overline{k}l$=*khl* was present in the output file of extra reflections, which remained after processing the X-ray diffraction data in the space group *R3* using *AGROVATA*. This confirmed the space group as *R32*.

The crystal density of both crystal forms was determined to be 1.17g/cm^3 using the Ficoll method. Assuming a molecular mass of 83.5kDa in the asymmetric unit, gave a computed V_m (volume of asymmetric unit/molecular weight) of 2.47Å^3/Da and 2.24Å^3/Da for crystal form #1 and #2 respectively. These V_m values gave solvent compositions of 49.8% for crystal form #1 and 50.2% for crystal form #2. These values are within

the range of values reported by Matthews (1977).

By recalculating the density from the solvent content, the density of the crystal in each crystal form was found to be 1.17g/cm^3. These independent calculations of density indicate that the asymmetric unit of the B800–820 antenna complex is a trimer of molecular assemblies with each assembly consisting of $\alpha_1\alpha_2\beta_1\beta_2$ apoproteins, 6 bacteriochlorophyll *a* molecules and 3 carotenoids.

The rotation function shows the presence of a local two–fold axis which is parallel to the *z* axis. Analysis of the rotation function for local three–fold symmetry gave a peak corresponding to the crystallographic three–fold axis parallel to the *z* axis. If local three-fold symmetry is present and parallel to the *z* axis then it would be obscured by this peak.

In view of the chromophore stoichiometry and the results of X-ray diffraction data, a tentative model for the arrangement of α–helices in the asymmetric unit was proposed. This is similar to the model proposed by Papiz (unpublished results, 1990) for the B800–850 antenna complex from *Rhodopseudomonas acidophila* strain 10050. The close similarity in molecular weight, crystal density, unit cell dimensions and space group suggests a similar asymmetric unit in both the B800–820 and the B800–850 antenna complexes.

CHAPTER 6. Summary and Discussion

6.1. Summary and Discussion

The first steps in photosynthesis are mediated by pigment–protein complexes in the photosynthetic membrane. In order to understand how these light–harvesting antenna complexes capture and transfer light at a molecular level, it is necessary to use X-ray crystallography to determine the three-dimensional structures of such complexes at atomic resolution. This would then give further insight as to why some species of purple bacteria possess the ability to synthesise different types of additional light–harvesting complexes.

An example of such a complex is the B800–820 light-harvesting antenna complex from the 7750 strain of *Rhodopseudomonas acidophila*, which is synthesised in response to temperatures of 20-25°C and low light intenstity (Gardner A.T., (1992), Personal communication).

An investigation into the structure and function of the B800–820 light–harvesting antenna complex from the 7750 strain of *Rhodopseudomonas acidophila* requires the isolation of a pure antenna preparation. The isolation procedure was described in **Chapters 2** and **3** of this thesis. The purified antenna complex displayed the same absorption maxima as the whole cells from which it was derived. This is a clear indicator that the native structure had been retained during isolation and purification. Secondary structural analysis of the native, purified antenna complex in **Chapter 3**, using ultra violet circular dichroism, confirmed the presence of α helix which had been suggested from primary structural analysis (Bissig, 1988). Infrared circular dichroism spectroscopy showed that carotenoid pigments in the antenna complex are influenced by their environment and show strong, induced optical activity. The circular dichroism spectra of the near infrared region showed a strong bacteriochlorophyll *a* Q_y absorption which differed from

the observed absorption of bacteriochlorophyll *a* in organic solvent. This may be due to the environment in which the bacteriochlorophylls are situated or possibly interactions between them (exciton coupling). Similar near infrared CD absorption has also been reported for other species of purple photosynthetic bacteria (Cogdell *et al.*, 1985). Both ultra violet and infrared circular dichroism spectra demonstrated that exchanging the antenna complex into different detergents had no deterimental effect on conformation of the antenna complex.

After isolation of the native, detergent–exchanged antenna complex, both pigment and protein content in the complex was assessed. The stoichiometric ratio of bacteriochlorophyll *a*: carotenoids was determined to be 2:1, which is is the same ratio obtained for purified chromatophores containing B800–820 antenna complex from *Rhodopseudomonas acidophila* strain 7750 by Evans in 1989.

The polypeptide composition of the antenna complex was investigated using tricine SDS polyacrylamide gel electrophoresis, which overcomes the problems associated with traditional SDS PAGE, in the examination of low molecular weight polypeptides. After denaturation of the antenna complex two sets of two bands were observed, which corresponded to the so-called α and β apoproteins. The presence of these apoproteins (α_1, α_2,β_1 and β_2) was confirmed by reverse phase HPLC (Zuber, H., (1992), Personal communication). The M_{APP}s of these polypeptides were determined to be 2550, 3350, 6300 and 6500 Da. Although three of these apoproteins have been sequenced (Bissig, 1988), the amphiphilic nature of these proteins means that their apparent molecular weight (M_{APP}) differs from the weight determined using primary structure analysis (α_1 5567 Da, α_2–not determined,β_1 4721 Da and β_2 4520 Da) . This makes it impossible to assign specific bands

on the gel to specific peptides. Electrospray ionisation mass spectrometry indicated that the molecular weight of the α_2 apoprotein (5906 Da) may be greater than any of the molecular weights reported for the other α/β apoproteins. A lack of time hampered a thorough investigation of this method. Further work would concern the optimisation of a suitable carrier solvent to prevent precipitation of the protein on injection and also to assess the effects of salt on the analysis, which would then enable the examination of the contents of a solution containing re-dissolved crystals.

The undenatured complex migrated on an SDS gel as a pigmented band with an apparent molecular weight of approximately 92kDa, which shows that the complex exists as an aggregate of the four apoproteins together with associated pigments. This is in the range of molecular weights reported for native antenna complexes and similar to 84kDa reported for the B800-850 antenna complex from the 10050 strain of *Rhodopseudomonas acidophila* (Papiz *et al.*, 1989). The smallest possible structural unit consists of an $\alpha_1\alpha_2\beta_1$ β_2 which binds six bacteriochlorophyll *a* molecules and three carotenoid molecules. The smallest oligomeric assembly, consistent with the apparent molecular weight of 92kDa is a trimer of this structural unit.

As a prerequisite to crystallisation trials, the stability of the antenna complex was determined with respect to different physical parameters (**Chapter 4**). The most important of these were found to be temperature and pH. The antenna complex was stable at a pH of 8.5 or greater, and temperatures of less than 25°C. Small amphiphiles were also added to the protein and shown to have no effect on protein integrity. The precipitation point using the inorganic salt di-potassium hydrogen orthophosphate was determined to be approximately 1M, and 10% for polyethylene glycol 6000. This precipitation point was raised upon addition of benzamidine hydrochloride

as detailed in **Chapter 4** .The effects of detergent were previously examined in **Chapter 3**, with the antenna complex stable in all of the detergents used. There was a slight change in the relative heights of absorbance of the two bacteriochlorophyll Q_y bands at 800 and 820nm after exchange into the alkyl glucoside detergents, which could be reversed by re–exchanging the complex back into LDAO. This transitory effect may arise because of subtle local changes in the conformation of bacteriochlorophyll. Sodium dodecyl sulphate was not used due to its strongly denaturing effects on this class of complexes (Cogdell *et al.*, 1991).

Trials were initially undertaken using different inorganic salts and the organic polymer polyethylene glycol 6000 as precipitants, in the presence of the detergent β–octyl glucoside. Small crystals were only obtained using a combination of di-potassium hydrogen orthophosphate in the drop in the presence of a small amphiphile, concentrated against a reservoir of ammonium sulphate at pHs of 9.0 and 9.5. Small crystals were obtained in all detergents in the presence of benzamidine hydrochloride, except the bile salt derivatives CHAPS and CHAPSO. It has been reported that these detergents may be better suited to membrane proteins of eukaryotic origin (Hjemeland *et al.*, 1983). Changing the small amphiphile to piperidine 2-carboxylic acid only enabled the growth of crystals using LDAO. The small amphiphile heptane-1, 2, 3-triol, used successfully in the crystallisation of the photosynthetic reaction centre from *Rhodopseudomonas viridis* (Michel, 1982), failed to yield any crystals of the B800–820 light–harvesting antenna complex. Alkyl glucoside detergents with different chain lengths were used to determine the optimal micelle size for formation of protein-protein contacts, which occurs during the process of crystallisation (Michel, 1983). It would seem from these studies that β octyl–glucoside possesses micelles of

the correct diameter. The importance of the alkyl chain length was also observed during crystallisation of the photosynthetic reaction centre from *Rhodopseudomonas viridis* (Michel, 1983). The photosynthetic reaction centre could not be crystallised when *N*,*N*-dimethyldodecylamine-*N*-oxide was replaced by *N*,*N*-dimethyldecylamine-*N*-oxide. Even replacement of the former detergent by the latter in the crystals by soaking led to disorder. The effect of the small amphiphile must however also be considered. Using SANS (small angle neutron scattering) it has been demonstrated that the overall diameter of the LDAO micelle was reduced with increasing concentration of heptane-1, 2, 3-triol (Timmins *et al.*, 1991). Benzamidine hydrochloride may be exerting a similar effect on the β–octyl glucoside micelles. By repeating the SANS experiments it would be possible to clarify this. It is possible that benzamidine hydrochloride might replace detergent molecules at positions critical for the formation of a crystal lattice (Michel & Oestorhelt, 1980, Garavito & Rosenbusch, 1980). Specific interactions of benzamidine hydrochloride with the antenna complex are also possible. This is indicated again from studies on the photosynthetic reaction centre, which would crystallise only in the presence of the *threo*-form of heptane-1, 2, 3-triol, but not the *erythro*-form (Michel, 1991).

Crystals which diffracted X-rays to low resolution could be grown only in the presence of the detergents β–octyl glucoside and NAD. Large crystals grown using NAD diffracted X-rays to a resolution of 15Å. β–octyl glucoside yielded small crystals which diffracted to a superior resolution of 10Å. These crystals were the subject of an optimisation to obtain an improvement in the resolution of X-ray diffraction.

The first crystallisation parameters to be optimised were the protein purity index and protein concentration used in trials. It was found that a

protein concentration of 8mg/ml gave the biggest tabular plate crystals with dimensions of 0.9mm X 0.4mm X 0.2mm. These crystals diffracted X-rays to 4.27Å resolution and were used in subsequent structural studies (crystal form #1). By changing the concentration of di–potassium hydrogen orthophosphate used in the drop from 0.9 to 1.0M a slight change in the unit cell was observed, but there were no noticable changes in the crystal dimensions or habit (Crystal form #2). The purity index of the protein, determined from the last detergent exchange step in the purification protocol had no bearing on the X-ray diffraction quality of the crystals. The time taken for the formation of these large crystals was improved by slightly increasing the temperature of incubation from 15°C to 20°C, giving crystals in 6 weeks. This is due to an increase in the speed of vapour diffusion. Attempts at "fine tuning" the reservoir pH made no difference to crystal size, shape or most importantly X-ray diffraction quality.

No attempt was made in this project to determine if residual LDAO was still present in the final detergent–exchanged protein. This could be easily qualified by isolating the B800–820 antenna complex using radioactively labelled [^{13}Carbon] LDAO and monitoring the removal of the radioactively labelled detergent during the concentration and detergent–exchange step.

Due to the length of time needed for the preparation of protein samples for crystallisation, the range of detergents and small amphiphiles used in this study were by no means exhaustive. Future work would enable both the range of small amphiphiles and classes of detergents used e.g polyoxyethylenes to be extended.

Crystallographic studies of the B800–820 light–harvesting antenna complex were described in **Chapter 5**. X-ray diffraction data were collected on two forms of tabular plate crystal (#1 and #2). Crystal form #1 showed

pseudosymmetry similar to that obtained for the B800–850 antenna complex from the 10050 strain of *Rhodopseudomonas acidophila*, leading to an initially mis-indexed cell which was subsequently indexed correctly as a hexagonal cell. This pseudosymmetry was not present in the second crystal form (#2) which was also 10Å shorter in the *c* axis than crystal form #1. This difference suggests a tighter packing of the complex in the second crystal form. Both crystal forms belonged to the space group *R32*.

The crystal density of both crystal forms was determined to be 1.17g/cm^3. Assuming a molecular mass of 83.5kDa (trimer of tetramers together with associated photosynthetic pigments) in the asymmetric unit gives a V_m of 2.47Å^3/Da and 2.42Å^3/Da for crystal forms #1 and #2 respectively. The V_m values give solvent compositions of 49.8% for crystal form #1 and 50.2% for crystal form #2. These values are within the range of values reported by Matthews (1977). Using the percentage solvent, the density was back calculated as 1.17g/cm^3. This indicates that the antenna complex exists as a trimer of tetramers. This is consistent with the stoichiometric ratio obtained for bacteriochlorophyll *a*: carotenoid.

The close similarity in unit cell, space group and also the z=0 section of the Patterson map of the B800–820 and B800–850 antenna complexes suggests a similar asymmetric unit in both cases. The Patterson map shows regular ordering of distinct sets of peaks, with interatomic vector lengths consistent with distances between α helices arranged as a trimer of tetramers. Analysis of plots of the Rotation function indicated the presence of a non-crystallographic two-fold axis parallel to the z axis (ϕ=0°,ψ=0°, χ=180°). This local axis may relate helices in the individual tetramers. Analysis of a plot of the Rotation function for three-fold symmetry indicated a peak corresponding to a crystallographic three-fold axis parallel to

the z axis (ϕ=0°,ψ=0°, χ=120°). If local three-fold symmetry is present then it is at a few degrees or parallel to this z axis.

On the basis of both the biochemical and crystallographic data a similar model to that obtained for the B800–850 light–harvesting antenna complex from *Rhodopseudomonas acidophila* strain 10050 was postulated. This model can only be verified by determining the structure of the B800–820 antenna complex at high resolution. There are several options available to pursue this. The first is to use isomorphous replacement and the Patterson function to determine the phases of reflections. Although a lack of time prevented any more progress in this area, initial heavy atom trials indicated that the B800–820 antenna complex was stable in the same solutions as the B800–850 light–harvesting antenna complex. This would facilitate a quick cross-section of heavy atom soaking conditions. Determination of an initial set of phases using isomorphous replacement could then be combined with molecular averaging using non- crystallographic symmetry to improve the quality of these phases. At low resolution (6Å) it would be possible to use diffraction data collected on the B800-850 antenna complex to obtain an initial set of phases. At this resolution one would hope to see rod-like regions in the electron density map corresponding to α helices.

Given the similarity between the B800–820 antenna complex and the B800–850 antenna complex, molecular replacement would be a second option for phase determination. This approach was used to show that the structures of the photosynthetic reaction centres from *Rhodobacter sphaeroides* and *Rhodopseudomonas viridis* were homologous (Allen *et al.*, 1986), (Chang *et al.*, 1986).

Aagaard, J. & Sistrom, W.R. (1972). Control of synthesis of reaction center bacteriochlorophyll in photosynthetic bacteria. *Photochem. Photobiol.* **15**, 209–225.

Allen, J.P., Feher, G., Yeates, T.O., Komiya, H. & Rees, D.C. (1987a). Structure of the reaction centre from *Rhodobacter sphaeroides*: the protein subunits. *Proc. Natl. Acad. Sci. USA.* **84**, 5730–5734.

Allen, J.P., Feher, G., Yeates, T.O., Komiya, H. & Rees, D.C. (1987b). Structure of the reaction centre from *Rhodobacter sphaeroides*: the protein subunits. *Proc. Natl. Acad. Sci. USA.* **84**, 6162–6166.

Allen, J.P., Feher, G., Yeates, T.O., Komiya, H. & Rees, D.C. (1988). In *The photosynthetic bacterial reaction centre* NATO AS1 Series A: Life sciences (Breton, J. & Vermeglio, A., eds) pp. 5–72 Plenum Press, New York.

Bissig, I., Wagner-Huber, R.V., Brunisholz, R.A. & Zuber, H. (1990). Multiple antenna complexes in various purple photosynthetic bacteria. In *Molecular biology of membrane-bound complexes in phototrophic bacteria* (Drews, G. and Dawes, E.A. eds) pp. 161–180. Plenum Press, New York.

Blundell, T.L. & Johnson, L.M. (1976). Crystallisation of proteins. In *Protein Crystallography* pp 59–82. Academic Press, London.

Bolotina, I.A., Chekov, V.O., Lugauskas, V.Y. & Pisyn, O.B. (1981). Determination of the secondary structure of proteins from circular dichroism spectra. III. Protein derived reference spectra for antiparallel and parallel β structures. *J. Mol. Biol.* **15**, 130–137.

Breton, J. & Nabedryk, E. (1984). Transmembrane orientation of α-helices and organisation of chlorophyll in photosynthetic pigment-protein complexes. *FEBS Lett.* **176**, 335–359.

Breton, J., Martin, J.L., Migus, A., Antonetti, A & Orzag, A. (1986). Femtosecond spectroscopy of excitation energy transfer and initial charge separation in the reaction centre of the photosynthetic bacterium *Rhodopseudomonas viridis. Proc. Natl. Acad. Sci. USA.* **83**, 5121–5125.

Bril, C. (1958). Action of a non-ionic detergent on chromatophores of *Rhodopseudomonas sphaeroides. Biochim. Biophys. Acta*, **29**, 458.

Broglie, R.M., Hunter, C.N., Delepelaire, P., Niederman, R.A., Chua, N.-H. & Clayton, R.K. (1980). Isolation and characterisation of the pigment-protein complexes of *Rhodobacter sphaeroides* by lithium dodecyl sulfate. *Proc. Natl. Acad. Sci. USA.* **77**, 87–91.

Brunie, S., Bolin, J., Gewirth, D. & Sigler, P.B. (1985). The refined crystal structure of dimeric phospholipase A_2 at 2.5Å. *J. Biol. Chem.* **260**, 9742–9749.

Brunisholz, R.A., Cuendet, P.A., Theiler, R. & Zuber, H. (1981). The complete amino acid sequence of the single light-harvesting protein from chromatophores of *Rhodospirillum rubrum* G9$^+$. *FEBS Lett.* **129**. 150–154.

Brunisholz, R.A., Suter, F. & Zuber, H. (1984). The light-harvesting polypeptides of *Rhodospirillum rubrum. Hoppe-Seyler's Z. Physiol. Chem.* **365**, 675–688.

Brunisholz, R.A., Zuber, H., Valentine, J., Lindsay, J.G., Woolley, K. J. & Cogdell, R.J. (1986). The membrane location of the B890-complex from *Rhodospirillum rubrum* and the effect of carotenoid on the conformation of its two apoproteins exposed at the cytoplasmic surface. *Biochem. Biophys. Acta* **849**, 295–303.

Brunisholz, R.A., Bissig, I., Niederer, E., Suter, F. & Zuber, H. (1987). Structure studies on the light-harvesting polypeptides of *Rhodopseudomonas acidophila.* In *Progress in Photosynthesis Research II* (Biggins, J., ed.) Martinus Nijhoff, The Netherlands.

Chang, C.H., Tiede, D., Tang, J., Smith, U., Norris, J. & Schiffer, M. (1986). Structure of the reaction center from *Rhodobacter sphaeroides* R–26. *FEBS Lett.* **205**, 82–86.

Chang, C.H., Elkabbani, O., Tiede, D., Norris, J. & Schiffer, M. (1991). Structure of the membrane bound protein photosynthetic reaction centre from *Rhodobacter sphaeroides. Biochemistry* **30**, 5352–5360.

Clayton, R.K. (1962). Primary reactions in bacterial photosynthesis. I. Nature of light-induced absorption changes in chromatophores; evidence for a special bacteriochlorophyll component. *Photochem. Photobiol.* **1**, 201.

Clayton, R.K. (1966). Spectroscopic analysis of bacteriochlorophylls *in vivo*. *Photochem. Photobiol.* **5**, 669–677.

Clayton, R.K. & Clayton, B.J. (1972). Relations between pigments and proteins in the photosynthetic membranes of *Rhodobacter sphaeroides*. *Biochim. Biophys. Acta*, **283**, 492–504.

Clayton, R.K. & Haselkorn, R. (1972). Protein components of bacterial photosynthetic membranes. *J. Mol. Biol.* **68**, 97–105.

Clayton, R.K. (1978). Physiochemical mechanisms in reaction centres of photosynthetic bacteria. In *The Photosynthetic Bacteria* (Clayton, R.K. and Sistrom, W.R. eds) pp. 387–396. Plenum Press, New York.

Cogdell, R.J., Parson, W.W. & Kerr, M.A. (1976). The typre, location and energy transfer properties of the carotenoid from *Rhodopseudomonas sphaeroides. Biochim. Biophys. Acta* **430**, 89–93.

Cogdell, R.J., Lindsay, J.G., Valentine, J. & Durant, I. (1982). A further characterisation of the B890 light-harvesting pigment-protein complexes from *Rhodospirillum rubrum* strain S1. *FEBS Lett.* **150**, 151–154.

Cogdell, R.J. (1983a). Light-harvesting complexes in the purple photosynthetic bacteria. In *Encyclopaedia of Plant Physiology New Series*, Vol. 19, (Stalhelin, L.A. and Arntzen, C.J., eds) pp. 252.

Cogdell, R.J., Durant, I., Valentine, J., Lindsay, J.G. & Schmidt, K. (1983b). The isolation and partial characterisation of the light-harvesting pigment-protein complement from *Rhodopseudomonas acidophila* strain 10050. *Biochim. Biophys. Acta* **722**, 427–455.

Cogdell, R.J. & Scheer, H. (1985). Circular dichroism of light-harvesting complexes from purple photosynthetic bacteria. *Photochem. Photobiol.* **42**, 669–689.

Cogdell, R.J., Woolley, K.J., MacKenzie, R.C., Lindsay, J.G., Michel, H., Dobler, J. & Zinth, W. (1985). Crystallisation of the B800–850 complex from *Rhodopseudomonas acidophila* strain 7750. In *Springer series in Chem. Phys.* **42**, 85–89.

Cogdell, R.J., Woolley, K.J., Dawkins, D.J. & Lindsay, J.G. (1986). In *Microbial Energy Transduction Current Communications in Molecular Biology* (Youvan, D.C. and Daldal, F., eds) pp. 47–51, Cold Spring Harbor Symposium, Cold-Spring Harbor, New York.

Colman, & Matthews, B.W. (1971). Symmetry, molecular weight and crystallographic data for sweet potato β-amylase. *J. Mol. Biol.* **60**, 163–168.

Cotton, T.M., Loach, P.A., Katz, J.J. & Ballscmiter, K. (1978). Studies of Chl-Chl and Chl-ligand interactions by visible absorption and infrared spectroscopy at low temperatures. *Photochem. Photobiol.* **27**, 735–749.

Davidson, E. & Cogdell, R.J. (1981). Reconstitution of carotenoids into the light-harvesting pigment–protein complexes from the carotenoidless mutant *Rhodobacter sphaeroides* R26. *Biochim. Biophys. Acta* **635**, 295-303.

Deinum, G., Otte, S.C.M., Gardiner, A.T., Aartsma, T.J., Cogdell, R.J. & Amesz, J. (1991). Antenna organisation of *Rhodopseudomonas acidophila* : A study of the excitation migration. *Biochim. Biophys. Acta* **1060**, 125–131.

Deisenhofer, J., Epp, O., Miki, K., Huber, R. & , Michel, H. (1984) X-ray structural analysis of a membrane protein complex. *J. Mol. Biol.* **180**, 385–398.

Deisenhofer, J., Epp, O., Miki, K., Huber, R. & Michel, H. (1985). Structure of the protein subunits in the photosynthetic reaction centre of *Rhodopseudomonas viridis* at 3Å resolution. *Nature* **318**, 618–624.

Deisenhofer & Michel, H. (1989). The photosynthetic reaction centre from the purple bacterium *Rhodopseudomonas viridis*. *EMBO J.* **8**, 2149–2170.

Diamond, R. (1969). Profile analysis in single crystal diffractometry. *Acta Cryst.* **A25**, 43–55.

Dole, M., Mack, L.L., Hines, R.L., Mobley, R.C., Ferguson, L.D. & Alice, M.B. (1968). Molecular beams of macroions. *J. Chem. Phys.* **49**, 2240–2249.

Drews, G. (1985). Structure and functional organisation of the light- harvesting complexes and photochemical reaction centres in membranes of photosynthetic bacteria. *Microbiol. Rev.* **49**, 59–70.

Dutton, P.L. (1986). Energy Transduction in Anoxygenic Photosynthesis. In "Photosynthesis III (*Staelhelin L.A. and Arntzen, C.J. eds*) Encyclopedia of Plant Physiology" Vol. 19, Springer-Verlag.

Emerson, R. & Arnold, W. (1932). Photochemical reactions in photosynthesis. *J. Gen. Physiol.* **16**, 191-205.

Engelhardt, H., Gukenberger, R., Hegerl, R. & Baumeister, W. (1985). High resolution shadowing of freeze-dried bacterial photosynthetic membranes: multivariate statistical analysis and surface relief reconstruction. *Ultramicroscopy* **16**, 395–409.

Evans, M.B. (1989). "The Structure and Function of the Light-Harvesting Antenna Complexes from Purple Photosynthetic Bacteria" PhD Thesis, University of Glasgow.

Feher, G. & Kam, Z. (1985). Nucleation and growth of protein crystals: general principles and assays. *Meth. Enzymol.* **114**, 77–112.

Fenna, R.E. & , Matthews B.W. (1975). Chlorophyll arrangement in a bacteriochlorophyll protein from *Chlorobium*. *Nature* **258**, 573–577.

Fenna, R.E., Ten Eyck, L.F. & Matthews, B.W. (1977). Atomic coordinates for the chlorophyll core of a bacteriochlorophyll *a* protein from green photosynthetic bacteria. *Biophys. Res. Comm.* **75**, 751–756.

Fleming, G.R., Martin, J.L.M. & Breton, J. (1988). Rates of primary electron transfer in photosynthetic reaction centres and their mechanistic implications. *Nature* **333**, 190–192.

Ford, R.C., Picot, D. & Garavito, R.M. (1987). Crystallisation of the photosystem I reaction centre. *EMBO J.* **6**, 1581–1586.

Fowler, G.J.S., Visschers, R.W., Grief, G.G., Van Grondelle, R. & Hunter, C.N. (1992). Genetically modified photosynthetic antenna complexes with blueshifted absorbancy bands. *Nature* **355**, 848–850.

Fox, G.C. & Holmes, K.C. (1966). An alternative method of solving the layer scaling equations of Hamilton, Rollet and Sparks. *Acta Cryst.* **20**, 886–891.

Frenkel, A.W. & Nelson, R.A. (1971). Bacterial Chromatophores. *Meth. Enzymol.* **23**, 256-268.

Gabellini, N., Bowyer, J.R., Hurt, E., Melandri, B.A. & Hauska, G. (1982). A cytochrome bc_1 complex with ubiquinol-cytochrome c_2 oxidoreductase activity from *Rhodobacter sphaeroides* GA. *Eur. J. Biochem.* **126**, 105–111.

Garavito, R.M. & Rosenbusch, J.P. (1980). Three-dimensional crystals of an integral membrane protein: initial X-ray analysis. *J. Cell. Biol.* **86**, 327–329.

Garavito, R.M., Jenkins, J., Jasonius, J.N., Karlsson, R. & Rosenbusch, J.P. (1983). X-Ray diffraction analysis of matrix porin, an integral membrane protein from *Escherichia coli* outer membranes. *J. Mol. Biol.* **164**, 313–327.

Garavito, R.M., Hinz, U. & Neuhaus, J.M. (1984). The crystallisation of outer membrane proteins from *Escherichia coli. J. Biol. Chem.* **259**, 4254–4257.

Garavito, R.M., Markovic-Housley, Z. & Jenkins, J.A. (1986). The growth and characterization of membrane protein crystals. *J. Crystal Growth* **76**, 701–709.

Garcia, A., Vernon, L.P. & Hilton M. (1966) Properties of chromatophore particles obtained by treatment with Triton X-100. *Biochem.* **5**, 2399-2407.

Gottstein, J. & Scheer, H. (1983). Long-wavelength absorbing forms of BChl *a* in solutions of Triton X–100. *Proc. Natl. Acad. Sci. USA.* **80**, 2231–2234.

Green, D.W., Ingram, V.M. & Perutz, M.F. (1954). The structure of haemoglobin. *Proc. Roy. Soc.* **A225**, 287–295.

Greenfield, N. & Fasman, G.D. (1969). Computed circular dichroism for the evaluation of protein conformation. *Biochemistry* **24**, 6955–6962.

Griffiths, M., Sistrom, W.R., Cohen-Bazire, G. & Stanier, R.Y. (1955). Function of carotenoids in photosynthesis. *Nature* **176**, 1211–1214.

Hanson, L.K. & Hofrichter, J. (1985). Absorption of methylbacteriophaeophorbide *a* in single crystals: spectral shifts due to π-π interactions *Photochem. Photobiol.* **41**, 247–249.

Hayashi, H., Nozawa, M., Hatano, M. & Morita, S. (1981). Circular dichroism of bacteriochlorophyll *a* in light-harvesting bacteriochlorophyll protein complexes from *Chromatium vinosum*. *J. Biochem.* **89**, 1853–1861.

Hayashi, H., Nozawa, M., Hatano, M. & Morita, S. (1982a). Circular dichroism of bacteriochlorophyll *a* in light-harvesting bacteriochlorophyll protein complexes from *Rhodopseudomonas palustris*. *J. Biochem.* **91**, 1029–1038.

Hayashi, H., Nakono, M. & Morita, S. (1982b). Comparative studies of protein properties and bacteriochlorophyll contents of bacteriochlorophyll- protein complexes from spectrally different types of *Rhodopseudomonas palustris*. *J. Biochem.* **92**, 1805–1811.

Helenius, A. & Simons, K. (1975). Solubilisation of membranes by detergents. *Biochim. Biophys. Acta* **415**, 29–79.

Helenius, A., McCaslin, D.R., Fries, E. & Tanford, C. (1979). Properties of detergents. *Meth. Enzymol.* **56**, 734–799.

Hermans, J. (1982). Excluded volume theory of polymer–protein interactions based on polymer chain statistics. *J. Chem. Phys.* **77**, 2193–2203.

Hjerten, S. (1962). Chromatographic separation according to size of macromolecules and cell particles on columns of agarose suspensions. *Arch. Biochem. Biophys.* **99**, 466–475.

Holmes, K.C. & Blow, D.M. (1966). *The use of X-ray diffraction in the study of protein and nucleic acid structure*, Interscience, New York.

Howard, A.J., Gilliland, G.L., Finzel, B.C., Poulos, T.L., Ohlendorf, D.H. & Salemme, F.R. (1987). The use of an imaging proportional counter in macromolecular crystallography. *J. Appl. Cryst.*, **20**, 383–387.

Imhoff, J.F., Trüper, H.G. & Pfennig, N. (1984). Rearrangement of the species and genera of the phototrophic purple nonsulfur bacteria. *Init. J. Syst. Bacteriol.* **34**, 340–343.

Imhoff, J.F. (1988). Anoxgenic phototrophic bacteria. In *Methods in Aquatic Biology* (Austin, B., ed.) John Wiley and Sons, London.

Iribane, J.V. & Thomson, B.A. (1976). On the evaporation of small ions from charged droplets. *J. Chem. Phys.* **64**, 2287-2294.

Jackson, J.B. & Crofts, A.R. (1969). The high energy state in chromatophores from *Rhodobacter sphaeroides. FEBS Lett.* **4**, 185–189.

Jardine, I. (in press). In "Current Research in Protein Chemistry" (Villafranca, J. ed.) Academic Press, San Diego, California.

Jay, F., Lambillotte, M. & Mühlethaler, K. (1983). Localisation of *Rhodopseudomonas viridis* reaction centre and light-harvesting proteins using ferritin-antibody labelling. *Eur. J. Cell Biol.* **30**, 1–8.

Jones, M.R. & Hunter, C.N. (1992). Engineering Biological Electron Transfer Systems. *SERC Bulletin* **12**, 5.

Kabsch, W. (1988). Automatic indexing of rotation diffraction patterns. *J. Appl. Cryst.* **21**, 67–71.

Katz, J.J., Sipman, L.L., Cotton, T.M. & Janson, T.R. (1977). In *The Porphyrins* (Dolphin, D. ed.), Academic Press, New York.

King, M.V. (1954). An efficient method for mounting wet protein crystals for X-ray studies. *Acta Cryst.* **7**, 601–602.

Laemmli, U.K. (1970). Cleavage of structural proteins during the assembly of the head of bacteriophage T4. *Nature* **227**, 680.

Lee, J.C. & Lee, L.L.Y. (1981). Preferred solvent interactions between protein and polyethylene glycols. *J. Biol. Chem.* **256**, 625–631.

Loo, J.A., Udseth, H.R. & Smith, R.D. (1989). Peptide and protein analysis electrospray ionisation-mass spectrometry and capillary electrophoresis-mass spectrometry. *Anal. Biochem.* **179**, 404–412.

Lowry, O.H., Rosebrough, N.J., Farr, A.L. & Randall, R.J. (1951). Protein measurement with the folin reagent. *J. Biol. Chem.* **193**, 265–275.

MacPherson, A. (1982). *The preparation and analysis of protein crystals* Chapter 3, John Wiley & Sons, New York.

McElroy, J.D., Feher, G. & Mauzerall, D.C. (1969). On the nature of the free radical formed during the primary process of bacterial photosynthesis. *Biochim. Biophys. Acta* **172**, 180–183.

Markwell, M.A.K., Haas, S.M., Bieber, L.L. & Tolbert, N.E. (1987). A modification of the Lowry procedure to simplify protein determination in membrane and lipoprotein samples. *Analytical Biochemistry* **87**, 206–210.

Matthews, B.W. (1968). Solvent content of protein crystals. *J. Mol. Biol.* **33**, 491-497.

Matthews B.W. (1977). In *Proteins* (Neurath, H. & Hill, R.L., eds), vol. 3, pp. 403–590, Academic Press, London.

Matthews, B.W. (1985). Determination of Protein Molecular Weight, Hydration, and Packing from Crystal Density. *Meth. Enzymol.* **114**, 176–187.

Mejbaum-Katzenellenbogen S,. & Drobryszycka, W.J. (1959). New method for quantitative determination of serum proteins separated by paper electrophoresis. *Clin. Chim. Acta* **4**, 515–522.

Michel, H. & Oesterhelt, D. (1980). Three-dimensional crystals of membrane proteins: bacteriorhodopsin. *Proc. Natl. Acad. Sci., USA.* **77**, 1283–1285.

Michel, H. (1983). Crystallisation of membrane proteins. *Trends Biochem. Sci.* **8**, 56–59.

Michel, H. & Deisenhofer, J. (1986). X-ray diffraction studies on a crystalline bacterial photosynthetic reaction centre. In *Photosynthesis III: Photosynthetic Membranes and Light-harvesting Systems* Encyclopedia of Plant Physiology, New Series, vol. 19. (Staehelin, L.A. & Arntzen, C.J. eds).

Michel, H. (1991). General and practical aspects of membrane protein crystallisation. In *Crystallization of membrane proteins* (Michel, H., ed.) pp. 73–86 CRC Press, Florida.

Mikol V., Rodeau, J.-L. & Giege, R. (1989). Changes of pH during biomolecular crystallisation by vapour diffusion using ammonium sulphate as the precipitant. *J. Appl. Cryst.* **22**, 155–161.

Mikol V., Rodeau, J.-L. & Giege, R. (1990). Experimental determination of water equilibration rates in the hanging drop method of protein crystallisation. *Analytical Biochemistry* **186**, 332–339.

Miller, K.R. (1982). Three-dimensional structure of a photosynthetic membrane. *Nature* **300**, 53–55.

Mitchell, P. (1961). Coupling of phosphorylation to electron and hydrogen transfer by a chemi-osmotic type of mechanism. *Nature* **191**, 144–148.

Netzel, T.L., Rentzepis, P.M. & Leigh, J. (1973). Picosecond kinetics of reaction centres containing bacteriochlorophyll. *Science* **182**, 238–241.

Nicolls, D.G. (1982) *Bioenergetics- An Introduction to Chemiosmotic Theory*, Academic Press, New York.

Norris, J.R., Uphaus, R.A., Crespi, H.L. & Katz, J.J. (1971). Electron nuclear double resonance of bacteriochlorophyll free radicals *in vivo* and *in vitro*. *Proc. Natl. Acad. Sci. USA.* **68**, 625–628.

Norris, J.R., Druyan, M.E. & Katz, J.J. (1973). Electron nuclear double resonance of bacteriochlorophyll free radicals in vivo and vitro. *J. Am. Chem. Soc.* **95**, 1680–1682.

Oelze, J. & Drews, G. (1981). Membranes of phototrophic bacteria. In *Organisation of prokaryotic cell membranes* vol 2. (Ghosh, B.K. ed.) pp. 131–195 CRC Press, Boca Raton, Florida.

Papiz, M.Z., Hawthornthwaite, A.M., Cogdell, R.J., Woolley, K.J., Wightman, P.A., Ferguson, L.A. & Lindsay, J.G. (1989). Crystallisation and characterisation of two crystal forms of the B800-850 light-harvesting complex from *Rhodopseudomonas acidophila* strain 10050. *J. Mol. Biol.* **209**, 833–835.

Park, K., Perzcel, A. & Fasman, G.D. (1992). Differentiation between transmembrane helices and peripheral helices by the deconvolution of circular dichroism spectra of membrane proteins. In press.

Parkes-Loach, P., Sprinkle, J.R. & Loach, P.A. (1988). Reconstitution of the B873 light-harvesting complex of *Rhodospirillum rubrum* from separated α– and β– polypeptides and bacteriochlorophyll *a*. *Biochem.* **27**, 2718–2727.

Parson, W.W. & Holten, D. (1986). Primary electron transfer reactions in photosynthetic bacteria: energetics and kinetics of transient states. In *Photosynthesis III: Photosynthetic Membranes and Light-harvesting Systems* Encyclopedia of Plant Physiology, New Series, vol. 19. (Staehelin, L.A. & Arntzen, C.J. eds).

Patterson, A.L. (1934). Fourier series method for the determination of contacts and interatomic distances in crystals. *Phys Rev.* **46**, 372–376.

Pearlstein, R.M. & Zuber, H. (1985). Exciton state and energy transfer in bacterial membranes. The role of protein–pigment cyclic unit structures. In *Antennas and Reaction Centres of Photosynthetic Bacteria* (Michel-Beyerle, M.E. ed.) Springer-Verlag Series in Chemical Physics **42**, 56–59.

Pearlstein, R.M. (1987) In *Photosynthesis* (Amesz, J. ed.) Elsevier Science Publishers, pp. 299–315.

Perzcel, A., Hollosi, M., Tusnady, G. & Fasman, G.D. (1991). Convex constraint analysis: A natural deconvolution of circular dichroism curves of proteins. *Protein Engineering* **4**, 669–679.

Pfennig, N. (1969). *Rhodopseudomonas acidophila* sp. n., a new species of the budding nonsulphur purple bacteria. *J. Bacteriol.* **99**, 597–602.

Pfennig, N. & Trüper, H.G. (1971). Higher taxa of the phototrophic bacteria. *Int. J. Syst. Bacteriol.* **21**, 19.

Pfennig, N. & Trüper, H.G. (1974). The phototrophic bacteria In *Bergey's Manual of Determinative Bacteriology* (Buchanan, R.E. and Gibbons, N.E. eds) pp. 24–64. The Williams & Wilkins Co., Baltimore.

Picorel, R., Belanger, G. & Gingras, G. (1983). Antenna holochrome B880 of *Rhodospirillum rubrum* S1. Pigment, phospholipid and polypeptide composition. *Biochemistry* **22**, 2491–2494.

Picorel, R. & Gingras, G. (1988). Preparative isolation and characterisation of the B875 complex from *Rhodobacter sphaeroides* 2.4.1. *Biochem. Cell Biol.* **66**, 442–448.

Provencher, S.W. & Glöckner J. (1981). Estimation of Globular Protein Secondary Structure from Circular Dichroism. *Biochemistry* **20**, 33–37.

Reed, D.W. & Clayton, R.K. (1968). Isolation of a reaction centre fraction from *Rhodopseudomonas sphaeroides. J. Biol. Chem.* **244**, 4396–4941.

Reed, D.W. (1970). Isolation and composition of a photosynthetic reaction centre complex from *Rhodobacter sphaeroides. J. Biol. Chem.* **244**, 4936–4941.

Reiss-Husson, R., Gaucher J-F., Ducruix, A. & Arnoux, B. (1992). Structural studies of wild type *Rhodobacter sphaeroides* Y reaction center. *Photosynthesis Research* **34**, 85.

Robert, B. & Lutz, M. (1985). Structures of antenna complexes of several *Rhodospirillales* from their resonance Raman spectra. *Biochim. Biophys. Acta* **807**, 10–23.

Robertson, D.E. & Dutton, D.L. (1988). The nature and magnitude of the charge separation reactions of ubiquinone cytochrome c_2 oxidoreductase. *Biochim. Biophys. Acta* **935**, 273–291.

Rossmann, M.G. & Blow, D.M. (1962). The detection of sub–units within the crystallographic asymmetric unit. *Acta Cryst.* **15**, 24–31.

Sauer, K. & Austin, L.A. (1978). Isolation and characterisation of the pigment-protein complexes from *Rhodopseudomonas sphaeroides* by lithium dodecyl sulphate. *Biochemistry* **17**, 2011–2019.

Saxena, V.P. & Wetlaufer, D.B. (1971). A new basis form interpreting the circular dichroic properties of proteins. *Proc. Natl. Acad. Sci. USA.* **68**, 969–972.

Schägger H. & Von Jagow G. (1987). Tricine-sodium dodecyl sulfate- polyacrylamide gel electrophoresis for the separation of proteins in the range from 1 to 100 kDa. *Anal. Biochem.* **166**, 368–379.

Scherz, A. & Parson, W.W. (1984). Oligomers of bacteriochlorophyll and bacteriopheophytin with spectroscopic properties resembling those found in photosynthetic bacteria. *Biochim. Biophys. Acta.* **766**, 653.

Scherz, A., Rosenbach, V. & Malkin, S. (1986). Small oligomers of bacteriochlorophylla as *in vitro* models for the primary electron donors and light-harvesting pigments in purple photosynthetic bacteria. In *Antennas and Reaction Centres of Photosynthetic Bacteria* (Michel-Beyerle, M.E. ed.), Springer-Verlag, pp. 314–323.

Schmidt, K. (1971). Carotenoids of purple nonsulphur bacteria. Composition and biosynthesis of carotenoids of some strains of *Rhodopseudomonas acidophila*, *Rhodospirillum tenue*, and *Rhodocyclus purpureus*. *Arch. Microbiol.* **77**, 231.

Shreve, A.P., Cherepy, N.J., Franzen, S. Boxer, S.G. & Mathies, R.D. (1992). Rapid flow resonance Raman spectroscopy of bacterial photosynthetic reaction centres. *FASEB Journal* **6**, Article #578.

Sprague, S.G. & Varga, A.R. (1986). Topography, composition and assembly of photosynthetic membranes In *Photosynthesis III: Photosynthetic membranes and light-harvesting systems* Encyclopedia of Plant Physiology, New Series vol. 19 (Staehelin, L.A. & Arntzen, C.J. eds).

Stark, W., Kühlbrandt, W., Wildhaber, I., Wehrli, E. & Mühlethaler, K. (1984). The structure of the photoreceptor unit of *Rhodopseudomonas viridis*. *EMBO J.* **3**, 777–783.

Studier, F.W. (1973). Analysis of bacteriophage T7 early RNAs and proteins on slab gels. *J. Mol. Biol.* **79**, 237–248.

Tanford, C. & Reynolds, J.A. (1976) Characterisation of membrane proteins in detergent solutions. *Biochim. Biophys. Acta* **457**, 133–170.

Tanford, C. (1980). *The Hydrophobic effect*, John Wiley & Sons, New York.

Ten Eyck, L.F. (1973). Fast Fourier Transforms. *Acta Cryst.* **A29**, 486.

Thornber, J.P. (1970). Photochemical reactions of purple bacteria as revealed by studies of three spectrally different caroteno-bacteriochlorophyll protein complexes isolated from *Chromatium vinosum* strain D. *Biochemistry* **9**, 2688–2698.

Thornber, J.P. (1978). Bacteriochlorophyll-protein complexes from the light-harvesting antenna of photosynthetic bacteria. *Biochemistry* **17**, 2011–2019.

Thornber, J.P., Cogdell, R.J., Pierson, B.K. & Seftor, R.E.B. (1983). Pigment-protein complexes of purple photosynthetic bacteria: an overview. *J. Cell. Biochem.* **23**, 159–169.

Thornber, J.P. (1986). Biochemical characterisation and structure of pigment–proteins of photosynthetic organisms. In *Photosynthesis III: Photosynthetic Membranes and Light-harvesting Systems* (Staehelin, L.A. and Arntzen, C.J. eds) Encyclopedia of Plant Physiology, New Series, vol. 19, Springer-Verlag.

Timmins, P.A., Hauk, J. & Welte, W. (1991). The influence of heptane-1, 2, 3-triol on the size and shape of LDAO micelles (Implications for the crystallisation of membrane proteins). *FEBS Lett.* **280**, 115–120.

Trüper, H.G. & Pfennig, N. (1978). Taxonomy of the Rhodospirillales. In *The Photosynthetic Bacteria* (Clayton, R.K. and Sistrom, W.R. eds) pp. 19–27. Plenum Press, New York.

Ueda, T., Morimoto, Y. Sato, M., Kakuno, T., Yamashita, J. & Horio, T. (1985). Isolation, characterisation and comparison of a ubiquitous pigment–protein complex consisting of a reaction centre and light-harvesting bacteriochlorophyll proteins present in photosynthetic bacteria. *J. Biochem.*, **98**, 1487–1498.

Van Niel, C.B. (1941). The bacterial photosyntheses and their importance for the general problem of photosynthesis. *Adv. Enzymol.* **1**, 263–328.

Vredenberg, W.J. & Amesz, J. (1967). Absorption characteristics of bacteriochlorophyll types in purple bacteria and efficiency of energy transfer between them. *Brookhaven Symp. Biol.* **19**, 49–54.

Wacker, T., Gadon, N., Becker, A., Mäntele, W., Kreutz, W., Drews, G. & Welte, W. (1986) Crystallisation and spectroscopic investigation with polarised light of the reaction centre B875 light-harvesting complexes of *Rhodopseudomonas palustris*. *FEBS Lett.* **197**, 267–273.

Welte, W., Wacker, T., Leis, M., Kreutz, W., Shiozawa, J., Gadon, N. & Drews, G. (1985). Crystallisation of the photosynthetic light-harvesting pigment-protein complex B800–850 of *Rhodopseudomonas capsulata. FEBS Lett.* **182**, 260–264.

Westbrook, E.M. (1985). Crystal density measurements using aqueous Ficoll solutions. *Meth. Enzymol.* **114**, 187–196.

Weyer, K.A., Schäfter, W., Lottspeich, F. & Michel, H. (1987). The cytochrome subunit of the photosynthetic reaction centre from *Rhodopseudomonas viridis* is a lipoprotein. *Biochemistry* **26**, 2909–2914.

Williams, J.C., Steiner, L.A., Feher, G. & Simon, M.I. (1983). Primary structure of the L subunit of the reaction centre from *Rhodopseudomonas sphaeroides. Proc. Natl. Acad. Sci. USA.* **81**, 7303–7307.

Woolley, K.J., MacKenzie, R.C., Cogdell, R.J., Lindsay, J.G. & Michel, H. (1986). Crystallisation of the B800–850 complex from *Rhodopseudomonas acidophila* strain 7750. *Biochem. Soc. Trans.* **14**, 57–62.

Xuong N.H., Nielsen, C., Hamlin, R. & Anderson, D. (1985). Strategy for data collection from protein crystals using a multiwire counter area detector diffractometer. *J. Appl. Cryst.* **18**, 342–350.

Yeates, T.O., Komiya, H., Rees, D.C., Allen, J.P.& Feher, G. (1987). Structure of the reaction centre from *Rhodobacter sphaeroides* R–26: membrane protein interactions. *Proc. Natl. Acad. Sci.* **84**, 6438–6442.

Yeates, T.O., Komiya, H., Chirino, A., Rees, D.C., Allen, J.P. & Feher, G. (1988). Structure of the reaction centers from *Rhodobacter sphaeroides* R–26 and 2.4.1.: Symmetry relations and sequence comparisons between different species. *Proc. Natl. Acad. Sci. USA.* **85**, 9012–9025.

Zuber, H. (1985). Yearly review: structure and function of light-harvesting complexes and their polypeptides. *Photochem. Photobiol.* **42**, 821–844.

Zuber, H. (1986). Structure of light-harvesting antenna complexes of photosynthetic bacteria, cyanobacteria and red algae. *Trends Biochem. Sci.* **11**, 414–419.

Zuber, H (1987). Structural principles of the antenna system of photosynthetic organisms. In *Progress in photosynthesis research* (Biggins, J. ed) vol. II, Martinus Nijhoff Publishers, Dordrecht.

Zuber, H. (1990). Considerations on the structural principles of the antenna complexes of phototrophic bacteria. In *Molecular biology of membrane-bound complexes in phototrophic bacteria* (Drews, G. and Dawes, E.A. eds) pp. 161–180, Plenum Press, New York.

Zuber, H. & Brunisholz, R.A. (1991). Structure and Function of Antenna Polypeptides and Chlorophyll-Protein Complexes: Priciples and Variability. In *Chlorophyll Proteins* pp. 627–680, CRC Press, Boca Raton, Florida.

Appendix A: Compositions of Growth Media

Pfennig's Medium	**per litre**
potassium dihydrogen orthophosphate	1.00g
magnesium sulphate (hepta-hydrate)	0.40g
sodium chloride	0.40g
sodium succinate	1.50g
calcium chloride(di-hydrate)	0.05g
ammonium chloride	0.50g
ferric citrate solution	5ml
trace elements solution	10ml

Adjust to pH 5.2 using 10M HCl

Ferric Citrate Solution	**per litre**
ferric citrate	1.00g

Trace Elements Solution	**per litre**
EDTA	0.50g
ferrous sulphate	0.01g
manganous chloride	0.003g
boric acid	0.03g
cobalt chloride	0.02g
calcium chloride	0.001g
nickel chloride	0.002g
sodium molybdate	0.003g

Adjust to pH 3.4 using 10M HCl

Agar Culture Medium

yeast extract	0.30g
casamino acids	0.20g
agar	1.50g
tap water	100ml

Heat to 100 ^{o}C, pour into universal bottles and autoclave.

Appendix B: Detergents used in Circular Dichroism and Crystallisation Studies

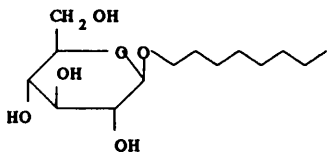

n-Octylglucoside

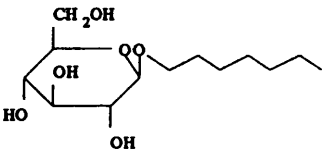

n-Heptylglucoside (7OG)

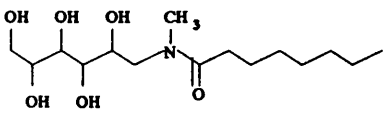

Octanoyl-N-methylglucamide (MEGA-8)

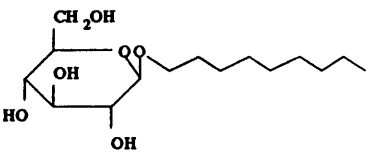

n-Nonylglucoside (9OG)

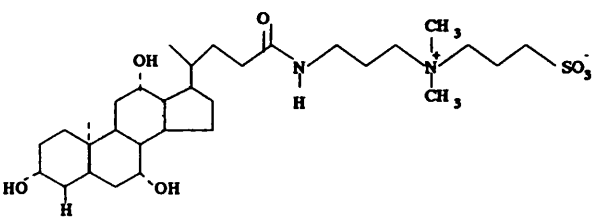

3-[(3-Cholamidopropyl)dimethylammonio]-1-propane sulphonate (CHAPS)

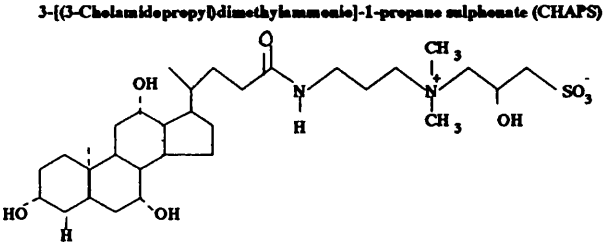

3-[(3-Cholamidopropyl)dimethylammonio]-2-hdroxy-1-propane sulphonate (CHAPSO)

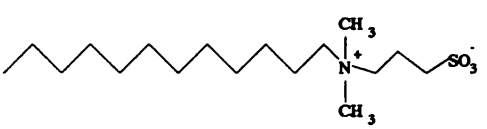

N-Dodecyl-N,N-dimethyl-3-ammonio-1-propane-sulphonate (NDA)

Appendix C: Compositions of Solutions for Tricine-SDS Polyacrylamide Gel Electrophoresis (after Laemmli)

Acrylamide Stock Solution	**per 100ml**
49.5% acrylamide	48.0g
1.5% bis-acrylamide	1.5g

Gel Buffer	**per 500ml**
Tris-HCl	181.65g
sodium dodecyl sulphate	1.50g

Adjust to pH 8.45 using 10M HCl

Electrode Buffers	**per litre**
Anode	
Tris-HCl	1.21g

Adjust to pH 8.9 using 10M HCl

Cathode	
Tris-HCl	12.1g
tricine	17.9g
sodium dodecyl sulphate	1.0g

Adjust to pH8.25 using 10M HCl

Sample Buffer (Boiling Solution)	**per 50ml**
tris-HCl	0.30g
sodium dodecyl sulphate	1.0g
glycerol	5.0g
mercaptoethanol	1.0g
bromophenol blue	0.05g

Gel Staining Solution	
isopropanol	625ml
acetic acid	250ml
coomassie blue	1.0g
distilled water	1625ml

Gel Destaining Solution	**per litre**
methanol	100ml
glacial acetic acid	200ml
distilled water	700ml

Appendix C cont: Tricine-SDS Polyacrylamide Gel Preparation

	Stacking	Spacer	Separating
acrylamide	1.6ml	4.0ml	10.0ml
gel buffer	4.96ml	6.0ml	10.0ml
glycerol	——	——	4.0ml
water	to 20ml	to 20ml	to 30ml
ammonium persulphate	200µl	200µl	300µl
TEMED	20µl	20µl	30µl

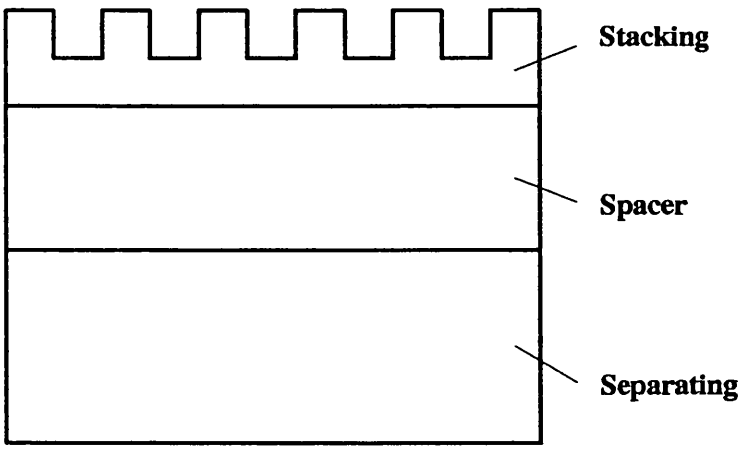

Appendix D: Low Molecular Weight Marker Proteins

Marker	Molecular Weight
myoglobin (1-153)	16,950 Da
myoglobin I+II (1-131)	14,440 Da
myoglobin I+III (56-153)	10,600 Da
myoglobin I (56-131)	8,160 Da
myoglobin II (1-55)	6,210 Da
glucagon	3480Da
myoglobin III (132-153)	2,510 Da

Amino acid residue no.	1	55	131	153
Molecular weight	6210	8160	2510	

Appendix E: Compositions of Solutions for SDS Polyacrylamide Gel Electrophoresis

Acrylamide Stock Solution	**per 100ml**
30% acrylamide	39.0g
0.8% bis-acrylamide	1.0g

Running Gel Buffer	**per 250ml**
Tris-HCl	43.55g
sodium dodecyl sulphate	1.0g

Adjust to pH 8.80 using 10M HCl

Stacking Gel Buffer	**per 250ml**
Tris-HCl	15.1g
sodium dodecyl sulphate	1.0g

Adjust to pH 6.80 using 10M HCl

Electrode Buffer	**per litre**
Tris-HCl	3.0g
sodium dodecyl sulphate	1.0g
glycine	14.6g

Adjust to pH 8.30 using 10M HCl

Sample Buffer (Boiling Solution)	**per 50ml**
Tris-HCl	0.30g
sodium dodecyl sulphate	1.0g
glycerol	5.0g
mercaptoethanol	1.0g
bromophenol blue	0.05g

Gel Staining Solution	
isopropanol	625ml
acetic acid	250ml
coomassie blue	1.0g
distilled water	1625ml

Gel Destaining Solution	**per litre**
methanol	100ml
glacial acetic acid	200ml
distilled water	700ml

Appendix E cont: SDS-Polyacrylamide Gel Preparation

		Separating Gel			
	Stacking Gel	13.5%	15%	16.5%	18%
stacking gel buffer	5ml	—	—	—	—
running gel buffer	—	5ml	5ml	5ml	5ml
30% acrylamide	3ml	9ml	10ml	11ml	12ml
H_2O	12ml	—	—	—	—
70% sucrose	—	6ml	5ml	4ml	3ml
10% ammonium per-sulphate	60µl	100µl	100µl	100µl	100µl
TEMED	20µl	12.5µl	12.5µl	12.5µl	12.5µl

Appendix F: Composition of Protein Assay Solutions

Tannin Assay

1M HCl	196ml
tannic acid	20g
phenol	4g

Heat to 80 ^{o}C, filter when cool and store at 4 ^{o}C.

gum arabic	0.4g in 200ml d. H_2O

Modified Lowry Assay

Solution A

sodium carbonate	10g
sodium hydroxide	2g
sodium potassium tartrate	0.8g
sodium dodecyl sulphate	5g

make volume up to 500ml with d.H_2O

Solution B	**per 100ml**
copper sulphate(penta hydrate)	4g

Solution C

1ml of **Solution B** per 100ml of **Solution A**

(fresh on day of the assay)

Solution D

Folin-Ciocalteau reagent diluted with an equal volume of water.